



University
of Glasgow

Rauf, Sakandar (2010) *Quantum dot encoded magnetic beads for multiplexed fluorescence biosensing*. PhD thesis.

<http://theses.gla.ac.uk/1647/>

Copyright and moral rights for this thesis are retained by the author

A copy can be downloaded for personal non-commercial research or study, without prior permission or charge

This thesis cannot be reproduced or quoted extensively from without first obtaining permission in writing from the Author

The content must not be changed in any way or sold commercially in any format or medium without the formal permission of the Author

When referring to this work, full bibliographic details including the author, title, awarding institution and date of the thesis must be given.

Quantum Dot Encoded Magnetic Beads for Multiplexed Fluorescence Biosensing

Sakandar Rauf

©

A Thesis Submitted in
Fulfilment of the Requirements for the
the Degree of Doctor of Philosophy

**Department of Electronics and Electrical Engineering
Faculty of Engineering
University of Glasgow
March 2010**

Abstract

In recent years, the use of encoded beads has received considerable attention due to their potential for measuring multiple analytes in solution.⁽¹⁻⁴⁾ This can be achieved without the need for knowledge of their spatial position, as in the case of microarray technology. Encoded bead technology also relies on the solution kinetics rather than diffusion to a fixed surface as in the case of microarray technology, offering the possibility of developing rapid high throughput screening methods.

This thesis describes the production, characterisation and application of quantum dot encoded beads prepared using layer-by-layer assembly of different colour quantum dots around a magnetic bead. To achieve this, two different strategies were used to make “coloured” barcodes. The first strategy used thiol chemistry to immobilise quantum dots in a layer-by-layer assembly onto magnetic beads whereas the second strategy uses the interaction between quantum dot-biotin and quantum dot-streptavidin conjugates to create constructs on the magnetic bead surface. The development of both of these immobilisation strategies was characterisation using X-ray photoelectron spectroscopy and fluorescence spectroscopy of immobilised quantum dot structures onto a plain glass substrate.

After the preparation of encoded beads, they were characterised using single bead fluorescence spectroscopy. It was found that attempts to prepare barcodes by layer-by-layer assembly of CdSe/ZnS quantum dots using thiol chemistry onto magnetic beads did not comply with the necessary barcode characteristics i.e., different colour coded beads could not be distinguished from each other. However, the encoded beads prepared using layer-by-layer assembly of quantum dot-biotin and quantum dot-streptavidin conjugates onto streptavidin coated magnetic beads gave distinct multicolour coded bead spectra. These barcodes were characterised in terms of different spectral responses, stability at raised temperatures, stability in biotin solutions, and long-term stability after storage.

Encoded beads prepared using layer-by-layer assembly of quantum dot-biotin and quantum dot-streptavidin conjugates onto streptavidin coated magnetic beads were then used to develop multiplexed immunoassays. Four different barcodes were prepared and used to perform model multiplexed immunoassays. The barcodes were identified upon the basis of different spectral response measured using single bead fluorescence spectroscopy.

Finally, a quantitative immunoassay for human IgG was performed using these barcodes, which showed that different concentrations of human IgG can be determined in solution.

References

1. Wilson R, Cossins AR, Spiller DG. Encoded microcarriers for high-throughput multiplexed detection. *Angewandte Chemie-International Edition* 2006;45(37):6104-6117.
2. Battersby BJ, Trau M. Optically encoded particles and their applications in multiplexed biomedical assays. *Australian Journal of Chemistry* 2007;60(5):343-353.
3. Sukhanova A, Nabiev I. Fluorescent nanocrystal-encoded microbeads for multiplexed cancer imaging and diagnosis. *Critical Reviews in Oncology Hematology* 2008;68(1):39-59.
4. Birtwell S, Morgan H. Microparticle encoding technologies for high-throughput multiplexed suspension assays. *Integrative Biology* 2009;1(5-6):345-362.

Publications

Journals

Rauf S, Glidle A, Cooper JM. Application of quantum dot barcodes Prepared using biological self-Assembly to multiplexed Immunoassays. *Chemical Communications* 2010; DOI: 10.1039/b927149j.

Rauf S, Glidle A, Cooper JM. Production of quantum dot barcodes using biological self-assembly. *Advanced Materials* 2009;21(40):4020-4024.

Conference (Poster Presentation)

Rauf S, Glidle A, Cooper JM. Production of Quantum Dot Barcodes using Layer-by-Layer Assembly of Biotin and Streptavidin Conjugated Quantum Dots. ESF-EMBO Symposium on Biological Surfaces and Interfaces; 27 June-2 July 2009, Sant Feliu de Guixols, Spain.

Table of Contents

List of Tables	1
List of Figures	1
List of Schemes	6
Acknowledgement	7
Author's Declaration	8
Chapter 1-Introduction and Review of Literature	9
1.1. Introduction	9
1.2. Biosensors	10
1.2.1. Biological Sensing Elements	10
1.2.2. Transduction Techniques	12
1.2.3. Quantum Dots	14
1.3. Barcode Technology for Biological Sensing	15
1.3.1. Lithographic Approaches for Barcode Fabrication	16
1.3.2. Microfluidic Production of Barcodes	19
1.3.3. Graphical Encoding	21
1.3.4. Encoding Based on Raman and Infrared Signatures	22
1.3.5. Physical Encoding	24
1.3.6. Chemical Encoding	25
1.3.7. Barcoded Fluorescent Beads	27
1.3.7.1. Encapsulation of Quantum Dots into the Beads	28
1.3.7.2. In-Situ Incorporation of Quantum Dots into Polymer Beads	32
1.3.7.3. Immobilisation of Quantum Dots on Bead Surface	32
1.4. Applications of Barcodes in Multiplexing Bioanalysis	33
1.5. Outline of the Approach to Barcode Generation and Multiplexed Assays Employed in This Thesis	36
1.6. References	38
Chapter 2-Materials and Methods	47
2.1. Layer-by-Layer Assembly of Quantum Dots onto Glass Slides and Magnetic Beads using Thiol Chemistry	47
2.1.1. Materials	47
2.1.2. Layer-by-Layer Assembly of Quantum Dots onto Glass Slides	48

2.1.3.	Immobilisation of Quantum Dots on Thiol (-SH) Modified Magnetic Beads	49
2.2.	Immobilisation of Quantum Dot Bioconjugates using Layer-by-Layer Biological Self- Assembly onto Glass Slides and Magnetic Beads	51
2.2.1.	Materials	51
2.2.2.	Layer-by-Layer Assembly of QD-Streptavidin and QD-Biotin Conjugates onto Plain Glass Substrates	52
2.2.3.	Layer-by-Layer Assembly of QD-Biotin and QD-Streptavidin Conjugates onto Magnetic Beads	53
2.2.3.1.	Comparison of Quantum Dot Conjugates Prepared with and without using a PEG-Linker for the Production of Quantum Dot Barcodes	55
2.3.	X-Ray Photoelectron Spectroscopy (XPS)	55
2.4.	Fluorescence Spectroscopy Measurements	57
2.4.1.	Measurement of Number of Quantum Dots	58
2.5.	Stability Studies of Quantum Dot Barcodes Prepared using Layer-by-Layer Assembly of QD-Biotin and QD-Streptavidin Conjugates onto Magnetic Beads	59
2.5.1.	Thermal Stability	59
2.5.2.	Stability in Biotin Solutions	60
2.5.3.	Long-Term Stability	61
2.6.	Application of Quantum Dot Barcodes to Multiplexed Immunoassays	61
2.6.1.	Materials	61
2.6.2.	Multiplexed Immunoassay using FITC-Labelled Anti-IgGs	61
2.6.2.1.	Immobilisation of Protein A-Biotin or Protein G-Biotin	62
2.6.2.2.	Immobilisation of Different Immunoglobulins (IgGs)	63
2.6.2.3.	Detection of Different IgGs	63
2.7.	Binding Inhibition Immunoassay	63
2.7.1.	Immobilisation of Protein A-biotin	64
2.7.2.	Immobilisation of Human IgG onto Barcode \bullet -B ₆₀₅ S ₆₅₅	65
2.7.3.	Optimisation of FITC Labelled Anti-Human IgG	65
2.7.4.	Calibration Curve for the Determination of Human IgG in Solution	65
2.8.	References	66
Chapter 3-Layer-by-Layer Assembly of Quantum Dots		67
3.1.	Layer-by-Layer Assembly of Quantum Dots onto Glass Substrate using a Dithiol Linker	67

3.1.1.	X-Ray Photoelectron Spectroscopy (XPS)	68
3.1.2.	Fluorescence Spectroscopy	72
3.2.	Production of Quantum Dot Barcodes using a Dithiol Linker Via Layer-by-Layer Assembly onto Magnetic Beads	75
3.3.	Layer-by-Layer Assembly of Quantum Dot-Biotin and Quantum Dot-Streptavidin Conjugates onto Glass Substrates	78
3.3.1.	X-Ray Photoelectron Spectroscopy (XPS)	78
3.3.2.	Fluorescence Spectroscopy	81
3.4.	References	85
Chapter 4-Production, Characterisation and Stability of Quantum Dot Barcodes		87
4.1.	Production of Quantum Dot Barcodes	87
4.2.	Characterisation of Quantum Dot Barcodes	89
4.3.	Stability Studies of Quantum Dot Barcodes	96
4.3.1.	Thermal Stability	97
4.3.2.	Stability in Biotin Solution	98
4.3.3.	Long-Term Stability	101
4.4.	References	103
Chapter 5-Applications of Quantum Dot Barcodes in Immunoassays		105
5.1.	Application of Quantum Dot Barcodes in Multiplexing Bioanalysis	105
5.2.	Binding Inhibition Immunoassay using Quantum Dot Barcodes	114
5.3.	References	117
Chapter 6-Summary, Conclusions and Future Prospects		118
	References	123

List of Tables

Table 2-1: Shows the filter set combinations used for the fluorescence spectroscopy measurements.	58
---	----

List of Figures

Figure 1-1: Schematic of an Immunoglobulin.	11
Figure 1-2: Jablonski diagram showing the mechanism for fluorescence emission.	13
Figure 1-3: (a) Shows emission spectra of different quantum dots; (b) Biomolecule conjugated quantum dot.	14
Figure 1-4: (a) Shows a microarray platform, which uses positional encoding for multiplexed analysis; (b) Barcoded beads labelled with different recognition molecules (antibodies, DNA or RNA sequence).	16
Figure 1-5: Shows the sequence of steps for the fabrication of encoded microparticles.	17
Figure 1-6: Shows the process of preparing microparticles from a spectrally encoded porous silicon film.	18
Figure 1-7: Schematic of the process for manufacturing nano-embossed SU8 microbars.	19
Figure 1-8: Shows the schematic diagram for the preparation of dot-coded particles.	20
Figure 1-9: Shows the set-up for the production of photonic crystals using a microfluidic device.	21
Figure 1-10: White light image of micron size glass rods encoded with different fluorescent rare-earth ions.	22
Figure 1-11: Synthesis of barcode particles.	23

Figure 1-12: Scheme showing aggregation of seeded silver nanoparticles and raman labels in silver nitrate solution to produce coins.	23
Figure 1-13: Time-dependent UV-Vis spectra showing the conversion of silver nanospheres to nanoprisms.	24
Figure 1-14: Shows schematic of nanobeads formation.	25
Figure 1-15: Overview of NanoString nCounter gene expression system.	26
Figure 1-16: Ten different coloured CdSe/ZnS quantum dots excited with a UV-lamp give different emission maxima.	28
Figure 1-17: Schematic diagram of optical coding based on wavelength and intensity multiplexing.	29
Figure 1-18: Schematic illustration of quantum dot encapsulation; (b) Fluorescence images of hydrogel spheres and corresponding fluorescence spectra of the hydrogel spheres.	30
Figure 1-19: Shows barcode production process.	31
Figure 1-20: Shows two different doping strategies of quantum dot and iron oxide nanoparticles into mesoporous beads.	31
Figure 1-21: Shows the strategy for the preparation of quantum dot barcodes using polyelectrolyte layer-by-layer assembly.	33
Figure 1-22: Shows the multiplexed DNA hybridisation assay where three different quantum dot encoded beads based barcodes were used to detect three different DNA sequences.	34
Figure 1-23: Shows different formats of immunoassays. The upper panel shows the situation before immunobinding and lower panel shows the situation after immunobinding.	34

Figure 1-24: Schematic of the multiplexed immunoassay using three different encoded silica colloidal crystal beads.	36
Figure 2-1: Schematic of an XPS set up shows X-ray source for the production of X-rays and detector to measure kinetic energy and number of electrons.	56
Figure 2-2: Schematic diagram of fluorescence measurement configuration used for single bead fluorescence spectroscopy.	57
Figure 3-1: Comparison of XPS survey spectra of four different samples.	69
Figure 3-2: Comparison of S(2p) high resolution XPS spectra.	70
Figure 3-3: Comparison of Zn(2p) high resolution XPS spectra of quantum dots immobilised with or without using MPTS.	72
Figure 3-4: Comparison of Cd(3d) high resolution XPS spectra of quantum dots immobilised with or without using MPTS.	72
Figure 3-5: Layer-by-layer assemblies of CdSe/ZnS quantum dots (QD ₆₂₆) onto glass substrate.	73
Figure 3-6: Layer-by-layer assemblies of QD ₆₂₆ and QD ₅₅₅ onto glass substrates.	74
Figure 3-7: Single bead fluorescence spectra of barcode •-QD ₆₂₆ (left) and barcode •-QD ₆₂₆ QD ₅₅₅ (right). A weak QD ₆₂₆ signal appeared in the barcode •-QD ₆₂₆ QD ₅₅₅ .	76
Figure 3-8: Single bead fluorescence spectra (left) and fluorescence micrograph (right) of barcode •-QD ₆₂₆ QD ₅₅₅ .	77
Figure 3-9: N(1s) high resolution XPS spectra of aminosilane film on the glass substrate.	79
Figure 3-10: Comparison of XPS survey spectra of four different samples.	80

Figure 3-11: Comparison of Cd(3d) high resolution XPS spectra of quantum dots immobilised with or without using biotin-streptavidin interaction. —————	82
Figure 3-12: Layer-by-layer assemblies of quantum dot-streptavidin 655nm (S_{655}) and quantum dot-biotin 655 (B_{655}) conjugates onto glass substrate. —————	83
Figure 3-13: Layer-by-layer assemblies of quantum dot-streptavidin 525nm (S_{525}) and quantum dot-biotin 655 (B_{655}) conjugates onto glass substrate. —————	84
Figure 4-1: Characterisation of barcodes prepared by layer-by-layer assembly of QD_{605} -biotin, QD_{605} -streptavidin and QD_{655} -streptavidin. —————	90
Figure 4-2: Single bead fluorescence emission spectra of barcode \bullet - $B_{605}S_{655}$ and \bullet - $S_{605}S_{655}$ shown in red and blue, respectively. —————	91
Figure 4-3: Batch to batch difference in the preparation of barcodes. —————	92
Figure 4-4: Fluorescence spectra after immobilisation of QD_{655} ITK TM -streptavidin (S_{655}^*) quantum dot conjugate on magnetic bead having QD_{605} -biotin quantum dot conjugate (\bullet - B_{605}). —————	93
Figure 4-5: Fluorescence micrographs of barcode \bullet - $B_{605}S_{655}$ and \bullet - $B_{605}S_{655}$ -fluorescein beads in the absence (top) and presence (bottom) of green band pass filter (500 nm-550 nm). —————	95
Figure 4-6: Fluorescence microscopy image of barcodes \bullet - $B_{605}S_{655}(B_{605}S_{605})_1$ and \bullet - $B_{605}S_{655}$ -fluorescein beads in the absence (top) and presence (bottom) of a green band pass filter. —————	96
Figure 4-7: Heat treatment of barcode \bullet - $B_{605}S_{655}(B_{605}S_{605})_1$. Barcoded beads were heated and maintained at 95°C for 15min in PBS containing 0.15% BSA. Single bead fluorescence spectra were taken before and after the treatment. —————	97

- Figure 4-8: Statistical distribution of (QD₆₀₅ to QD₆₅₅) fluorescence intensity ratio of barcode ●-B₆₅₅S₆₀₅(B₆₀₅S₆₀₅)₁ incubated for 1400min at different concentrations of biotin (0-100mM). Data collected from 100 beads for each concentration. ————— 99
- Figure 4-9: Statistical distribution of QD₆₀₅ to QD₆₅₅ fluorescence intensity ratio of barcode ●-B₆₅₅S₆₀₅(B₆₀₅S₆₀₅)₁ incubated in 100mM biotin solution at 37°C for different time intervals. ————— 100
- Figure 4-10: Long term stability of barcode ●-B₆₀₅S₆₅₅(B₆₀₅S₆₀₅)₁. Single bead fluorescence spectra were measured before (red) and after the storage of the barcode at 4°C for two months (blue). ————— 102
- Figure 5-1: Single bead fluorescence spectra of four different barcodes prepared using layer-by-layer assembly of quantum dot biotin (QD₆₀₅-biotin) and quantum dot streptavidin (QD₆₅₅, QD₆₀₅ and QD₅₆₅) conjugates on a streptavidin coated magnetic bead (●-). ————— 107
- Figure 5-2: Single bead fluorescence spectra of four different barcodes measured before and after performing multiplexed immunoassay. ————— 109
- Figure 5-3: Multiplexed immunoassay using four different IgGs immobilised on four different barcodes. ————— 110
- Figure 5-4: Multiplexed immunoassay using four different IgGs immobilised on four different barcodes. ————— 111
- Figure 5-5: Control experiment showing the single bead spectra of the barcode ●-B₆₀₅S₅₆₅ before and after incubation in a cocktail of four different FITC-labelled anti-IgGs. The shoulder peak around 530 nm did not appear after incubation of the barcode in the FITC-labelled anti-IgGs. ————— 112
- Figure 5-6: Shows fluorescence micrographs of barcodes ●-B₆₀₅S₆₅₅ and ●-B₆₀₅S₆₅₅(B₆₀₅S₆₀₅)₁ containing rabbit IgG and human IgG, respectively after the addition of FITC-

labelled anti-rabbit IgG in the absence (left) and presence (right) of a green band pass filter (500 nm-550 nm). 113

Figure 5-7: Optimisation of FITC labelled anti-human IgG concentration for performing binding inhibition immunoassay for human IgG using the barcode ●-B₆₀₅S₆₅₅. -115

Figure 5-8: Shows the binding inhibition immunoassay using the barcode ●-B₆₀₅S₆₅₅ for the determination of different concentrations of human IgG. 116

List of Schemes

Scheme 2-1: Schematic layout of the steps followed for the preparation of quantum dots 626nm(QD₆₂₆) layer-by-layer assembly onto the glass substrate. For the preparation of mixed multilayers of quantum dots, QD₆₂₆ and QD₅₅₅ were immobilised in an alternate fashion. Figures are not to scale. 49

Scheme 2-2: Shows the multilayer assembly of QD₆₂₆ and QD₅₅₅ using layer-by-layer assembly onto magnetic bead. A dithiol linker (1,9-nonanedithiol) was used to prepare multilayer assemblies. Figures are not to scale. 50

Scheme 2-3: Schematic representation of immobilisation of QD₅₂₅-streptavidin (S₅₂₅) conjugate and QD₆₅₅-biotin conjugate (B₆₅₅) using layer-by-layer biological self-assembly. Figures are not to scale. 52

Scheme 2-4: Barcode production using biological self-assembly of quantum dot-biotin and quantum dot-streptavidin conjugates. 54, 88

Scheme 2-5: Immunoassay scheme for a single rabbit IgG-anti-rabbit IgG pair and multiplexed immunoassay scheme showing rabbit IgG (red), human IgG (blue), mouse IgG (pink) and goat IgG (green) immobilised on barcoded beads. 62, 106

Scheme 2-6: Binding inhibition immunoassay of human IgG. 64, 114

Acknowledgment

I am thankful to Almighty Allah, whose grace and mercy enabled me to accomplish this piece of work. All respect for the Holy Prophet Muhammad (Peace Be Upon Him), whose teachings are an asset of my life.

I would like to express my gratitude to Prof. Jon Cooper for giving me opportunity to accomplish this research work. His kindness, guidance and support are greatly appreciated. I would also like to pay thanks to Dr. Andrew Glidle for his guidance, productive discussions and suggestions throughout my research work. I would like to thank all my lab fellows and friends for their cooperation and nice company. I am thankful to Research Councils, UK for the award of Dorothy Hodgkin's Postgraduate Award (DHPA) for my PhD studies.

Thanks to my parents for their prayers and support during my studies. I want to express my deepest gratitude to my wife, Amber, for her cooperation, moral support and motivation. Thanks to my brothers and sister for their prayers and support.

Author's Declaration

The work presented in this thesis was conducted by me and has not previously been submitted for a degree or diploma at this University or any other institution.

Sakandar Rauf

Chapter 1

Introduction and Review of Literature

In this chapter, a brief introduction to biosensing technologies is presented and different methods for producing barcodes are described. In this context, barcode production is divided into different categories namely: lithographic approaches for barcode fabrication; microfluidic production of barcodes; graphical encoding; encoding based on Raman and Infrared signatures; physical encoding; chemical encoding; barcoded fluorescent beads. An overview of each category is presented. A section detailing biosensing applications of barcodes is also described. At the end of the chapter, the concept behind the studies presented in this thesis is introduced.

1.1. Introduction

The convergence of materials science and biology has emerged as a new and exciting field of research known as nanobiotechnology which has resulted in the development of novel analytical tools with promising applications in the environment, health and industrial sectors.^(1, 2) To meet the growing challenges of healthcare in this era of nanotechnology, the demands of biological sensing have continually increased over the last two decades. The treatment of many health symptoms often requires an accurate, reliable and faster diagnosis. Biosensors can be used for the detection and quantification

of many different biological target analytes, such as DNA, RNA, immunoglobulins and many other molecules of interest related to different diseases.

A biosensor consists of biological sensing elements such as enzymes, DNA, antibodies, cells and tissues, immobilised or retained on a sensor or transducer surface.⁽³⁾
⁴⁾ Biosensors can be classified depending on the nature of the biological sensing elements and type of the transducer. Several books and review articles can be found on this topic covering a range of different types of biosensors and their applications.⁽⁴⁻¹⁰⁾

1.2. Biosensors

As mentioned above biosensors comprise two parts i.e biological sensing element and sensor or a transducer. Following is a brief introduction to some of the biological sensing elements and transduction techniques.

1.2.1. Biological Sensing Elements

The biological sensing element can be classified into five major categories, namely DNA, antibodies or antigens, enzymes, cells and biomimetic materials.⁽³⁾ The specificity and selectivity of the biological sensing element plays a key role in the development of a biosensor: for example biosensors used for the determination of DNA hybridisation utilise highly specific single stranded probe DNA immobilised on the sensor to detect a particular DNA sequence. This information which arises due to the precise nature of Watson-Crick bonding, could be used for the detection of tumours, genetic disorders, pathogenic bacteria and viruses.⁽¹¹⁾

Biosensors produced by using enzymes as the biological sensing element are based on the catalytic reaction in the presence of a particular substrate. For example in the case of a glucose biosensor, glucose oxidase (an enzyme) is immobilised on the transducer and in the presence of oxygen catalyses the conversion of D-glucose into D-gluconic acid and hydrogen peroxide which can then be determined using different strategies.⁽¹²⁾ Different enzymes have been used as a biological sensing element to produce biosensors for the determination of glucose,⁽¹³⁻¹⁶⁾ ascorbic acid,^(17, 18) cholesterol,^(19, 20) choline,⁽²¹⁾ ethanol,⁽²²⁾ , for example.

Antibodies or antigens also are used as the biosensing element because of their capability to bind to a specific structure. An antibody or immunoglobulin binds to its antigen in a lock and key (or “hand in glove”) mechanism.⁽³⁾ When an organism is exposed to a foreign antigen, B cells produce immunoglobulins in response to the antigen. Immunoglobulins have unique antigen binding sites that recognise the antigen.⁽²³⁾ Immunoglobulins can be divided into five major types IgM, IgG, IgA, IgE and IgD.⁽²⁴⁾ Each of these immunoglobulins has different characteristics, which helps the immune system to response against different antigens in different conditions throughout the body.⁽²⁴⁾

Immunoglobulins or antibodies have a Y shaped structure, which consists of two main structural regions namely, the variable region or antigen binding site and the Fc region. The variable region or antigen-binding region specifically binds with an epitope on an antigen and the Fc portion is responsible for the clearance of antigen from the body and to promote immune response.⁽²⁵⁾ **Figure 1-1** shows the structure of Immunoglobulins (variable region and Fc region), which consists of two identical light chains and two heavy chains held together by disulphide bonds.⁽²⁶⁾ Enzymatic cleavage of IgG with papain yields two Fab and one Fc fragments by breaking at hinge region.^(25, 27)

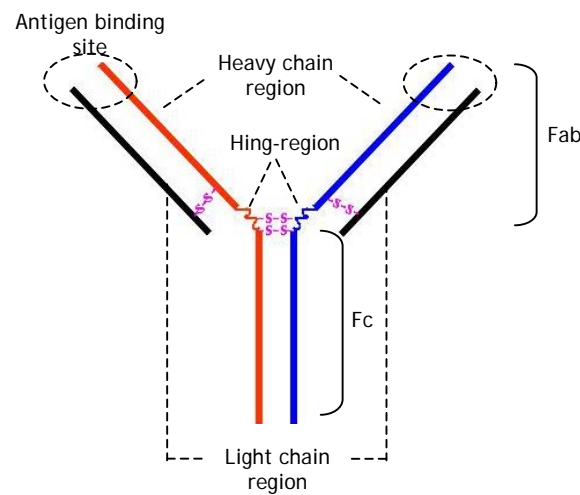


Figure 1-1: Schematic of an Immunoglobulin. -S-S- shows disulphide bridge.

Antibodies or immunoglobulins can either be monoclonal or polyclonal in nature depending on the method of production. "A monoclonal antibody is defined as a uniform homogeneous antibody directed at a single epitope or antigenic determinant and produced continuously from one cell clone"⁽²⁸⁾ whereas polyclonal antibodies are produced by immunisation across animal species or within species.^(25, 27, 28) Polyclonal antibodies have certain disadvantages when used in assays like batch-to-batch variation in the specificity and reactivity, variation in specificity and reactivity among antibodies within an antiserum.⁽²⁸⁾ Different immunosensors have been developed using Immunoglobulins or antibodies due to their specific affinity for antigens.⁽²⁹⁻³¹⁾

1.2.2. Transduction Techniques

A transducer or sensor translates the biological event as a result of the interaction of biological sensing element with the analyte into a measurable signal. There are many types of sensors which include electrochemical, optical and piezoelectric, for example.⁽³⁾ However, in this section only electrochemical and optical transducers are discussed briefly.

Electrochemical transducers convert the biological recognition event into a useful electrical signal.⁽³²⁾ Commonly used electrochemical transducers are amperometric and potentiometric sensors. Amperometric transducers are based on the application of a constant potential and "monitoring the current associated with the reduction or oxidation of an electroactive species involved in the biological recognition process".⁽³²⁾ In contrast, in the case of potentiometric transducers, the change in potential is used as the measure of the occurrence of events due to the biological sensing element-analyte interaction.⁽³²⁾ Electrochemical transducers have been used for applications in enzyme based biosensors,⁽³³⁾ DNA hybridisation,^(34, 35) DNA damage detection⁽³⁶⁾ and immunoassays.^(37, 38)

Optical transduction technologies rely on the measurement of photons or photonic interactions rather than electrons as in the case of electrochemical transducers.⁽³⁹⁾ More common optical transduction methods are based on absorbance, reflectance, fluorescence, infrared and Raman.⁽³⁹⁾ Optical transduction using fluorescence has gained most attention due to its high specificity and sensitivity in the detection of different target molecules.⁽⁴⁰⁾ In the context of this thesis fluorescence is discussed in detail.

The fluorescence of a molecule is the light emitted spontaneously due to transitions from excited singlet states (usually S_1) to various vibration levels of the electronic ground state, i.e. ($S_{1,0}$ to $S_{0,v}$)⁽⁴¹⁾ as shown in Figure 1-2. Fluorescence can be characterised using fluorescence intensity at a given wavelength i.e emission spectrum, quantum yield, lifetime and polarisation.⁽⁴¹⁾ A fluorescence emission spectrum is a plot of fluorescence intensity versus wavelength (nanometers) or wavenumber (cm^{-1}).⁽⁴²⁾

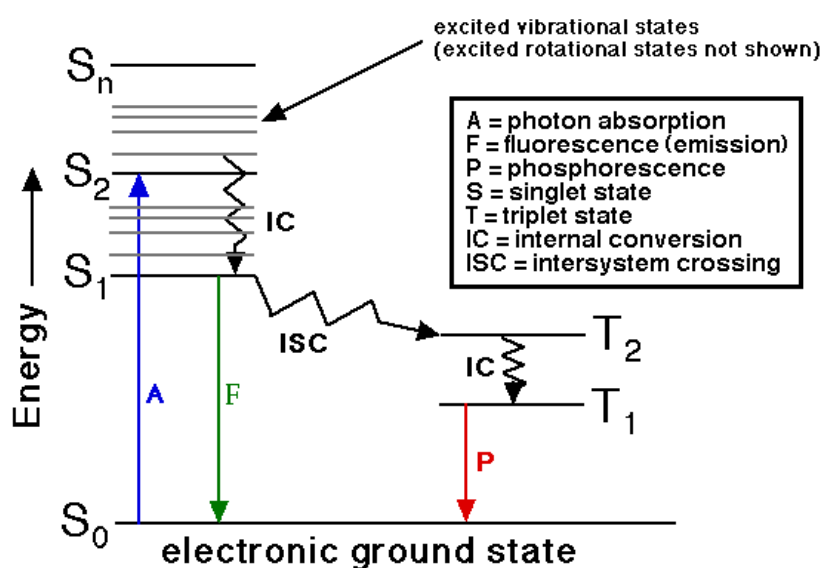


Figure 1-2: Jablonski diagram showing the mechanism for fluorescence emission, taken from (43). Reproduced with permission. Copyright © 1996 by Dr. Thomas G. Chasteen.

Fluorescence typically occurs from aromatic molecules usually called fluorophores or fluorescent dyes. Different fluorescent dyes have been used in different biosensor formats for biological applications.^(22, 44, 45) However, in addition to the organic fluorophores or fluorescent dyes, semiconductor nanocrystals called quantum dots also exhibit fluorescent properties that have been used in many applications.^(46, 47)

1.2.3. Quantum Dots

Quantum dots are highly luminescent and monodisperse nanocrystals (CdSe/ZnS or CdTe, for example) that are currently of great interest especially due to their use as labels in bioanalytical applications.⁽⁴⁸⁾ Quantum dots are often composed of atoms from group II-VI or III-V elements in the periodic table, and are defined as particles with physical dimensions smaller than the exciton Bohr radius.⁽⁴⁹⁾

Quantum dots offer good photostability, high fluorescence intensity and broad tunability that make these an excellent choice as a chromophore.⁽⁵⁰⁾ Different methods of synthesis of quantum dot nanocrystals have been reported but the formation of quantum dots in colloidal form via solution chemistry is an easy and successful route to realise quantum dots.⁽⁵¹⁻⁵⁵⁾ Quantum dot emission wavelengths are dependent on the size of the quantum dots.^(55, 56) Different sizes of quantum dot nanocrystals give a different spectral response. Figure 1-3 shows the dependence of emission spectra with the size of the quantum dots and biomolecules functionalised CdSe/ZnS quantum dot.

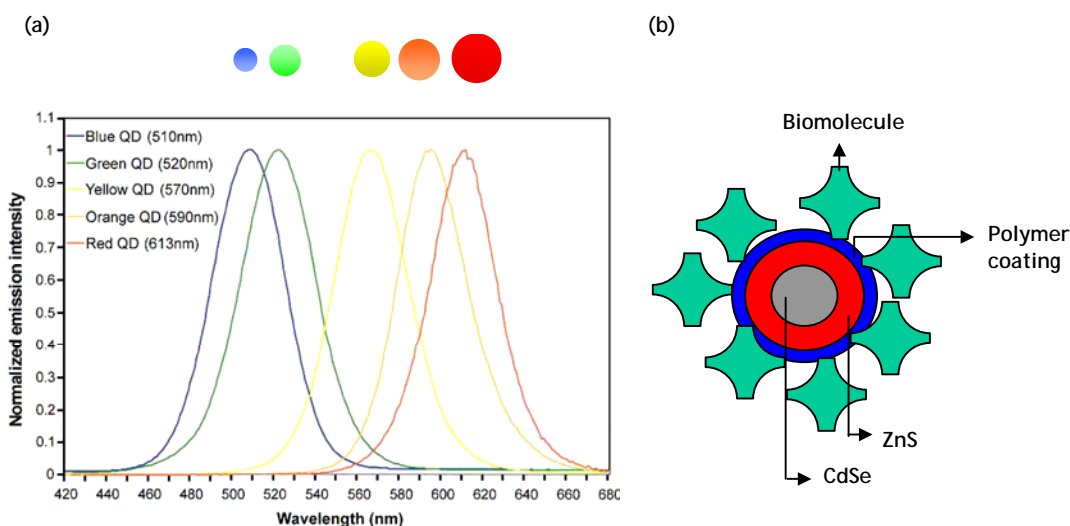


Figure 1-3: (a) Shows emission spectra of different quantum dots, taken from (57); (b) Biomolecules conjugated quantum dot (not to scale), reproduced from (58).

The surface properties of the quantum dots can be easily manipulated by the addition or removal of organic functional groups during a chemical synthesis without altering the intrinsic optical properties.⁽⁵⁹⁾ Quantum dots functionalised with different biomolecules (streptavidin, biotin, oligonucleotides or peptides, for example) have been used as fluorescent labels in many applications. Examples include immunoassays and DNA assays.⁽⁶⁰⁻⁶²⁾

1.3. Barcode Technology for Biological Sensing

Particular to the biological detection, a large number of materials and assays have been developed to detect and quantify different biomolecules including for example antigens, antibodies, and nucleic acid sequences related to different diseases. The detection of these biomolecules may require the measurement of more than one analyte at the same time, in a sample. This need has led to the development of multiplexed assays to detect biomolecules.

Microarray technologies, including those associated with proteins, RNA and DNA are the most popular approaches for analysing hundreds of targets in parallel.⁽⁶³⁾ However, the development of barcoded beads or lithographically encoded particles has opened up new possibilities for multiplexing analysis of biomolecules. This technology has the potential to replace microarray technology by overcoming some of their limitations. For example, in optical microarray technology, a large number of different biomolecular binding events can be identified from their characteristic response and their position on a two-dimensional grid, a technology that has become synonymous with high density screening.⁽⁶⁴⁾ A variety of methods have been proposed for such assays, including the use of fluorescent dyes and quantum dots. The very nature of the microarray, however, often results in relatively slow reaction events; as a consequence, the geometry of the chip and mass transfer limit transduction at a solid surface, **Figure 1-4a**.

In contrast, tags based upon either micrometer- and nanometer-dimensioned encoded particles, known as *barcodes*, provide a technique that can perform many hundreds of individual tests in parallel, in solution⁽⁶⁵⁾, without the need for a knowledge of their spatial position on a chip, **Figure 1-4b**. These barcodes may benefit from better solution kinetics, high surface to volume ratios, as well as robust assay modification and development of high throughput screening methods.⁽⁶⁶⁾

Current techniques used to fabricate such barcodes range from using elegant solution chemistries to assemble fluorescent dyes or quantum dots, to the application of highly sophisticated and relatively expensive lithographic techniques to make patterned structures (e.g. using UV or electron beam lithography).⁽⁶⁷⁾ Depending upon the basis of the encoding strategy used, barcodes have generally been created with an optical signal transduction technique, as the assay can be read out in parallel. Current techniques may include fluorescence, Surface Enhanced (Resonance) Raman Scattering, SE(R)RS, scattering or reflectivity.

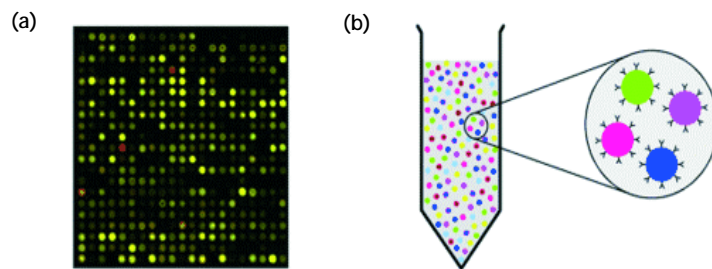


Figure 1-4: (a) Shows a microarray platform, which uses positional encoding for multiplexed analysis; (b) Barcoded beads labelled with different recognition molecules (antibodies, DNA or RNA sequence), taken from (63). Copyright Wiley-VCH verlag GmbH & Co. KGaA. Reproduced with permission.

A number of different strategies have been used for the production of barcodes. Broadly these can be classified as lithographic and different non-lithographic strategies. As stated, most of the barcodes produced involve optical methods as detection technique.

1.3.1. Lithographic Approaches for Barcode Fabrication

Encoded microparticles have been fabricated using a combination of different techniques that include “photolithography, lift-off, electroplating-through-mask, metal thermal evaporation, and wet etching processes.”⁽⁶⁸⁾ **Figure 1-5** shows the sequence of steps used to fabricate the encoded microparticles. Here, the thickness (~2 μ m) of the particles was controlled by the current density and duration of electrodeposition.

The coding pattern and dimensions ($100 \times 200 \mu\text{m}$) of the particles in **Figure 1-5** were defined by a photomask. A pattern of 1-10 dots was used as the coding element and two dots were fixed at the starting and ending points in order to define the coding area.⁽⁶⁵⁾ The authors reported that this coding scheme has the potential for $2^8 = 254$ types of particles. The level of multiplexing could be increased exponentially by increasing the number of dots and their arrangement in the pattern. These encoded microparticles were used to register and identify the biomolecules attached to the barcode surface.^(65, 68)

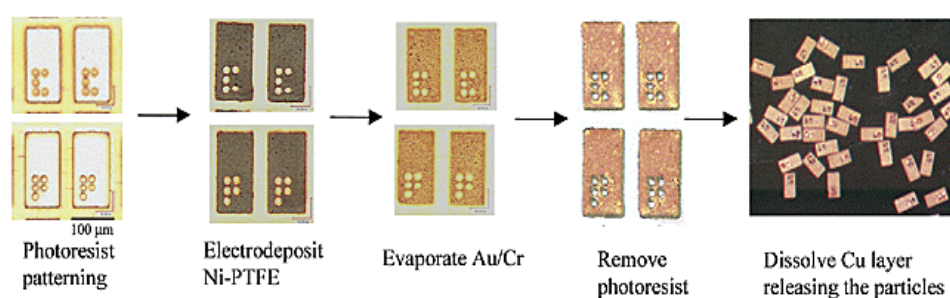


Figure 1-5: Shows the sequence of steps for the fabrication of encoded microparticles. "SU-8 photoresist was first photolithographically patterned as the particle template on a Cu-coated glass substrate; Ni-PTFE (electroplating solution containing nickel sulfamate and fine polytetrafluoroethylene particles) layers ($\sim 6 \mu\text{m}$ thick) were electrodeposited on the open areas of the photoresist-patterned microwells. After evaporation of Cr (20 nm) and Au (300 nm) from the whole chip surface, metallised SU-8 photoresist was lift-off using SU-8 remover. Finally, the particles were released from the underlying substrate by dissolution of the Cu sacrificial layer." Reprinted With permission from (68). Copyright © 2003 American Chemical Society.

Using a different approach, micron-scale freestanding porous silicon photonic crystal particles containing spectral barcodes have been fabricated by using standard photolithographic process and electropolishing.⁽⁶⁹⁾ "An electrochemically prepared film of porous silicon on a crystalline silicon substrate was patterned with an SU8-25 photoresist."⁽⁶⁹⁾ The mask used was a square array of circles, each $25\mu\text{m}$ in diameter with a pitch of $35\mu\text{m}$ and the unmasked porous silicon was removed with reactive ion etching

process. Electropolishing was used to remove the porous microparticles formed.

Figure 1-6 shows the scheme used to fabricate these encoded microparticles along with the image and reflection spectra of a microparticle. The encoding capacity of this process was estimated to be $\sim 10^4$ microparticles from a 1.33 cm^2 wafer surface.⁽⁶⁹⁾

Silicon microbeads have also been fabricated by using standard microfabrication techniques that can be identified on the basis of their different optical signatures.⁽⁷⁰⁾ Although the barcodes were fabricated with distinctive optical signatures their dimensions were large ($1000 \mu\text{m} \times 500 \mu\text{m} \times 100 \mu\text{m}$).

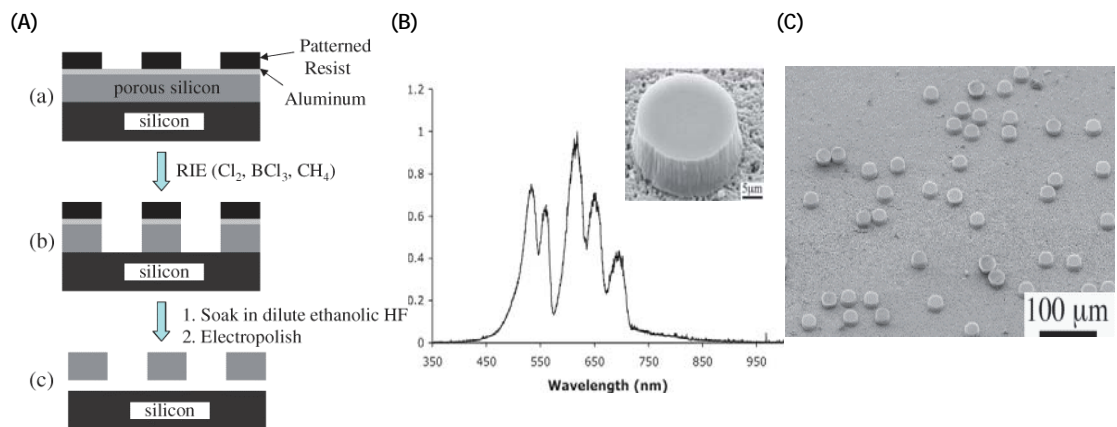


Figure 1-6: (A) Shows the process of preparing microparticles from a spectrally encoded porous silicon film, (a) first a photopattern was fabricated, (b) porous silicon was etched by using plasma etching and (c) finally photoresist was removed and particles were released; (B) Reflection spectrum of a single porous silicon microparticle; (C) SEM images of microfabricated porous silicon photonic crystal particles, taken from (69). Copyright Wiley-VCH verlag GmbH & Co. KGaA. Reproduced with permission.

Finally, Electron beam lithography and nanoimprint lithography have been used to fabricate barcoded beads of SU8 photoresist.^(71, 72) These barcodes are based on different

grating structures created on an SU8 surface that allow distinguishing via diffraction properties. Figure 1-7 shows an array of nanoimprinted SU8 microbarcodes. In this case, SU8 bars were pre-fabricated using a standard lithography protocol and electron beam lithography or nanoimprint lithography were used afterwards to make grating structures in the SU8 bars.^(71, 72) It was estimated that approximately 10^9 barcodes could be produced on a 50 μm long barcodes.⁽⁷¹⁾

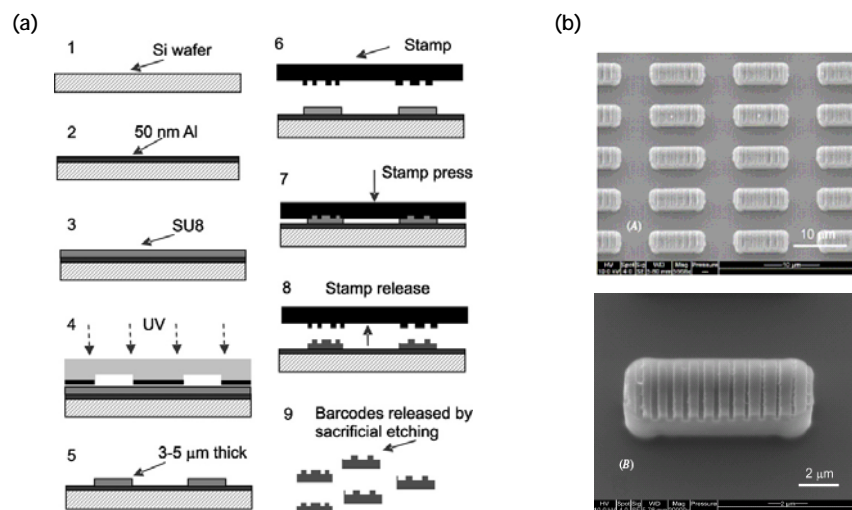


Figure 1-7: (a) “Schematic of the process for manufacturing nano-embossed SU8 microbars. An Al sacrificial layer and a layer of SU8 are spun onto a Si wafer (1-3). The SU8 is illuminated with UV light through a mask to cross-link the SU8, and uncross-linked SU8 washed away to leave the microbars (4 and 5). The nano-embossing stamp is pressed into the SU8 to pattern it (6 and 7), with baking during step 7. Finally the patterned bars are released (8) by etching away the Al layer”⁽⁷²⁾; (b) SEM images of barcode tags prepared by nanoimprint lithography, taken from⁽⁷²⁾. Copyright ICP Publishing Ltd. Reproduced with permission.

1.3.2. Microfluidic Production of Barcodes

Continuous flow lithography approaches have also been used to fabricate encoded particles.⁽⁷³⁾ These approaches involved adjacent flow of two monomers through a

microfluidic channel (Figure 1-8). In the experiment, one monomer was loaded with a dye and the second monomer was an acrylate modified probe. The continuous-flow lithography technique was used to polymerise these monomers as they passed through the channel. The advantage of this approach is that the morphology and chemistry of each particle can be controlled both by using a photomask and by changing the composition of the flowing monomer streams, respectively. The encoding capacity for these barcodes was reported over a million (2^{20}) codes.⁽⁷³⁾

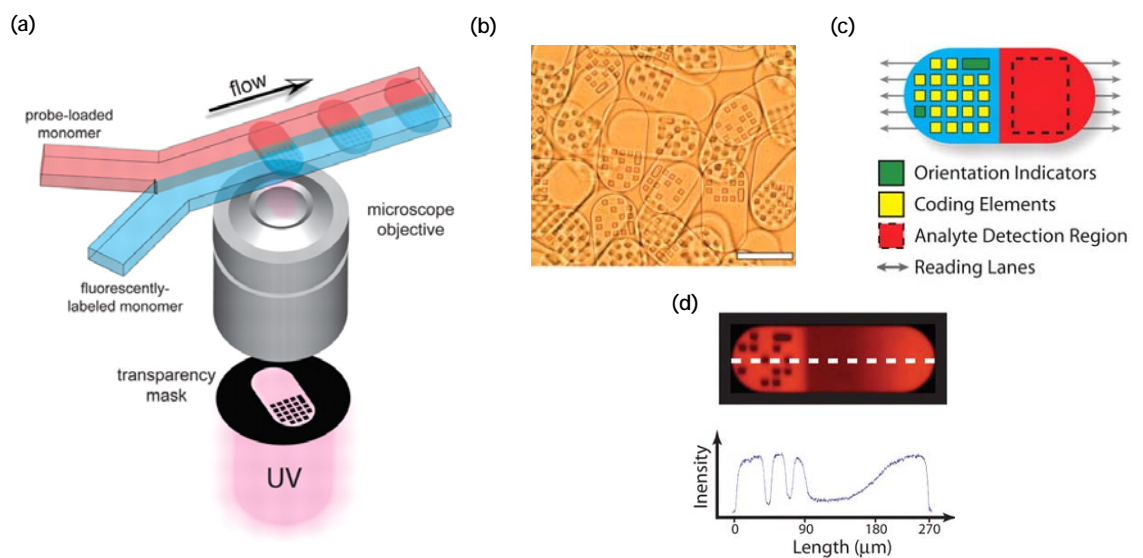


Figure 1-8: (a) Shows the schematic diagram for the preparation of dot-coded particles; (b) Microscopic image of the particles prepared in scheme a. Scale bar is $100\mu\text{m}$; (c) Diagram shows different regions of the dot-coded particle; (d) Fluorescence intensity measured on a dot-coded particle, taken from (73). Reprinted with permission from AAAS.

Photonic crystal hydrogel beads have been prepared by generating droplets of monodisperse silica nanoparticles in poly (ethylene glycol) diacrylates (PEG-DA) using a microfluidic device.⁽⁷⁴⁾ These droplets were then irradiated with UV-light to polymerise the hydrogel. The silica nanoparticles were trapped in the hydrogel network and give photonic crystal features, which have different optical reflectivities (Figure 1-9).

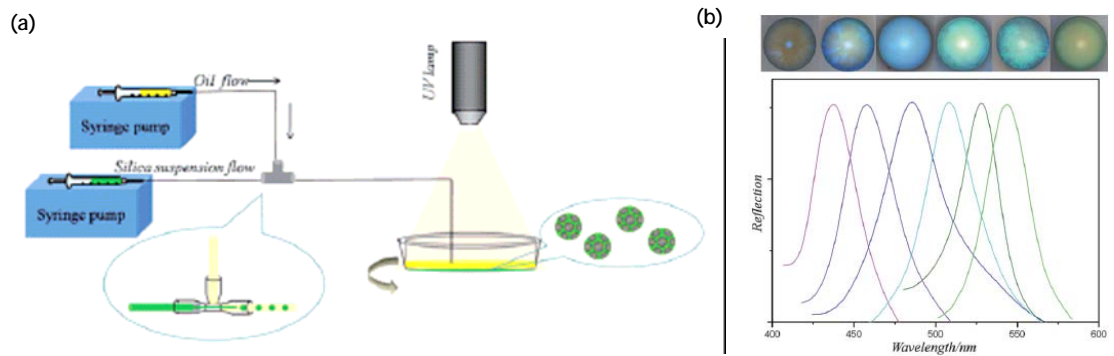


Figure 1-9: (a) shows the set-up for the production of photonic crystals using a microfluidic device; (b) The reflection spectra of different photonic crystal hydrogel beads, taken from (74). Reproduced by permission of The Royal Society of Chemistry.

The barcodes prepared using lithographic and microfluidic techniques have high encoding capacity. However, the size of the barcode produced is large, typically 50-200 μm . Moreover, the applications of these barcodes for a multiplexed bioassay require multiple separation and washing steps. Often this is done by centrifugation of the barcodes prepared using lithographic and microfluidic approaches, however magnetic separation can be a more convenient and faster method.

1.3.3. Graphical Encoding

Graphical encoding relies on the physical properties of the barcoding element.⁽⁶³⁾ For example, glass barcodes containing patterns of different fluorescent materials have been fabricated in micrometer dimensions. These materials can be identified by using their unique fluorescent signatures when excited with a UV lamp.⁽⁷⁵⁾ RE (Rare earth)-doped alkaline earth aluminosilicate glass compositions for a particular colour were mixed, and optimal doping levels were obtained by maximising the relative fluorescence intensity as a function of the RE (RE_2O_3) concentration. This product was drawn out into a ribbon fiber (20 μm thick, 100 μm wide), which was cut into 20 μm sections at a rate of 5 mms^{-1} with 800-nm femtosecond laser pulses (100mW average power) on a computer-controlled stage^(63, 75) (Figure 1-10).

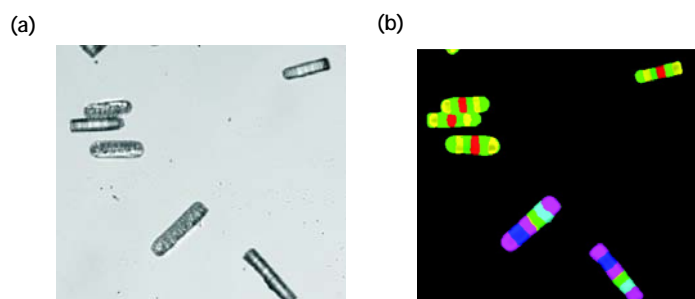


Figure 1-10: (a) White light image of micron size glass rods encoded with different fluorescent rare-earth ions; (b) Fluorescence image of (a) when excited with UV-light and using a 420 nm long pass filter, taken from (75). Copyright (2003) National Academy of Sciences, U.S.A.

In another method different metals (Pt, Pd, Ni, Co, Ag, Cu, and Au) were incorporated as segments of a micro- or nanorod like structure by sequential electrochemical deposition of metal ions into uniformly sized pores using Al_2O_3 membrane as a template⁽⁷⁶⁾ (Figure 1-11). Optical microscopy was used to identify the striped patterns based upon the metal's reflectivity. Protein and DNA bioassays performed using these barcodes showed that the readout mechanism did not interfere with the analyte detection using fluorescence.⁽⁷⁶⁾

1.3.4. Encoding Based on Raman and Infrared Signatures

Raman and Infrared (IR) spectroscopic signatures of different molecules have been utilised to produce barcodes. Su *et al.*,⁽⁷⁷⁾ "prepared a new type of barcodes called composite organic-inorganic nanoparticles (COINs). The method allows the incorporation of a broad range of organic compounds into COINs to produce a large number of surface enhanced Raman scattering (SERS)-like signatures,"⁽⁷⁷⁾ as shown in Figure 1-12.

Fenniri *et al.*,⁽⁷⁸⁾ synthesised different barcode resins that have infrared (IR) and Raman spectroscopic signatures using different styrene derivatives. Only 24 unique codes were reported using the unique vibrational signatures of all the six derivatives.

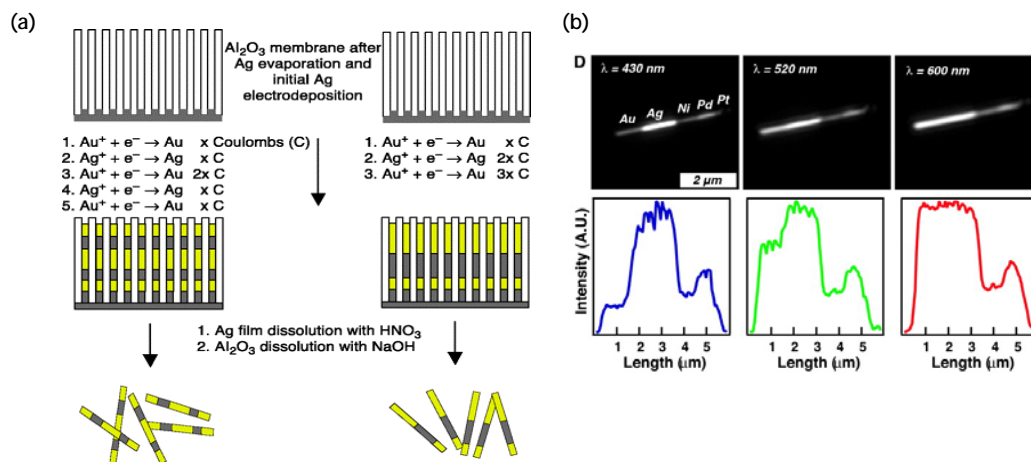


Figure 1-11: (a) Synthesis of barcode particles; (b) Reflectance optical microscopy images and line profiles for a particle of composition Au-Ag-Ni-Pd-Pt with illumination at 430 nm, 520 nm, and 600 nm, respectively, taken from (76). Reprinted with permission from AAAS.

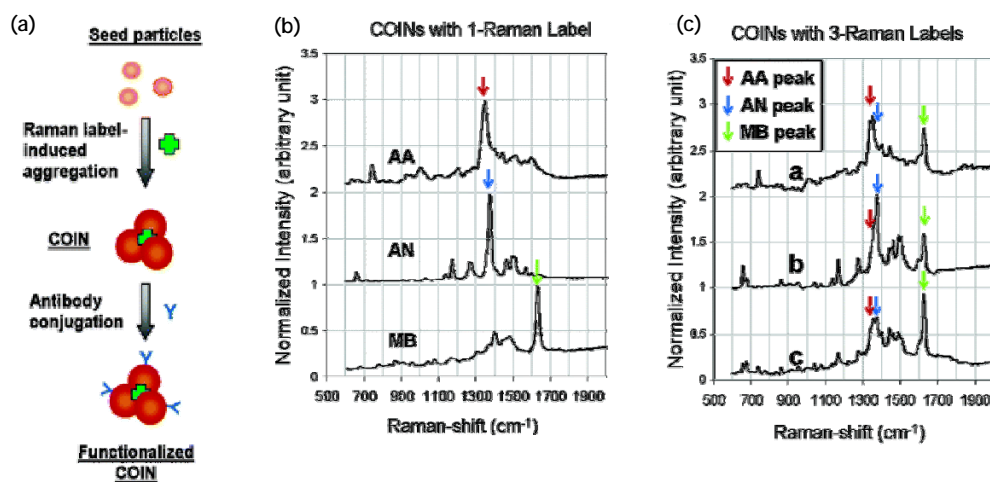


Figure 1-12: (a) Scheme showing aggregation of seeded silver nanoparticles and raman labels in silver nitrate solution to produce coins; (b) and (c) Shows coins prepared by using single raman dye label and multiple labels in one coin. Where AA= 8-azaadenine, AN=9-aminoacridine and MB= methylene blue. The arrows show representative peaks from three different dyes. Reprinted With permission from (77). Copyright © 2003 American Chemical Society.

1.3.5. Physical Encoding

Physical encoding relates to the shape and size of the barcodes that interact with light differently. A photo-induced method for converting silver nanospheres into triangular nanoprisms has been developed.⁽⁷⁹⁾ Figure 1-13 shows the change in UV-Vis spectra due to the change in shape and size of the particles.⁽⁷⁹⁾ This approach has been used to synthesize a distinct number of barcodes that can be identified in a multiplexing assay.

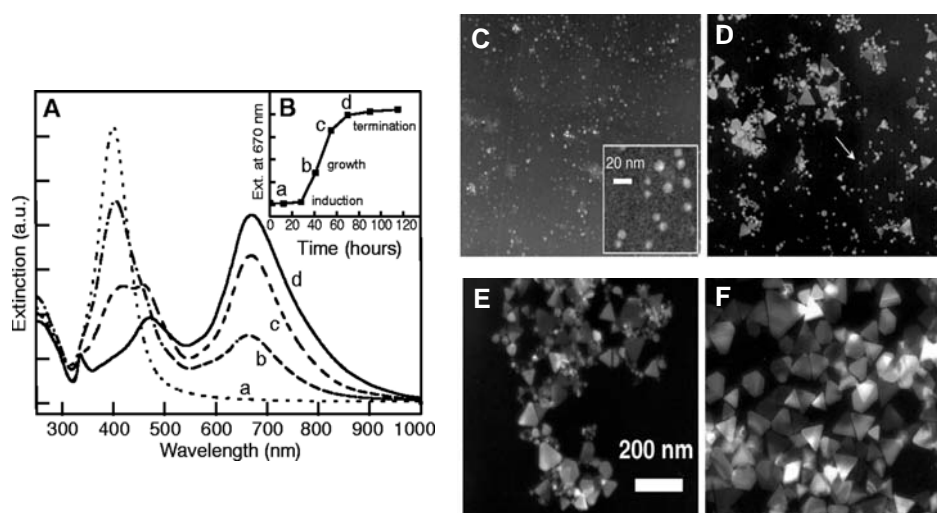


Figure 1-13: (A) "Time-dependent UV-Vis spectra showing the conversion of silver nanospheres to nanoprisms (a) before irradiation and after (b) 40, (c) 55, and (d) 70 hours of irradiation; (B) Corresponding extinction profiles at 670 nm as a function of time. TEM images mapping the morphology changes (C) before irradiation and after (D) 40; (E) 55; (F) 70 hours of irradiation. Except for the inset in (C), the scale bar is 200 nm for all four images," taken from (79). Reprinted with permission from AAAS.

1.3.6. Chemical Encoding

Quantum dot nanobarcode have been prepared by using quantum dot copolymer complexes. These complexes grow into nanobeads of narrow size distribution.⁽⁸⁰⁾ First, the quantum dots were precoated with poly(maleic anhydride-octadecene) (PMAO) via hydrophobic interaction. By increasing the solvent polarity, uniform quantum dot nanobeads were formed as shown in Figure 1-14.

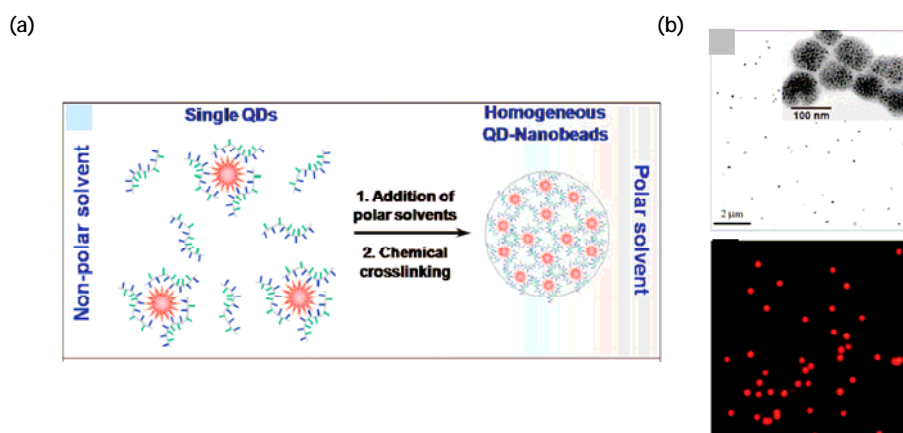


Figure 1-14: (a) Shows schematic of nanobeads formation; (b) TEM image of the nanobeads (upper) showing the size of the nanobeads 92 ± 13 nm and fluorescence image of the nanobeads (lower), Reprinted With permission from (80). Copyright © 2008 American Chemical Society.

Another oligonucleotide based barcoding technology has been developed which utilises colour coded oligonucleotide probe pairs as an encoding strategy. The technology named as “Nanostring technology” uses capture probe and reporter probe for multiplexing.⁽⁸¹⁾ The reporter probe contains different fluorescent dyes that encode a particular sequence, which results in barcoding of multiple sequences, Figure 1-15.

The barcode production strategies described above (Sections 1.3.3 to 1.3.6) have different advantages and disadvantages. For example, in case of graphical encoding, the size of the barcode is large ($20\mu\text{m}$) while the encoding speed is high. The barcodes

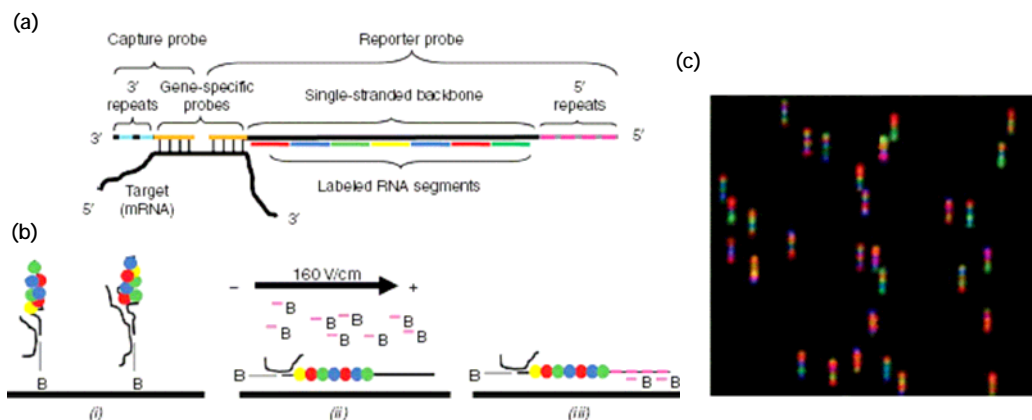


Figure 1-15: "Overview of NanoString nCounter gene expression system: (a) A schematic representation of the hybridised complex (not to scale). The capture probe and reporter probe hybridise to a complementary target mRNA in solution via the gene-specific sequences; (b) Schematic representation of (i) binding of purified complexes to a streptavidin-coated slide, (ii) electrophoresis, and (iii) immobilisation of reporters for imaging and counting; (c) False-colour image of immobilised reporter probes," taken from (81). Reprinted by permission from Macmillan Publishers Ltd.

produced using Raman and Infrared signatures, give a better control over identification of the barcodes. However, the barcoding capacity of these methods depends on the availability of number of different organic molecules that have distinct Raman or infrared signatures.

In the case of physical encoding methods, barcodes are produced on the basis of size and shape resulting in the limited number of barcodes that can be produced. Moreover, within one type of barcode, the variation in size and shape can influence the identification of the barcode. Encoding strategies based on quantum dot co-polymer complexes can be useful to produce nanobarcode, however, the lack of control over the size of the barcode and number of different quantum dots within one barcode results in higher variations. This influences the number of unique quantum dot barcodes that can be produced using this method. In case of oligonucleotide-based barcoding strategy, which relies on the use of different fluorescence dyes within one barcode. In order to identify

these barcodes, each fluorescent dye needs to be excited with a particular excitation wavelength within a barcode. This increases the measurement time and places more demands on the readout instrumentation. The encoding strategy based on the barcoded fluorescent beads offer a wide variety of methods for producing encoded beads and also have the potential of incorporating multiple functionalities such as magnetic bead based barcodes.

1.3.7. Barcoded Fluorescent Beads

The production of barcoded fluorescent beads can be classified into three different methods⁽⁸²⁾ namely: barcoded beads produced by the encapsulation of quantum dots or dyes into the beads; Incorporation of quantum dots during the synthesis of beads; and immobilisation of quantum dots or fluorescent dyes on the bead surface. In these methods, the beads act as carrier elements that host the quantum dots or fluorescent dyes and which act as the encoding element.

In the case of encapsulation, beads were first swelled in an organic solvent in the presence of encoding nanoparticles (e.g., quantum dots) or molecules (fluorescent dyes). Due to the swelling of the beads, nanochannels or nanopores were opened on the bead surface and allowed quantum dots or dye molecules to enter the pores. When these beads were placed in an aqueous solution, this closes the opened channels resulting in encapsulation of the quantum dots or dye molecules into the beads.⁽⁸³⁾ These beads provide an inert environment to the coding elements and prevent aggregation with their neighbours.^(83, 84)

In the second approach, quantum dots were first dispersed in the monomer solution and then initiator was added to form the beads encapsulated with quantum dots.⁽⁸⁵⁾ Thirdly, quantum dots or fluorescent dyes were immobilised on the bead surface.⁽⁸⁶⁾ The encoding elements used in these approaches consisted of fluorescent dyes, chromophores and quantum dots. By trapping different dyes or quantum dots onto a bead, distinctive spectral barcodes can be produced. The number of barcodes depended upon the number of dyes or quantum dots and "intensities according to the formula: $C = N^{m-1}$ (where C is the number of codes, N is the number of intensity levels and m is the number of colours)."⁽⁸⁴⁾

Quantum dots are superior to fluorescent dyes as an encoding element because of unique optical properties⁽⁴⁹⁾ and have several advantages over the fluorescent dyes. These advantages that they exhibit are: significantly less photobleaching as compared to fluorescent dyes; greater encoding capacity as a consequence of less spectral overlap between the symmetric and spectroscopically narrow fluorescence emission; excitation by a single, low wavelength excitation source which also gives a brighter signal placing less demand on detection equipment (Figure 1-16).^(73, 87)

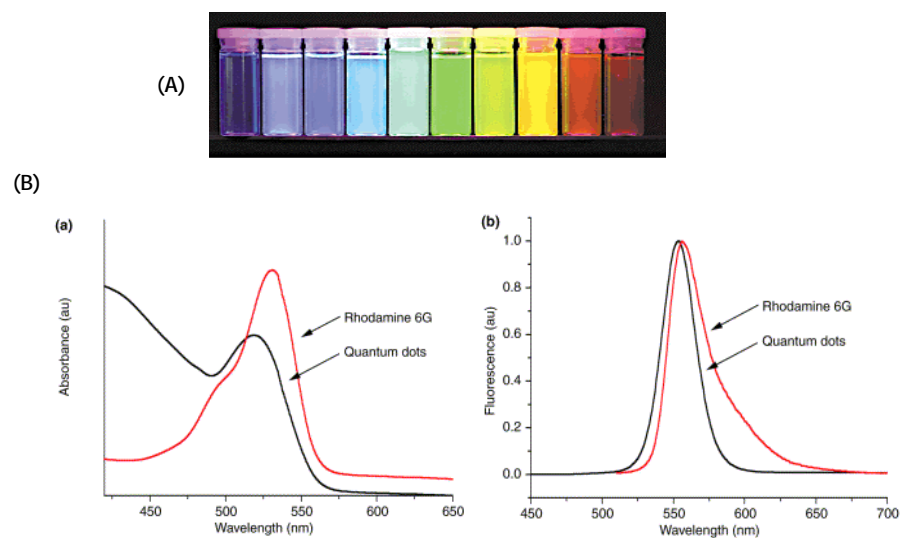


Figure 1-16: (A) Ten different coloured CdSe/ZnS quantum dots excited with a UV-lamp give different emission maxima (from left to right at 443, 473, 481, 500, 518, 543, 565, 587, 610, and 655 nm); (B) Comparison of (a) the excitation and (b) the emission profiles of rhodamine 6G (red) and CdSe/ZnS QDs (black), taken from⁽⁴⁹⁾. Reprinted with permission from Elsevier.

1.3.7.1. Encapsulation of Quantum Dots into the Beads

Based on the above advantages of the quantum dot nanocrystals, Han et al.,⁽⁸⁴⁾ developed barcodes using polystyrene beads as a 'cargo' and quantum dots as the encoding elements. Figure 1-17 represents the encoding principle to produce multicolour

encoded beads using quantum dots as encoding elements. The authors suggested that the number of codes can be increased exponentially by using multiple wavelengths and intensities of the encoding elements. For example, one million barcodes can be generated by using six colour and ten intensity levels. However, practical encoding capacity is lower because of spectral overlapping, optical intensity variations, and “signal-to-noise” requirements.⁽⁸⁴⁾

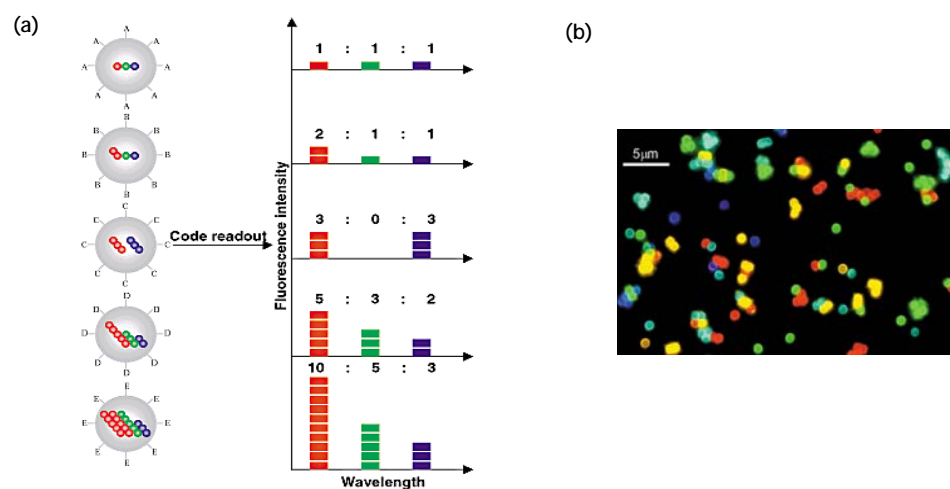


Figure 1-17: (a) Schematic diagram of optical coding based on wavelength and intensity multiplexing. On the left large spheres represent polystyrene beads embedded with quantum dots (small spheres); (b) Fluorescence micrograph showing a mixture of single colour encoded polystyrene beads, taken from (84). Reprinted by permission from Macmillan Publishers Ltd.

In another approach multicolour encoded microspheres were produced by incorporating CdTe nanocrystals with different sizes into N-isopropylacrylamide and 4-vinylpyridine co-polymer hydrogel spheres by utilising their stimuli responsive swelling properties.⁽⁸⁸⁾ This co-polymer swelled at pH 3 and took up the quantum dots. The hydrogel spheres shrunk at a higher pH to incorporate the quantum dots (Figure 1-18).

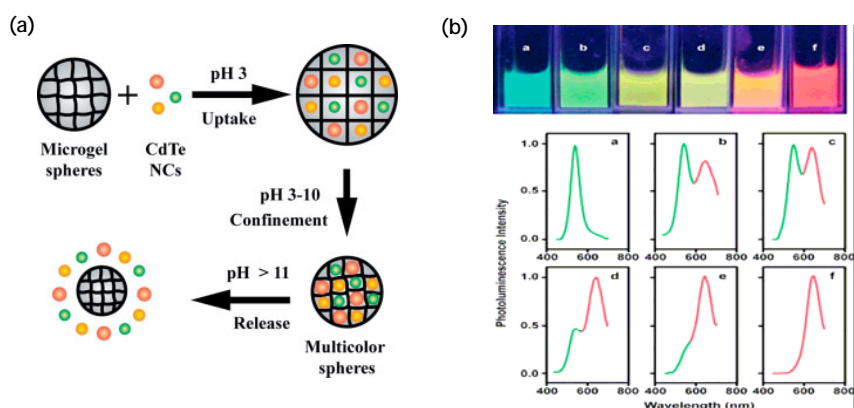


Figure 1-18: (a) Schematic illustration of quantum dot encapsulation; (b) Fluorescence images of hydrogel spheres and corresponding fluorescence spectra of the hydrogel spheres, taken from (88). Copyright Wiley-VCH verlag GmbH & Co. KGaA. Reproduced with permission.

Thiol (-SH) containing polystyrene beads have also been used to prepare barcodes by the incorporation of quantum dots through a swelling/doping strategy.⁽⁸⁹⁾ It was found that these barcodes were highly stable against leaching of quantum dots into different solvents due to the thiol-quantum dot interaction.⁽⁸⁹⁾ Mesoporous polystyrene beads were used to encapsulate quantum dots.⁽⁹⁰⁾ It was reported that the mesoporous beads were ~1000 times brighter than the same size non-porous beads of similar composition due to high loading and even distribution of quantum dots within the beads.⁽⁹⁰⁾

Quantum dots were encapsulated in the polymer matrix like poly(styrene-co-maleic anhydride) to prepare quantum dot barcodes. Quantum dots were mixed with poly(styrene-co-maleic anhydride) in the presence of chloroform to make a homogeneous suspension of the quantum dots.⁽⁹¹⁾ This solution was introduced into a nozzle system using a syringe pump along with water as a focusing fluid that intersect at the nozzle output, Figure 1-19. The polymer suspension was insoluble in water, which solidify the quantum dot polymer mixture into water making the barcodes.

Dual function bead based barcodes were produced by simultaneous or sequential incorporation of quantum dots and magnetic iron oxide nanoparticles into mesoporous silica, (Figure 1-20).⁽⁹²⁾ It was reported that the sequential and simultaneous doping

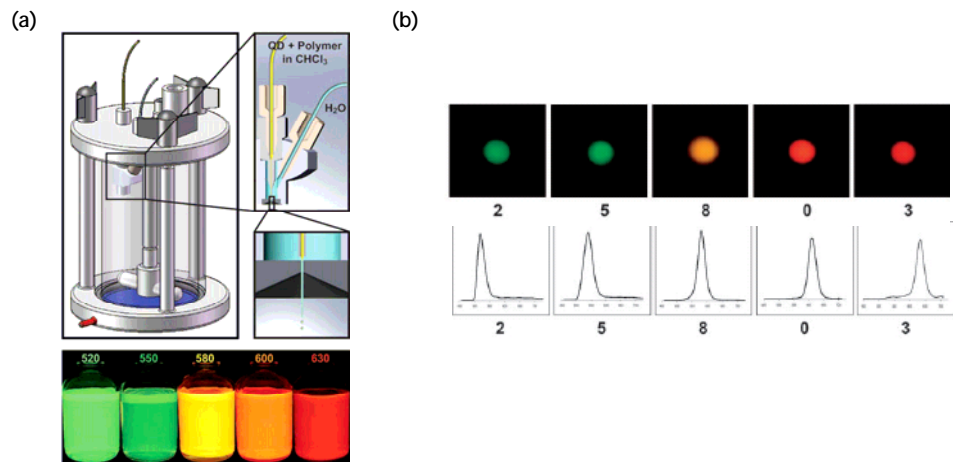


Figure 1-19: (a) Shows barcode production process. An enlargement shown on the right shows the working of the flow-focusing nozzle. The quantum dot mixture is introduced from the top and the flow focusing fluid is introduced from the right; (b) Shows fluorescence images of different barcoded beads along with their spectra, taken from (91). Copyright Wiley-VCH verlag GmbH & Co. KGaA. Reproduced with permission.

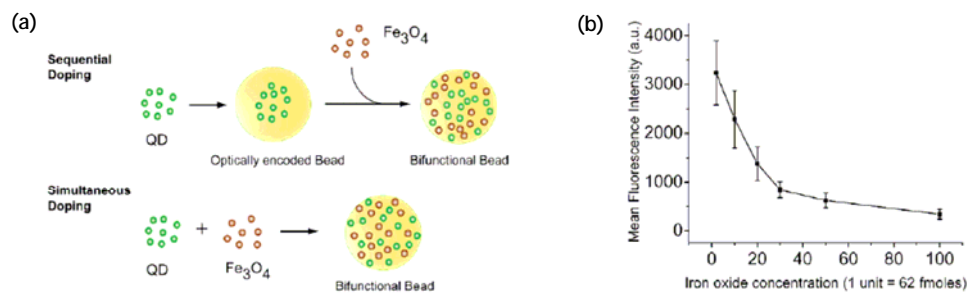


Figure 1-20: (a) Shows two different doping strategies of quantum dot and iron oxide nanoparticles into mesoporous beads; (b) The effect of iron oxide nanoparticles concentration on fluorescence intensity of barcodes. Reprinted With permission from (92). Copyright © 2006 American Chemical Society.

produced the same results in terms of optical and magnetic properties of the barcoded beads.⁽⁹²⁾ However, the fluorescence intensity of barcoded beads depended on the amount of iron oxide nanoparticles inside the bead. As the number of iron oxide nanoparticles increases, the fluorescence intensity decreases. Moreover, the variation in the fluorescence intensity ratio of green and red colour quantum dot encoded beads was found to be 15% and magnetic beads take 5 min to separate from the solution.⁽⁹²⁾

1.3.7.2. In-Situ Incorporation of Quantum Dots into Polymer Beads

In this strategy, barcoded beads are synthesised in the presence of quantum dots and starting monomer for the beads. Polystyrene beads encoded with CdS quantum dots were prepared by suspension polymerisation in the presence of CdS and styrene monomer.⁽⁹³⁾ Using this approach different sizes of barcoded beads can be prepared but the variation in fluorescence intensity from bead to bead is high as compared to other methods due to the variation in the size of the beads and number of quantum dots incorporated.⁽⁹⁴⁾

1.3.7.3. Immobilisation of Quantum Dots on Bead Surface

Quantum dots have been immobilised onto the beads and nanoparticles by covalent bonding or electrostatic interaction.⁽⁹⁵⁻⁹⁸⁾ Amphiphilic copolymer coated quantum dots were immobilised onto layer-by-layer polyelectrolyte coated beads to produce barcoded beads, as shown in Figure 1-21. In these studies, the relative standard deviation between the barcodes was found to be 20-22% for three different barcodes.⁽⁹⁶⁾

Magnetic beads have been used as a support for immobilisation of quantum dots by first coating the beads with polyamine and then quantum dots were assembled on the bead surface.⁽⁹⁸⁾ Finally beads were coated with silica nanoparticles, which serve as a support in functionalising quantum dot encoded beads for multiplexed applications.⁽⁹⁸⁾ Silica colloidal crystals beads were encoded with quantum dots using layer-by-layer assembly of poly(allylamine hydrochloride), poly(sodium 4-styrenesulfonate) and CdTe quantum dots.⁽⁹⁹⁾ A large number of barcodes could be generated using this method although the barcode size was relatively large i.e. 200µm.

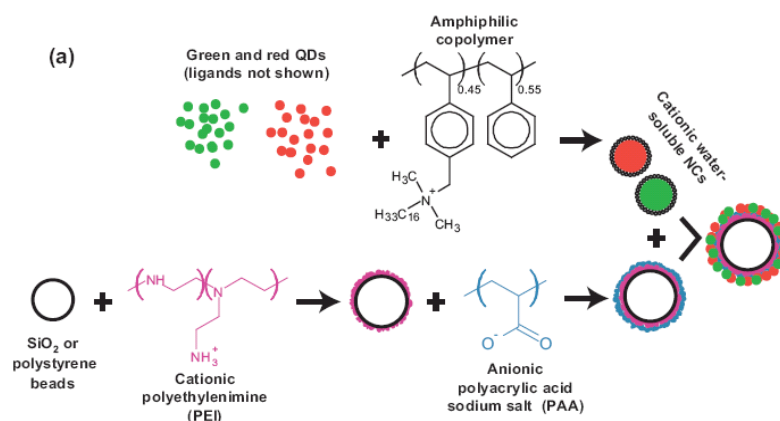


Figure 1-21: Shows the strategy for the preparation of quantum dot barcodes using polyelectrolyte layer-by-layer assembly, taken from (96). Copyright Wiley-VCH verlag GmbH & Co. KGaA. Reproduced with permission.

1.4. Applications of Barcodes in Multiplexing Bioanalysis

Many of the barcodes, which are discussed in Section 1.3 of this chapter, have been used to develop multiplexed bioassays including immunoassays and nucleic acid hybridisation assays. For example, polystyrene beads encoded with quantum dots were used for multiplexed hybridisation assays as shown in Figure 1-22.⁽⁸⁴⁾ Single bead fluorescence spectroscopy was used to read the barcodes and to detect different DNA sequences.

Similarly sub-micron metallic nanorods,⁽¹⁰⁰⁾ photonic crystal hydrogel beads,⁽⁷⁴⁾ quantum dot coated silica encoded beads,⁽¹⁰¹⁾ dot coded particles prepared by flow lithography⁽⁷³⁾ and spectrally encoded porous SiO₂ photonic crystals⁽¹⁰²⁾ have been used for multiplexed DNA hybridisation.

Barcodes prepared by different strategies have also been used for developing multiplexed immunoassays. In an immunoassay antibodies are used as an analytical reagent due to their high binding affinity and specificity for the analyte of interest (antigen) in the presence of many other substances in a sample.^(103, 104) Immunoassays are of different formats as shown in Figure 1-23.⁽³⁹⁾

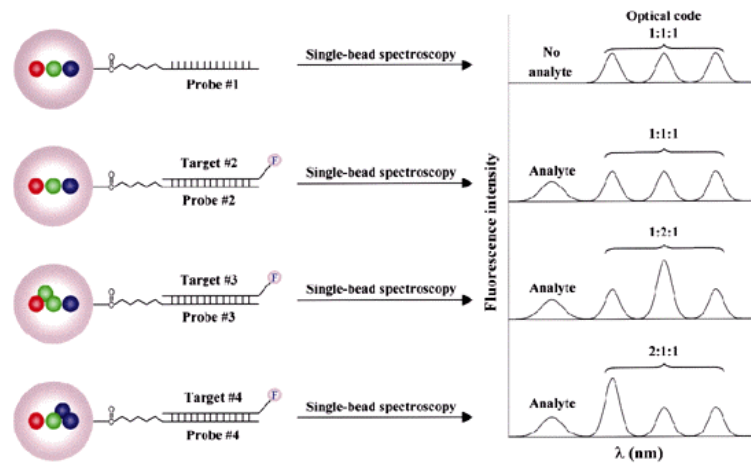


Figure 1-22: Shows the multiplexed DNA hybridisation assay where three different quantum dot encoded beads based barcodes were used to detect three different DNA sequences. The results showed that each sequence could be clearly identified using this encoding strategy, taken from (84). Reprinted by permission from Macmillan Publishers Ltd.

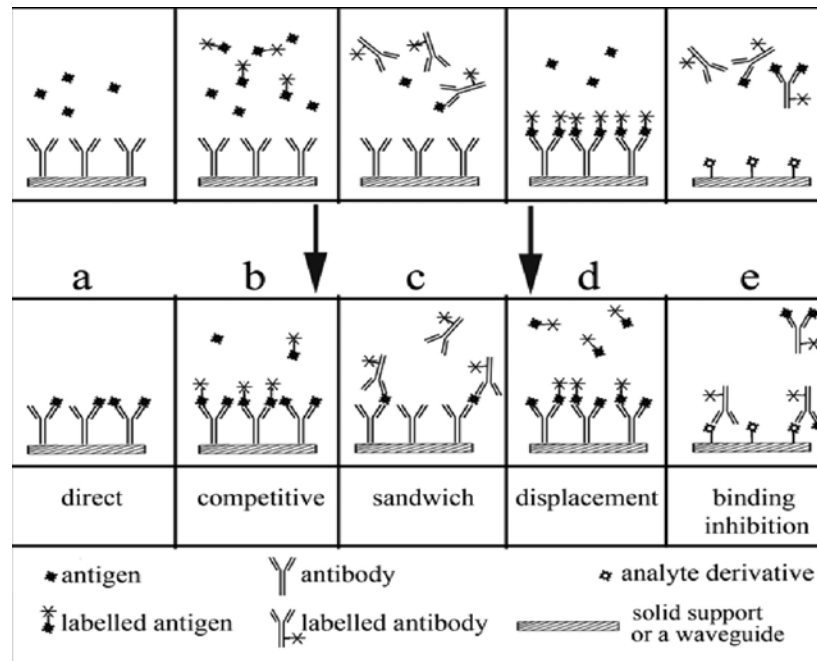


Figure 1-23: Shows different formats of immunoassays. The upper panel shows the situation before immunobinding and lower panel shows the situation after immunobinding. Reprinted With permission from (39). Copyright © 2008 American Chemical Society.

In the case of direct immunoassay, both antigen and antibody are not labelled and the binding event is measured using interferometric or electrochemical methods.^(39, 105) In case of competitive immunoassay, both labelled and unlabelled antigens compete for limited number of binding sites⁽¹⁰⁶⁾ whereas in a sandwich immunoassay antigen is first captured using an immobilised antibody and a second labelled antibody is used to detect the bound antigen.^(107, 108)

In the displacement immunoassay format an antibody coated surface is first saturated with a labelled antigen and after the introduction of the unlabelled antigen, displacement of the labelled antigen occurs resulting in the decrease in fluorescent signal of labelled antigen.^(39, 109) The response time in these type of assays is slow.⁽¹⁰⁹⁾

In a binding inhibition immunoassay format an immobilised antigen is used instead. The binding of the fluorescently labelled antibody is inhibited due to the binding of the antigen present in the solution.⁽³⁹⁾ The more the antigen present in the solution, the fewer antibodies bind to the antigen surface.

In a multiplexed immunoassay, more than one analyte (antigen) is determined simultaneously in a sample. Encoded silica colloidal crystal beads have previously been used for the multiplexed immunoassay.⁽¹¹⁰⁾ Three different kinds of silica colloidal crystal beads that can be distinguished upon the basis of different reflection spectra were used to immobilise three different immunoglobulins (human IgG, mouse IgG and rabbit IgG) for the immunoassay. Only two FITC labelled goat anti-human IgG and goat anti-mouse IgG were used in the analyte solution and it was shown that these FITC-labelled anti-IgGs bound to the corresponding IgGs immobilised on the encoded colloidal crystal beads (Figure 1-24).⁽¹¹⁰⁾

Similarly, different immunoglobulins (mouse, human, rabbit and guinea pig IgGs) were immobilised on diffractive microbarcodes of SU8 photoresist and multiplexed immunoassays were performed to show multiplexing capability of these barcodes.⁽⁶⁴⁾ In another study, pearl pigments were incorporated into polystyrene beads using droplet generation technique to produce multicolour polystyrene beads. These beads with different spectral characteristics were used to do multiplexed immunoassay using different antigen-antibody pairs.⁽¹¹¹⁾ Finally, quantum dot encoded beads prepared by using

poly(styrene-co-maleic anhydride) polymer⁽⁹¹⁾ were used to develop multiplexed immunoassay using different antigen labelled barcodes.

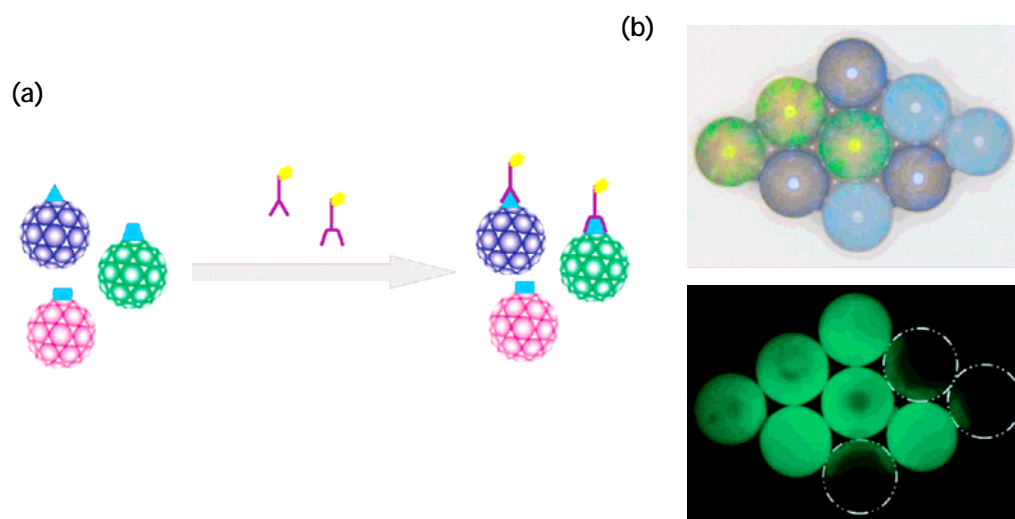


Figure 1-24: (a) Schematic of the multiplexed immunoassay using three different encoded silica colloidal crystal beads; (b) Reflection image (top) and fluorescence microscope image (bottom) of three different encoded silica colloidal crystal beads. FITC labelled anti-rabbit IgG was not added and the colloidal crystal beads correspond to the rabbit IgG have less or no fluorescent signal. Reprinted With permission from (110). Copyright © 2008 American Chemical Society.

1.5. Outline of the Approach to Barcode Generation and Multiplexed Assays Employed in this Thesis

This thesis describes the production and application of quantum dot barcodes produced by using layer-by-layer assembly of quantum dots onto magnetic bead surface. Two types of strategies are used. The first strategy uses thiol chemistry to immobilise quantum dots in a layer-by-layer assembly onto magnetic beads. In the second strategy,

the interaction between biotin and streptavidin has been exploited to create constructs on the bead surface, which can subsequently be read optically.

The streptavidin-biotin interaction is sufficiently strong ($K_d \cong 4 \times 10^{-14} \text{ M}$)⁽¹¹²⁾ that the assembled codes are stable over extended periods. The strategy that is proposed in this work has a number of advantages over traditional strategies: firstly, the nature of the streptavidin-biotin self-assembly provides a reagentless method to bring together modular components that may make up the barcode (analogous to biomolecular lego); secondly, this assembly process is stable at temperatures above ambient (for example, if the barcode were to be used in the polymerase chain reaction, PCR); thirdly the exploitation of the streptavidin-biotin conjugation has the potential to enable biological molecules subsequently to be bound to the encoded bead (e.g., using biotinylated DNA or antibodies to perform encoded ligand binding assays); and finally, importantly, it is well known from the microtiter plate industry that streptavidin provides a coating that shows minimal non-specific binding to proteins, thereby mitigating against significant cross-talk between particles, during and after their assembly.

The experimental work in this thesis can be divided into two parts. The first part concerns the layer-by-layer assembly of quantum dots onto the glass substrates to help characterise the immobilisation process using for example, X-ray photoelectron spectroscopy (XPS) and fluorescence spectroscopy. The second part of the thesis describes the production and application of quantum dot barcodes prepared by layer-by-layer assembly of quantum dots onto magnetic beads. To show the application of these barcodes, multiplexed immunoassays are performed.

The thesis contains six chapters including this chapter. Chapter 2 details materials and experimental methods used to carry out the experiments. Chapter 3 details the confirmation of immobilisation of quantum dots onto glass substrates using XPS and fluorescence spectroscopy. Chapter 4 details the results for the production, characterisation and stability of quantum dot barcodes produced by layer-by-layer assembly of quantum dot conjugates. Chapter 5 concerns the application of quantum dot barcodes for multiplexed immunoassay, and finally Chapter 6 discusses and draws conclusions from all the experiments and indicates possible future directions to exploit this barcoding technique.

1.6. References

1. Whitesides GM. The 'right' size in nanobiotechnology. *Nature Biotechnology* 2003;21(10):1161-1165.
2. Fortina P, Kricka LJ, Surrey S, Grodzinski P. Nanobiotechnology: the promise and reality of new approaches to molecular recognition. *Trends in Biotechnology* 2005;23(4):168-173.
3. Vo-Dinh T, Cullum B. Biosensors and biochips: advances in biological and medical diagnostics. *Fresenius Journal of Analytical Chemistry* 2000;366(6-7):540-551.
4. Cass AEG. *Biosensors : a practical approach*. Oxford, England ; New York: IRL Press at Oxford University Press; 1990.
5. Turner APF, Karube I, Wilson GS. *Biosensors : fundamentals and applications*. Oxford ; New York: Oxford University Press; 1987.
6. Cooper JM, Cass AEG, Knovel (Firm). *Biosensors a practical approach*. In. 2nd ed. Oxford ; New York: Oxford University Press; 2004. p. xvi, 251 p.
7. Gorton L, Knovel (Firm). *Biosensors and modern biospecific analytical techniques*. In. 1st ed. Amsterdam ; Boston: Elsevier; 2005. p. xxii, 635 p.
8. Freitag R. *Biosensors in analytical biotechnology*. Austin, TX: R.G. Landes; 1996.
9. Kerman K, Kobayashi M, Tamiya E. Recent trends in electrochemical DNA biosensor technology. *Measurement Science & Technology* 2004;15(2):R1-R11.
10. Rasooly L, K.E. H. *Biosensors and Biodetection: Methods and Protocols: Electrochemical and Mechanical Detectors, Lateral Flow and Ligands for Biosensors*: Springer; 2008.
11. Gooding JJ. Electrochemical DNA hybridization biosensors. *Electroanalysis* 2002;14(17):1149-1156.
12. Choi MMF. Progress in enzyme-based biosensors using optical transducers. *Microchimica Acta* 2004;148(3-4):107-132.
13. Hsu CT, Hsiao HC, Chen SH, Wu MH, Lin CK, Chang KC, et al. Evaluation of a New Self-Monitoring Blood Glucose System Bionime Rightest GM550 with Auto-Calibration for Alternative-Site Blood Glucose Tests. *Diabetes* 2009;58:A506-A506.
14. Garg SK, Jennings MK, Tideman A. Clinical evaluation of a new electrochemical system for self-monitoring of blood glucose. *Diabetes* 1997;46:1273-1273.
15. Chen WC, Lin YY. Glucose biosensor based on dextran-Fe₃O₄ nanocomposite modified spces. *Biomedical Engineering-Applications Basis Communications* 2009;21(6):437-440.

16. Li SK, Chou JC, Sun TP, Hsiung SK. Study on the potentiometric glucose biosensor based on the SnO₂/ITO/PET. *Biomedical Engineering-Applications Basis Communications* 2009;21(6):411-414.
17. Chou JC, Tsai YH, Chen CC. Development of a Disposable All-Solid-State Ascorbic Acid Biosensor and Miniaturized Reference Electrode Fabricated on Single Substrate. *Ieee Sensors Journal* 2008;8(9-10):1571-1577.
18. Fernandes JCB, Kubota LT, Neto GD. Potentiometric biosensor for L-ascorbic acid based on ascorbate oxidase of natural source immobilized on ethylene-vinylacetate membrane. *Analytica Chimica Acta* 1999;385(1-3):3-12.
19. Yildirimoglu F, Arslan F, Cete S, Yasar A. Preparation of a polypyrrole-polyvinylsulphonate composite film biosensor for determination of cholesterol based on entrapment of cholesterol oxidase. *Sensors* 2009;9(8):6435-6445.
20. Nien PC, Chen PY, Ho KC. Fabricating an Amperometric Cholesterol Biosensor by a Covalent Linkage between Poly(3-thiopheneacetic acid) and Cholesterol Oxidase. *Sensors* 2009;9(3):1794-1806.
21. Ding SN, Shan D, Sun YM. Bioelectrochemical response of a choline biosensor fabricated by using polyaniline. *Science in China Series B-Chemistry* 2009;52(12):2275-2280.
22. Jiang XY, Zhu LD, Yang DX, Mao XY, Wu YH. Amperometric ethanol biosensor based on integration of alcohol dehydrogenase with meldola's blue/ordered mesoporous carbon electrode. *Electroanalysis* 2009;21(14):1617-1623.
23. Diamandis E, Christopoulos T. *Immunoassay*. London: Academic Press, Inc; 1996.
24. Osborn LM. *Pediatrics*. 1st ed. Philadelphia, Pa.: Elsevier Mosby; 2005.
25. Murray PR, Rosenthal KS, Pfaller MA. *Medical microbiology*. 6th ed. Philadelphia: Mosby/Elsevier; 2009.
26. Murray RK, Knovel (Firm). *Harper's illustrated biochemistry*. In. 26th ed. New York: McGraw-Hill; 2003. p. x, 693 p.
27. Brändén C-I, Tooze J. *Introduction to protein structure*. 2nd ed. New York: Garland Pub.; 1999.
28. Nakamura RM, Kasahara Y, Rechnitz GA. *Immunochemical assays and biosensor technology for the 1990s*. Washington, D.C.: American Society for Microbiology; 1992.
29. Wei MY, Guo LH. Advances in the determination of environmental pollutants by immunosensors. *Progress in Chemistry* 2009;21(2-3):492-502.

30. Vidal JC, Duato P, Bonel L, Castillo JR. Use of polyclonal antibodies to ochratoxin A with a quartz-crystal microbalance for developing real-time mycotoxin piezoelectric immunosensors. *Analytical and Bioanalytical Chemistry* 2009;394(2):575-582.
31. Rao VK, Singh C. Effect of antibodies immobilization on the efficiency of carbon paste based immunosensors. *Sensor Letters* 2009;7(4):609-614.
32. Wang J. Electrochemical biosensors: Towards point-of-care cancer diagnostics. *Biosensors & Bioelectronics* 2006;21(10):1887-1892.
33. Gopalan AI, Lee KP, Ragupathy D, Lee SH, Lee JW. An electrochemical glucose biosensor exploiting a polyaniline grafted multiwalled carbon nanotube/perfluorosulfonate ionomer-silica nanocomposite. *Biomaterials* 2009;30(30):5999-6005.
34. Pournaghi-Azar MH, Ahour F, Hejazi MS. Differential pulse voltammetric detection of hepatitis C virus 1a oligonucleotide chain by a label-free electrochemical DNA hybridization biosensor using consensus sequence of hepatitis C virus 1a probe on the pencil graphite electrode. *Electroanalysis* 2009;21(16):1822-1828.
35. Levine PM, Gong P, Levicky R, Shepard KL. Real-time, multiplexed electrochemical DNA detection using an active complementary metal-oxide-semiconductor biosensor array with integrated sensor electronics. *Biosensors & Bioelectronics* 2009;24(7):1995-2001.
36. Wang CH, Zhao J, Zhang DP, Yang ZS. Detection of DNA damage induced by hydroquinone and catechol using an electrochemical DNA biosensor. *Australian Journal of Chemistry* 2009;62(9):1181-1184.
37. Namgung MO, Jung SK, Chung CM, Oh SY. Electrochemical immunosensor for prostate-specific antigen using self-assembled oligophenylethylenethiol monolayer containing dendrimer. *Ultramicroscopy* 2009;109(8):907-910.
38. Parker CO, Tothill IE. Development of an electrochemical immunosensor for aflatoxin M-1 in milk with focus on matrix interference. *Biosensors & Bioelectronics* 2009;24(8):2452-2457.
39. Borisov SM, Wolfbeis OS. Optical biosensors. *Chemical Reviews* 2008;108(2):423-461.
40. Thompson RB. Fluorescence sensors and biosensors. In. Boca Raton: CRC/Taylor & Francis; 2006. p. 395 p.
41. Hof M, Hutterer R, Fidler V, Springer E-books - York University., SpringerLink (Online service). Fluorescence spectroscopy in biology advanced methods and their

- applications to membranes, proteins, DNA, and cells. Berlin ; New York: Springer; 2005.
42. Lakowicz JR, Springer E-books - York University., SpringerLink (Online service). Principles of fluorescence spectroscopy. 3rd ed. New York: Springer; 2006.
 43. Chasteen TG. Relaxation mechanism for excited state molecules. 1996.
 44. Grate JW, Warner MG, Ozanich RM, Miller KD, Colburn HA, Dockendorff B, et al. Renewable surface fluorescence sandwich immunoassay biosensor for rapid sensitive botulinum toxin detection in an automated fluidic format. *Analyst* 2009;134(5):987-996.
 45. Lin CH, Chen HY, Yu CJ, Lu PL, Hsieh CH, Hsieh BY, et al. Quantitative measurement of binding kinetics in sandwich assay using a fluorescence detection fiber-optic biosensor. *Analytical Biochemistry* 2009;385(2):224-228.
 46. Stringer RC, Hoehn D, Grant SA. Quantum dot-based biosensor for detection of human cardiac Troponin I using a liquid-core waveguide. *Ieee Sensors Journal* 2008;8(3-4):295-300.
 47. Revesz E, Lai EPC, DeRosa MC. Towards a FRET-based ATP biosensor using quantum dot/aptamer-based complexes. *Journal of Biomolecular Structure & Dynamics* 2007;24(6):645-645.
 48. Nann T. Phase-transfer of CdSe@ZnS quantum dots using amphiphilic hyperbranched polyethylenimine. *Chemical Communications* 2005(13):1735-1736.
 49. Chan WCW, Maxwell DJ, Gao XH, Bailey RE, Han MY, Nie SM. Luminescent quantum dots for multiplexed biological detection and imaging. *Current Opinion in Biotechnology* 2002;13(1):40-46.
 50. Zimnitsky D, Jiang CY, Xu J, Lin ZQ, Tsukruk VV. Substrate- and time-dependent photoluminescence of quantum dots inside the ultrathin polymer LbL film. *Langmuir* 2007;23(8):4509-4515.
 51. Pang L, Tetz K, Shen YM, Chen CH, Fainman Y. Photosensitive quantum dot composites and their applications in optical structures. *Journal of Vacuum Science & Technology B* 2005;23(6):2413-2418.
 52. Wang Y, Suna A, Mahler W, Kasowski R. Pbs in Polymers - from Molecules to Bulk Solids. *Journal of Chemical Physics* 1987;87(12):7315-7322.
 53. Murray CB, Norris DJ, Bawendi MG. Synthesis and Characterization of Nearly Monodisperse Cde (E = S, Se, Te) Semiconductor Nanocrystallites. *Journal of the American Chemical Society* 1993;115(19):8706-8715.

54. Hines MA, Guyot-Sionnest P. Synthesis and characterization of strongly luminescing ZnS-Capped CdSe nanocrystals. *Journal of Physical Chemistry* 1996;100(2):468-471.
55. Gill R, Zayats M, Willner I. Semiconductor quantum dots for bioanalysis. *Angewandte Chemie-International Edition* 2008;47(40):7602-7625.
56. Alivisatos AP. Semiconductor clusters, nanocrystals, and quantum dots. *Science* 1996;271(5251):933-937.
57. Frasco MF, Chaniotakis N. Semiconductor quantum dots in chemical sensors and biosensors. *Sensors* 2009;9(9):7266-7286.
58. <http://www.invitrogen.com>.
59. Komarala VK, Rakovich YP, Bradley AL, Byrne SJ, Corr SA, Gun'ko YK. Emission properties of colloidal quantum dots on polyelectrolyte multilayers. *Nanotechnology* 2006;17(16):4117-4122.
60. Giraud G, Schulze H, Bachmann TT, Campbell CJ, Mount AR, Ghazal P, et al. Solution state hybridization detection using time-resolved fluorescence anisotropy of quantum dot-DNA bioconjugates. *Chemical Physics Letters* 2010;484(4-6):309-314.
61. Giraud G, Schulze H, Bachmann TT, Campbell CJ, Mount AR, Ghazal P, et al. Fluorescence lifetime imaging of quantum dot labeled DNA microarrays. *International Journal of Molecular Sciences* 2009;10(4):1930-1941.
62. Costa-Fernandez JM, Pereiro R, Sanz-Medel A. The use of luminescent quantum dots for optical sensing. *Trends in Analytical Chemistry* 2006;25(3):207-218.
63. Wilson R, Cossins AR, Spiller DG. Encoded microcarriers for high-throughput multiplexed detection. *Angewandte Chemie-International Edition* 2006;45(37):6104-6117.
64. Broder GR, Ranasinghe RT, She JK, Banu S, Birtwell SW, Cavalli G, et al. Diffractive micro bar codes for encoding of biomolecules in multiplexed assays. *Analytical Chemistry* 2008;80(6):1902-1909.
65. Zhi ZL, Morita Y, Yamamura S, Tamiya E. Microfabrication of encoded microparticle array for multiplexed DNA hybridization detection. *Chemical Communications* 2005(19):2448-2450.
66. Nolan JP, Sklar LA. Suspension array technology: evolution of the flat-array paradigm. *Trends in Biotechnology* 2002;20(1):9-12.
67. Douglas ES, Hsiao SC, Onoe H, Bertozzi CR, Francis MB, Mathies RA. DNA-barcode directed capture and electrochemical metabolic analysis of single mammalian cells on a microelectrode array. *Lab on a Chip* 2009;9(14):2010-2015.

68. Zhi ZL, Morita Y, Hasan Q, Tamiya E. Micromachining microcarrier-based biomolecular encoding for miniaturized and multiplexed immunoassay. *Analytical Chemistry* 2003;75(16):4125-4131.
69. Meade SO, Sailor MJ. Microfabrication of freestanding porous silicon particles containing spectral barcodes. *Physica Status Solidi-Rapid Research Letters* 2007;1(2):R71-R73.
70. Hoffmann D, O'Brien J, Brennan D, Loughran M. Optically encoded silicon microbeads: Detection and characterisation in a microfluidic system. *Sensors and Actuators B-Chemical* 2007;122(2):653-658.
71. Galitonov GS, Birtwell SW, Zheludev NI, Morgan H. High capacity tagging using nanostructured diffraction barcodes. *Optics Express* 2006;14(4):1382-1387.
72. Banu S, Birtwell S, Galitonov G, Chen YF, Zheludev N, Morgan H. Fabrication of diffraction-encoded micro-particles using nano-imprint lithography. *Journal of Micromechanics and Microengineering* 2007;17(7):S116-S121.
73. Pregibon DC, Toner M, Doyle PS. Multifunctional encoded particles for high-throughput biomolecule analysis. *Science* 2007;315(5817):1393-1396.
74. Hu J, Zhao XW, Zhao YJ, Li J, Xu WY, Wen ZY, et al. Photonic crystal hydrogel beads used for multiplex biomolecular detection. *Journal of Materials Chemistry* 2009;19(32):5730-5736.
75. Dejneka MJ, Streltsov A, Pal S, Frutos AG, Powell CL, Yost K, et al. Rare earth-doped glass microbarcodes. *Proceedings of the National Academy of Sciences of the United States of America* 2003;100(2):389-393.
76. Nicewarner-Pena SR, Freeman RG, Reiss BD, He L, Pena DJ, Walton ID, et al. Submicrometer metallic barcodes. *Science* 2001;294(5540):137-141.
77. Su X, Zhang J, Sun L, Koo TW, Chan S, Sundararajan N, et al. Composite organic-inorganic nanoparticles (COINs) with chemically encoded optical signatures. *Nano Letters* 2005;5(1):49-54.
78. Fenniri H, Ding LH, Ribbe AE, Zyrianov Y. Barcoded resins: A new concept for polymer-supported combinatorial library self-deconvolution. *Journal of the American Chemical Society* 2001;123(33):8151-8152.
79. Jin RC, Cao YW, Mirkin CA, Kelly KL, Schatz GC, Zheng JG. Photoinduced conversion of silver nanospheres to nanoprisms. *Science* 2001;294(5548):1901-1903.

80. Yang J, Dave SR, Gao XH. Quantum dot nanobarcodes: Epitaxial assembly of nanoparticle-polymer complexes in homogeneous solution. *Journal of the American Chemical Society* 2008;130(15):5286-5292.
81. Geiss GK, Bumgarner RE, Birditt B, Dahl T, Dowidar N, Dunaway DL, et al. Direct multiplexed measurement of gene expression with color-coded probe pairs. *Nature Biotechnology* 2008;26(3):317-325.
82. Sukhanova A, Nabiev I. Fluorescent nanocrystal-encoded microbeads for multiplexed cancer imaging and diagnosis. *Critical Reviews in Oncology Hematology* 2008;68(1):39-59.
83. Finkel NH, Lou XH, Wang CY, He L. Barcoding the microworld. *Analytical Chemistry* 2004;76(19):353a-359a.
84. Han MY, Gao XH, Su JZ, Nie S. Quantum-dot-tagged microbeads for multiplexed optical coding of biomolecules. *Nature Biotechnology* 2001;19(7):631-635.
85. Yang YH, Wen ZK, Dong YP, Gao MY. Incorporating CdTe nanocrystals into polystyrene microspheres: Towards robust fluorescent beads. *Small* 2006;2(7):898-901.
86. Grondahl L, Battersby BJ, Bryant D, Trau M. Encoding combinatorial libraries: A novel application of fluorescent silica colloids. *Langmuir* 2000;16(25):9709-9715.
87. Huang ZL, Zhao YD, Luo QM. Quantum-dot-tagged microbeads and their use as fluorescent biological probes. *Current Analytical Chemistry* 2006;2(1):59-66.
88. Kuang M, Wang DY, Bao HB, Gao MY, Mohwald H, Jiang M. Fabrication of multicolor-encoded microspheres by tagging semiconductor nanocrystals to hydrogel spheres. *Advanced Materials* 2005;17(3):267-+.
89. Behrendt JM, Afzaal M, Alexander LM, Bradley M, Hine AV, Nagel D, et al. Thiol-containing microspheres as polymeric ligands for the immobilisation of quantum dots. *Journal of Materials Chemistry* 2009;19(2):215-221.
90. Gao XH, Nie SM. Quantum dot-encoded mesoporous beads with high brightness and uniformity: Rapid readout using flow cytometry. *Analytical Chemistry* 2004;76(8):2406-2410.
91. Fournier-Bidoz S, Jennings TL, Klostranec JM, Fung W, Rhee A, Li D, et al. Facile and rapid one-step mass preparation of quantum-dot barcodes. *Angewandte Chemie-International Edition* 2008;47(30):5577-5581.
92. Sathe TR, Agrawal A, Nie SM. Mesoporous silica beads embedded with semiconductor quantum dots and iron oxide nanocrystals: Dual-function

- microcarriers for optical encoding and magnetic separation. *Analytical Chemistry* 2006;78(16):5627-5632.
93. Li Y, Liu ECY, Pickett N, Skabara PJ, Cummins SS, Ryley S, et al. Synthesis and characterization of CdS quantum dots in polystyrene microbeads. *Journal of Materials Chemistry* 2005;15(12):1238-1243.
 94. Sheng WC, Kim S, Lee J, Kim SW, Jensen K, Bawendi MG. In-situ encapsulation of quantum dots into polymer microspheres. *Langmuir* 2006;22(8):3782-3790.
 95. Wang DY, Rogach AL, Caruso F. Semiconductor quantum dot-labeled microsphere bioconjugates prepared by stepwise self-assembly. *Nano Letters* 2002;2(8):857-861.
 96. Allen CN, Lequeux N, Chassenieux C, Tessier G, Dubertret B. Optical analysis of beads encoded with quantum dots coated with a cationic polymer. *Advanced Materials* 2007;19(24):4420-+.
 97. Graf C, Dembski S, Hofmann A, Ruhl E. A general method for the controlled embedding of nanoparticles in silica colloids. *Langmuir* 2006;22(13):5604-5610.
 98. Wilson R, Spiller DG, Prior IA, Veltkamp KJ, Hutchinson A. A simple method for preparing spectrally encoded magnetic beads for multiplexed detection. *ACS Nano* 2007;1(5):487-493.
 99. Li J, Zhao XW, Zhao YJ, Hu J, Xu M, Gu ZZ. Colloidal crystal beads coated with multicolor CdTe quantum dots: microcarriers for optical encoding and fluorescence enhancement. *Journal of Materials Chemistry* 2009;19(36):6492-6497.
 100. Sha MY, Walton ID, Norton SM, Taylor M, Yamanaka M, Natan MJ, et al. Multiplexed SNP genotyping using nanobarcode particle technology. *Analytical and Bioanalytical Chemistry* 2006;384(3):658-666.
 101. Li J, Zhao XW, Zhao YJ, Gu ZZ. Quantum-dot-coated encoded silica colloidal crystals beads for multiplex coding. *Chemical Communications* 2009(17):2329-2331.
 102. Meade SO, Chen MY, Sailor MJ, Miskelly GM. Multiplexed DNA detection using spectrally encoded porous SiO₂ photonic crystal particles. *Analytical Chemistry* 2009;81(7):2618-2625.
 103. Diamandis EP, Christopoulos TK. *Immunoassay*. San Diego: Academic Press; 1996.
 104. Lakowicz JR, ebrary Inc. *Topics in fluorescence spectroscopy Volume 4, Probe design and chemical sensing*. In. New York: Kluwer Academic; 2002. p. xviii, 501 p.

105. Wang FC, Yuan R, Chai YQ. Direct electrochemical immunoassay based on a silica nanoparticles/sol-gel composite architecture for encapsulation of immunoconjugate. *Applied Microbiology and Biotechnology* 2006;72(4):671-675.
106. Nistor C, Oubina A, Marco MP, Barcelo D, Emneus J. Competitive flow immunoassay with fluorescence detection for determination of 4-nitrophenol. *Analytica Chimica Acta* 2001;426(2):185-195.
107. Vicennati P, Bensele N, Wagner A, Creminon C, Taran F. Sandwich immunoassay as a high-throughput screening method for cross-coupling reactions. *Angewandte Chemie-International Edition* 2005;44(42):6863-6866.
108. Sivagnanam V, Bouhmad A, Lacharme F, Vandevyver C, Gijss MAM. Sandwich immunoassay on a microfluidic chip using patterns of electrostatically self-assembled streptavidin-coated beads. *Microelectronic Engineering* 2009;86(4-6):1404-1406.
109. Sapsford KE, Charles PT, Patterson CH, Ligler FS. Demonstration of four immunoassay formats using the array biosensor. *Analytical Chemistry* 2002;74(5):1061-1068.
110. Zhao YJ, Zhao XW, Sun C, Li J, Zhu R, Gu ZZ. Encoded silica colloidal crystal beads as supports for potential multiplex immunoassay. *Analytical Chemistry* 2008;80(5):1598-1605.
111. Zhao XW, Liu ZB, Yang H, Nagai K, Zhao YH, Gu ZZ. Uniformly colorized beads for multiplex immunoassay. *Chemistry of Materials* 2006;18(9):2443-2449.
112. Holmberg A, Blomstergren A, Nord O, Lukacs M, Lundberg J, Uhlen M. The biotin-streptavidin interaction can be reversibly broken using water at elevated temperatures. *Electrophoresis* 2005;26(3):501-510.

Chapter 2

Materials and Methods

This chapter details the materials used in the experimental work for this thesis and the different techniques and procedures used to carry out the experiments.

2.1. Layer-by-Layer Assembly of Quantum Dots onto Glass Slides and Magnetic Beads using Thiol Chemistry

Quantum dots were immobilised on a plain glass substrate and magnetic beads using a thiol-quantum dot linkage,⁽¹⁾ in a layer-by-layer assembly approach. Immobilisation on glass substrates was used as a model for characterising interfacial chemistries (e.g. for XPS, Chapter 3), whilst that on magnetic beads was ultimately that used in bioassays. The materials used for this experiment and detail concerning each method is described below.

2.1.1. Materials

Quantum dots (CdSe/ZnS) dispersed in toluene having emission maximum wavelength at 626 nm (QD₆₂₆) and 555 nm (QD₅₅₅) were purchased from Evident technologies, USA. (3-mercaptopropyl)trimethoxysilane, a dithiol linker 1,9-nonanedithiol, cysteamine and toluene were purchased from Sigma-Aldrich. Absolute ethanol was

purchased from Fisher Scientific. Plain microscope glass slides, used for the preparation of layer-by-layer assembly of quantum dots were purchased from Menzel-Glaser and Thermoscientific. Decon 90, a surface active cleaning agent was purchased from Decon laboratories limited, UK.

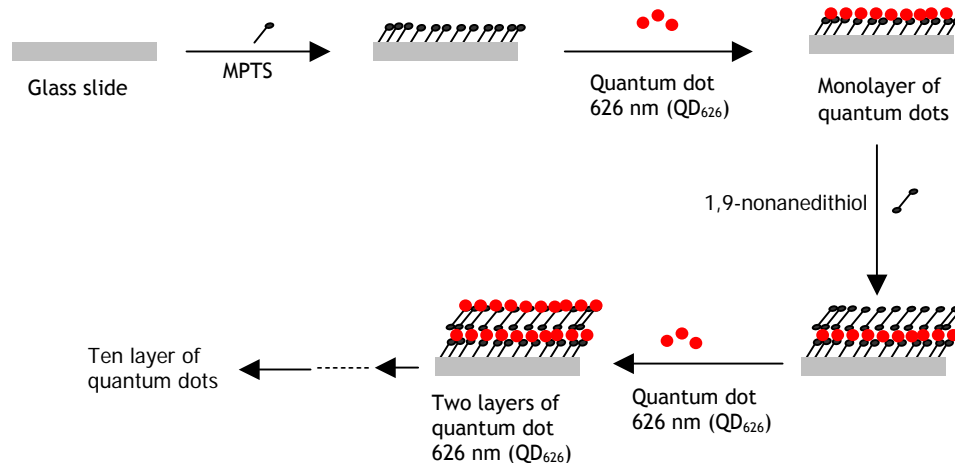
SiMAG-Thiol magnetic beads (1 μ m diameter) were purchased from Chemicell GmbH, Germany. These are aqueous dispersion of non-porous magnetic silica particles that are functionalised with thiol (-SH) group. These magnetic silica beads contain iron oxide nanoparticles encapsulated inside the beads. The dispersion of these magnetic beads contains 9.0×10^{10} beads/ml of suspension.

2.1.2. Layer-by-Layer Assembly of Quantum Dots onto Glass Slides

Glass slides were first cut into 1×1 cm² pieces and cleaned by sonication in 5% vol/vol solution of Decon 90 in de-ionised water for 15 min, rinsed with plenty of deionised water and dried with nitrogen gas. These glass slides were then modified with (3-mercaptopropyl)-trimethoxysilane (MPTS) to introduce thiol groups on the glass surface.⁽²⁾ Briefly, cleaned glass slides were placed in a wide neck round bottom flask equipped with a condenser and 400ml isopropyl alcohol (IPA) along with 10ml of water was added. To this mixture 10ml of MPTS was added and refluxed for 10 min in the boiling silane solution. After this, the flask was removed and allowed to cool. Glass slides were then rinsed with IPA and dried with nitrogen gas, **Scheme 2-1**. The same procedure was repeated three times to modify the glass slides.

After modification with MPTS, the glass slides were immediately incubated in 2 μ M solution of quantum dots 626 nm (stock solution of quantum dots was 14.0 μ M) in toluene for one hour at room temperature. After incubation, these glass slides were rinsed exhaustively with toluene and dried with nitrogen gas. For the preparation of multilayers of quantum dots, the glass slides were subsequently incubated in a solution of dithiol linker⁽³⁾ as shown in **Scheme 2-1**.

The glass slides were incubated in 10mM ethanolic solution of 1,9-nonanedithiol for one hour. After incubation, the glass slides were rinsed with ethanol and dried with nitrogen gas. These slides were then incubated in quantum dots solution (2 μ M) for one hour to make the second layer of quantum dots.



Scheme 2-1: Schematic layout of the steps followed for the preparation of quantum dots 626 nm (QD₆₂₆) layer-by-layer assembly onto the glass substrate. For the preparation of mixed multilayers of quantum dots, QD₆₂₆ and QD₅₅₅ were immobilised in an alternate fashion. Figures are not to scale.

In this way, by repeating the incubation in 1,9-nonanedithiol and quantum dots solutions, multilayers of quantum dots were formed. In these studies ten layers of quantum dots were formed on the glass slides using QD₆₂₆. Two different colour quantum dots QD₆₂₆ and QD₅₅₅ were also used to make layer-by-layer assembly using the same method as described above. These quantum dot multilayers were then characterised using X-ray photoelectron spectroscopy and fluorescence spectroscopy.

2.1.3. Immobilisation of Quantum Dots on Thiol (-SH) Modified Magnetic Beads

Thiol modified magnetic silica beads (1µm) were used for making the multilayers of quantum dots on the bead surface. By immobilising different quantum dots onto the magnetic beads, different fluorescent signatures can be created to produce different magnetic bead based barcodes. Magnetic beads were used in order to provide a simple technique to separate the beads from the incubation solution and washing solvent, using a magnet (MagnaRack, DNA Research Innovations, UK). The use of magnetic beads made

To make a second layer of quantum dots onto the magnetic beads, the magnetic beads modified with QD₆₂₆ were incubated in 500µl of 10mM solution of 1,9-nonanedithiol for one hour using the vortex mixer at a low speed. These beads were then washed with ethanol to remove excess and unbound dithiol linker. At this step, one thiol group of the bifunctional thiol linker was bound to the QD₆₂₆ and the second thiol group was available for binding the next layer of quantum dots. These beads were then incubated with 500µl of ethanol-toluene (50:50) mixture containing 5µl of QD₅₅₅ (stock solution 63.5 µM) quantum dots for one hour. After washing to remove unbound quantum dots, magnetic beads were redispersed in ethanol. In order to re-disperse the beads in water, these beads were then incubated in 10mM solution of cysteamine⁽¹⁾ for one hour. Cysteamine has one thiol (-SH) and one (-NH₂) functional group. The thiol functional group binds to the quantum dots and amino group helps to render the magnetic beads water dispersible. After washing with ethanol these barcoded beads were then re-dispersed in deionised water. Single bead fluorescence spectroscopy was used to characterise these beads.

2.2. Immobilisation of Quantum Dot Bioconjugates using Layer-by-Layer Biological Self-Assembly onto Glass Slides and Magnetic Beads

2.2.1. Materials

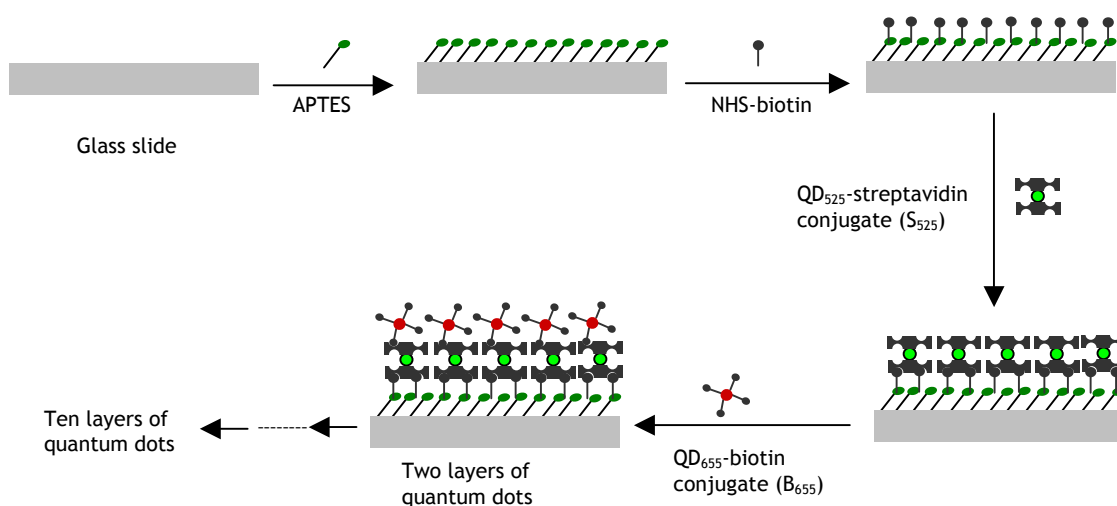
Plain microscope glass slides used for the preparation of layer-by-layer assembly of quantum dots were purchased from Menzel-Glaser and Thermoscientific. Decon 90 was purchased from Decon laboratories limited, UK. (3-Aminopropyl)triethoxysilane (APTES), biotin, biotinamidohexanoic acid 3-sulfo-N-hydroxysuccinimide ester sodium salt (NHS-biotin) and biotin-fluorescein were purchased from Sigma-Aldrich, UK. NHS-biotin has an aminocaproyl spacer which reduces steric hindrance in binding streptavidin quantum dot conjugates. NHS-biotin reacts with primary amines in the pH range 6.5-8.5.

Dynabeads M-280 streptavidin (2.8µm), streptavidin- and biotin-conjugated CdSe/ZnS quantum dots (QD₆₀₅-biotin, QD₆₅₅-biotin, QD₆₀₅-streptavidin, QD₆₅₅-streptavidin, QD₅₂₅-streptavidin, QD₅₆₅-streptavidin) were purchased from Invitrogen, UK. These quantum dot streptavidin or biotin conjugates are semiconductor nanocrystals of CdSe around which a semiconductor shell of ZnS is coated to improve the optical properties. These core-shell quantum dots are coated with a polymer shell, directly coupled to streptavidin or biotin molecules using a polyethylene glycol (PEG)-linker. The size of the

quantum dot streptavidin conjugate is ~15-20 nm and that of biotin conjugate is ~10-12 nm. The loading of streptavidin onto the quantum dots is estimated as 5-10 streptavidin/QD conjugate while in case of biotin conjugate is 5-7 biotin molecules/QD conjugate.^(4, 5) Another type of streptavidin conjugates (QD₆₅₅ ITK™-streptavidin conjugate and QD₆₀₅ ITK™-streptavidin conjugate) without a PEG-linker was also purchased from Invitrogen (**Section 2.2.3.1**). 10mM phosphate buffer pH 7.4 (adjusted to an ionic strength of 25mM using NaCl and containing 0.002% sodium azide and 0.15% BSA) was prepared using ultrapure MilliQ water ($\Omega > 18 \text{ M}\Omega\cdot\text{cm}$). The word “PBS” is used for this buffer without 0.15% BSA.

2.2.2. Layer-by-Layer Assembly of QD-Streptavidin and QD-Biotin Conjugates onto Plain Glass Substrates

The streptavidin and biotin interaction was used to immobilise quantum dots onto planar glass surface and magnetic beads. A layer-by-layer assembly approach was used to concentrate the quantum dots on to the substrate surface. The strategy to immobilise quantum dots onto the glass substrate is shown in **Scheme 2-3**. The glass slides were first



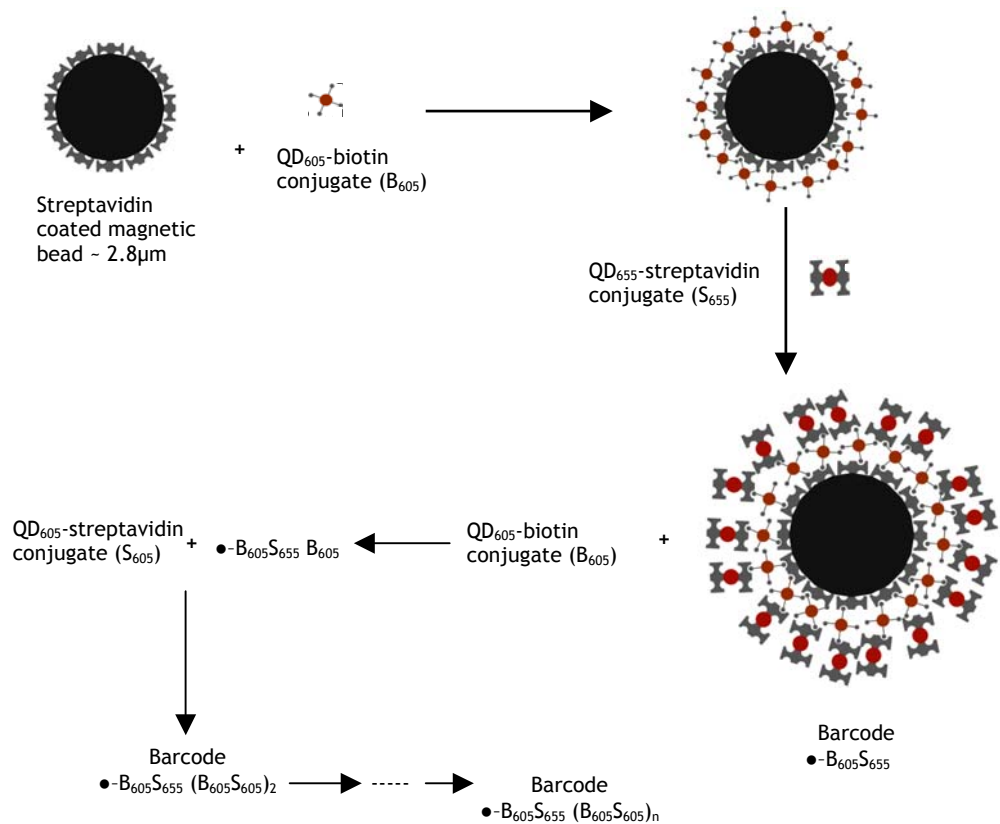
Scheme 2-3: Schematic representation of immobilisation of QD₅₂₅-streptavidin (S₅₂₅) conjugate and QD₆₅₅-biotin conjugate (B₆₅₅) using layer-by-layer biological self-assembly. Figures are not to scale.

cleaned by sonication in 5% vol/vol solution of Decon 90 for 15 min and then rinsed exhaustively with water and finally dried with nitrogen gas. To form an amino-terminated layer on the glass slides (**Scheme 2-3**), the substrates were immersed in a 3 vol% solution of 3-(aminopropyl)triethoxysilane (APTES) in 95% ethanol for 2h and thoroughly rinsed with ethanol and dried with nitrogen gas. The samples were further dried in an oven at 120°C for half an hour. After this, the samples were incubated in a solution of NHS-Biotin (1 mg/ml) for two hours. The solution of NHS-Biotin was prepared in 10mM phosphate buffer pH 7.4. After incubation in NHS-biotin, samples were rinsed with buffer and incubated in 0.15 % solution of bovine serum albumin (BSA) for half an hour. This step was used to block the non-specific adsorption of quantum dot conjugates. Samples were then incubated in 10 nM solution of QD₅₂₅-streptavidin conjugate (S₅₂₅) or QD₆₅₅-streptavidin for one hour. After washing with buffer, samples were incubated in 10 nM solution of QD₆₅₅-biotin (B₆₅₅) solution for one hour to make two layers of quantum dots as shown in **Scheme 2-3**. In this way, 2,4,6,8,10 layers of QD-streptavidin and QD-biotin conjugates were prepared.

2.2.3. Layer-by-Layer Assembly of QD-Biotin and QD-Streptavidin Conjugates onto Magnetic Beads

For making the first layer of QD₆₀₅-biotin conjugate (B₆₀₅), 2µl of streptavidin coated magnetic beads (●-) ($\cong 1.4 \times 10^6$ beads) from stock solution were added to 300µl of 10mM phosphate buffer pH 7.4 containing 0.15% BSA. To this, 2µl of B₆₀₅ conjugate was added from the stock solution (2.2µM) and incubated for one hour, agitated using a vortex mixer at a low speed (**Scheme 2-4**). After one hour, magnetic beads were separated from the quantum dot suspension using MagnaRack. The use of magnetic beads made it easy to separate the beads from the unreacted reagent using MagnaRack. It also made washing steps easier and faster as compared to the separation and washing using centrifugation. The beads were washed four times with the same PBS to remove any non-specifically adsorbed B₆₀₅ conjugate, and then were re-suspended in 300µl of PBS buffer containing 0.15% BSA. These beads were named ●-B₆₀₅.

In order to deposit an additional layer of quantum dots, 4µl of QD₆₅₅-streptavidin (S₆₅₅) conjugate (1µM stock) was added to the bead suspension and incubated for one hour. After separation, beads were washed four times with PBS



Scheme 2-4: Barcode production using biological self-assembly of quantum dot-biotin and quantum dot-streptavidin conjugates.

containing 0.15% BSA and re-suspended in 300 μ l of the same buffer to make the first barcode \bullet -B₆₀₅S₆₅₅. To make subsequent layers of quantum dots, magnetic beads containing \bullet -B₆₀₅S₆₅₅ were incubated in B₆₀₅ and QD₆₀₅-streptavidin (S₆₀₅) conjugates. **Scheme 2-4** shows how the assembly process was performed illustrating the creation of \bullet -B₆₀₅S₆₅₅, \bullet -B₆₀₅S₆₅₅(B₆₀₅S₆₀₅)₁, \bullet -B₆₀₅S₆₅₅(B₆₀₅S₆₀₅)₂ and to \bullet -B₆₀₅S₆₅₅(B₆₀₅S₆₀₅)_n. In this manner, using the layer-by-layer assembly of streptavidin-biotin, \bullet -B₆₀₅S₆₅₅, \bullet -B₆₀₅S₆₅₅(B₆₀₅S₆₀₅)₁ and \bullet -B₆₀₅S₆₅₅(B₆₀₅S₆₀₅)₂ barcodes were prepared. The barcodes prepared above were then stored at 4°C in PBS containing 0.15% BSA for further use. The use of BSA helps to stabilise the quantum dot conjugates immobilised onto the

magnetic beads. These barcodes were characterised using single bead fluorescence spectroscopy.

2.2.3.1. Comparison of Quantum Dot Conjugates Prepared with and without using a PEG-Linker for the Production of Quantum Dot Barcodes

As stated, two types of quantum dot streptavidin conjugates were purchased from Invitrogen. The QD-streptavidin conjugates described in **Section 2.2.1, 2.2.2 and 2.2.3** were prepared by covalently attaching streptavidin to the amphiphilic coating (a polymer coating) on the CdSe/ZnS quantum dots using a PEG-linker as a spacer between CdSe/ZnS and streptavidin. The other streptavidin conjugates were QD₆₅₅ ITK™-streptavidin conjugate and QD₆₀₅ ITK™-streptavidin conjugate which were also purchased from invitrogen. In these latter types of quantum dot-streptavidin conjugates, streptavidin is covalently attached to the amphiphilic coating on the quantum dots directly without the use of a PEG-linker. The **Scheme 2-4** was used to prepare the barcodes using these quantum dot conjugates. Two types of barcodes were prepared i.e. ●-B₆₀₅S*₆₅₅ and ●-B₆₅₅S*₆₀₅ where S*₆₅₅ is QD₆₅₅ ITK™-streptavidin conjugate and S*₆₀₅ is QD₆₀₅ ITK™-streptavidin conjugate. The fluorescence properties of these barcodes were studied using single bead fluorescence spectroscopy and compared with the barcodes prepared in **Section 2.2.3**.

2.3. X-Ray Photoelectron Spectroscopy (XPS)

XPS or electron spectroscopy for chemical analysis (ESCA) was used to confirm the immobilisation of CdSe/ZnS quantum dots onto the glass substrate. **Figure 2-1** shows the schematic of different components of XPS set-up and Scientia ESCA 300 spectrometer used in these experiments.

All the samples for XPS analysis were prepared on -1×1 cm² glass slides and stored in vacuum desiccator before taking measurements. All the XPS spectra were taken using the high resolution Scientia ESCA 300 spectrometer at Daresbury laboratories, UK. The Al K α radiation is provided with a rotating anode source and is focussed on the samples at a take off angle (TOA) of 45° after passing through the monochromators.^(6, 7) To study the immobilisation of CdSe/ZnS quantum dots on the glass substrates using dithiol chemistry,

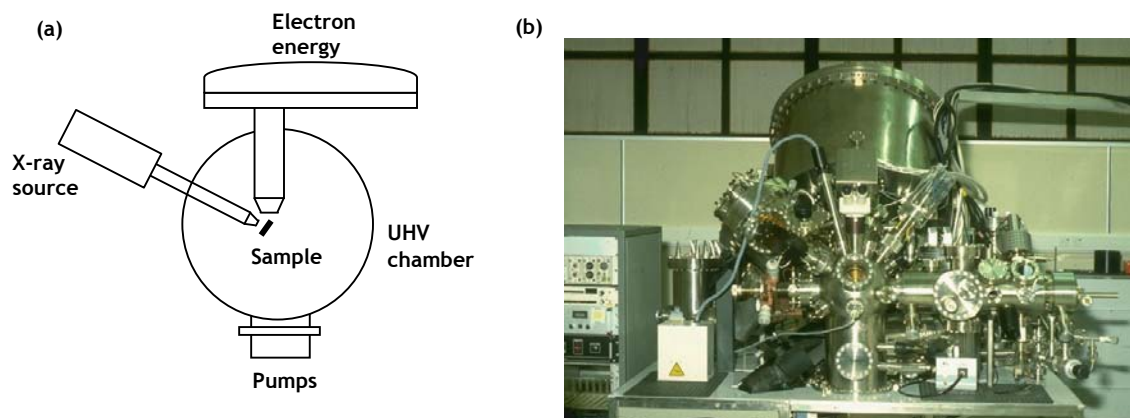


Figure 2-1: (a) Schematic of an XPS set up shows X-ray source for the production of X-rays and detector to measure kinetic energy and number of electrons (reproduced from (8)); (b) Photograph of Scienta ESCA 300 used in the current experiments.

in addition to the survey spectra for each sample, C(1s), N(1s), S(2p), Cd(3d) and Zn(2p) high resolution XPS spectra were also measured. Similarly for immobilisation of CdSe/ZnS quantum dots using biotin-streptavidin interaction, C(1s), N(1s), Cd(3d) and Zn(2p) high resolution XPS spectra were measured in addition to the survey scan for each sample. The slit width (0.8 mm) and channel resolution (0.05 eV) were kept constant in all the samples. All spectra were adjusted for an offset due to the flood gun by assigning 285 eV to the main C–H peak in the C(1s) spectrum as a reference.⁽⁷⁾ The deconvolution of the S(2p) peaks was performed using CasaXPS software, Casa Software Limited. When deconvoluting the S(2p) peaks, different sulphur species are present as doublets. The doublet appears as a consequence of the known 2:1 ratio of S(2p_{1/2}) and S(2p_{3/2}) spin orbit states.^(9, 10) The known binding energy difference between these spin orbit states is 1.18 eV.⁽⁹⁾ These values are used as constrained input parameters to the software during the deconvolution of the S(2p) peaks.

2.4. Fluorescence Spectroscopy Measurements

For fluorescence measurements, a Nikon microscope (Microphot-SA) (NA=0.85, 40× objective) was coupled with a Triax 320 spectrometer (Jobin Yvon) equipped with a symphony CCD detector, **Figure 2-2**. A true colour CoolSnap CCD camera was used to acquire optical images. The filter sets used for fluorescence measurements were from Nikon, and are listed in **Table 2-1**.

Figure 2-2 shows the experimental set-up with a variable aperture. When the aperture was fully closed, it produces a spot size of ~50µm diameter of excitation light. For the measurement of fluorescence signal from the quantum dots immobilised on the glass substrates, the aperture was closed and quantum dots were excited using filter set UV-2A and spectra were collected using the spectrometer with 0.1s acquisition time. In case of each layer assembly n=5 measurements were taken. Where “n” is the number of measurements taken on one sample at different places.

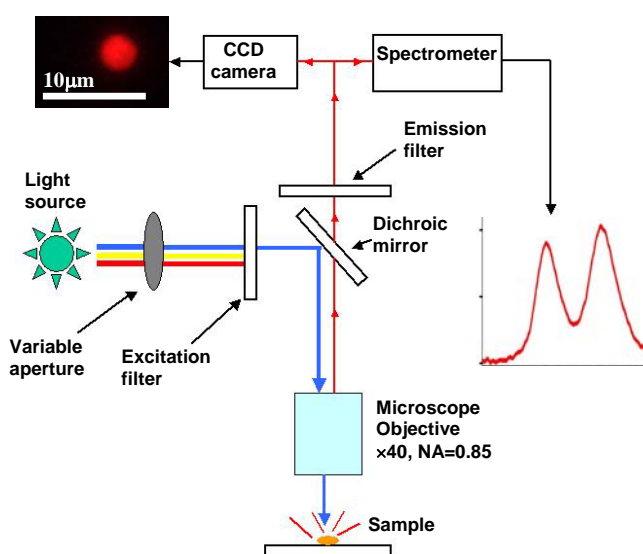


Figure 2-2: Schematic diagram of fluorescence measurement configuration used for single bead fluorescence spectroscopy.

Filter set	Exc.filter (nm)	Dichroic mirror (nm)	Em. Filter (nm)
UV-2A	330-380	400	420 long pass
B-2A	450-490	500	(i) 515 long pass or (ii) 500-550 band pass (Omega optical)
G-2A	510-560	565	590 long pass

Table 2-1: Shows the filter set combinations used for the fluorescence spectroscopy measurements.

For single bead fluorescence measurements, a single bead was focussed using the true colour CCD camera image in the middle of the 50 μ m spot of excitation light and spectra were measured by using the spectrometer with an acquisition time of 1s.

In this study, fluorescence intensity ratios of different quantum dots in a barcode were used to identify different barcodes. For the barcodes \bullet -B₆₀₅S₆₅₅, \bullet -B₆₀₅S₆₅₅(B₆₀₅S₆₀₅)₁, \bullet -B₆₀₅S₆₅₅(B₆₀₅S₆₀₅)₂ prepared in Section 2.2.3, after measuring the single bead fluorescence spectra of these barcodes, the ratio of QD₆₀₅ to QD₆₅₅ fluorescence intensity was determined for each barcode at 605 nm and 655 nm, respectively. These fluorescence intensity ratios were plotted against the number of counts (number of beads) of the barcodes in case of each barcode preparation.

For the detection of fluorescein isothiocyanate (FITC), B-2A filter set with a band pass filter (500-550 nm, Omega optical) was used to distinguish between the FITC and non-FITC labelled barcodes. Fluorescence micrographs were collected using a true colour CCD camera.

2.4.1. Measurement of Number of Quantum Dots

The number of quantum dots per bead was calculated from fluorescence emission intensities before and after incubation with magnetic beads, using Eq.2-1 and Eq.2-2.⁽¹¹⁾

$$L_b = (I_o - I_r) / I_o \cdot [L_o] \quad \text{Eq. 2-1}$$

$$\text{Number of quantum dots/bead} = (L_b \cdot N_A) / n \quad \text{Eq. 2-2}$$

Where L_b is the concentration of quantum dots bound to the beads, I_o and I_r are the background corrected fluorescence intensities of quantum dots before and after incubation with the bead suspension, respectively. L_o is the initial concentration of quantum dots, N_A is the Avogadro's number and n is the number of beads per litre.

2.5. Stability Studies of Quantum Dot Barcodes Prepared using Layer-by-Layer Assembly of QD-Biotin and QD-Streptavidin Conjugates onto Magnetic Beads

The stability studies of quantum dot barcodes prepared in Section 2.2.3 were carried out in terms of thermal stability, stability in biotin solution and long term stability of the barcodes. The procedure for these studies is detailed below.

2.5.1. Thermal Stability

The information concerning the thermal stability of the barcodes is important for their use in different applications involving prolonged storage or applications at higher temperatures. For thermal stability studies, barcode $\bullet\text{-B}_{605}\text{S}_{655}(\text{B}_{605}\text{S}_{605})_1$ was chosen. The barcode $\bullet\text{-B}_{605}\text{S}_{655}(\text{B}_{605}\text{S}_{605})_1$ was prepared as described in Section 2.2.3. First, single bead fluorescence spectroscopy was performed to measure the fluorescence intensity ratio of the barcoded beads before heat treatment and then these barcoded beads were treated at an elevated temperature (95°C) for 15 min in the PBS containing 0.15% BSA. For heat treatment, a beaker with de-ionised water was heated to the desired temperature and an eppendorf tube containing PBS buffer with 0.15% BSA was immersed in the beaker. At this point, the barcoded magnetic beads $\bullet\text{-B}_{605}\text{S}_{655}(\text{B}_{605}\text{S}_{605})_1$ were added to the PBS buffer containing 0.15% BSA and treated for 15 min. After this the eppendorff tube was allowed to cool and kept at 4°C before performing the single bead fluorescence measurements and measuring the fluorescence intensity ratios.

2.5.2. Stability in Biotin Solutions

The quantum dot barcodes in Section 2.2.3 were prepared using the biotin-streptavidin interaction of QD-biotin and QD-streptavidin conjugates onto streptavidin coated magentic beads using a layer-by-layer assembly approach. Stability studies in a biotin solution helps to understand the disassociation behaviour of these assemblies. For this purpose barcode $\bullet\text{-B}_{655}\text{S}_{605}(\text{B}_{605}\text{S}_{605})_1$ was selected. This barcode has inner layer of QD₆₆₅-biotin conjugate and QD₆₀₅-streptavidin, QD₆₀₅-biotin and QD₆₀₅-streptavidin as the outer layers. This enable us to study the unwinding of the barcode down to the last layer of the barcode using fluorescence intensity ratio (QD₆₀₅ to QD₆₅₅) measurements.

After the preparation of the barcoded beads in 300 μ l PBS buffer with 0.15% BSA, they were divided into five equal portions i.e. 60 μ l in each of five eppendorf tubes. A stock solution of 100mM biotin was prepared separately in PBS containing 0.15% BSA. From each eppendorf tube, 60 μ l of buffer was removed after collecting the beads using MagnaRack. To these five different samples, an appropriate amount of biotin stock solution (100 mM) was added to make 300 μ l total volume having biotin concentrations of 0, 1, 10, 50 and 100 mM. The total volume was made upto 300 μ l using PBS buffer with 0.15 %BSA. To the sample tube with 0 mM biotin, only 300 μ l of PBS buffer with 0.15% BSA was added. These five different samples were incubated at room temperature for 1400 min. The fluorescence intensity ratio (QD₆₀₅ to QD₆₅₅) was measured using single bead fluorescence spectroscopy for 100 beads for each sample and data was plotted as a histogram. In another experiment, the barcode $\bullet\text{-B}_{655}\text{S}_{605}(\text{B}_{605}\text{S}_{605})_1$ was incubated for different time intervals from 0, 50, 200, 600, 1000, 1400 min in 100mM biotin solution at 37°C. The fluorescence intensity ratios for all the samples were measured and plotted as a histogram (100 bead samples were measured in each case).

2.5.3. Long-Term Stability

The long-term stability of the barcode is an important parameter which indicates the shelf life of the barcodes. For these studies, barcode $\bullet\text{-B}_{605}\text{S}_{655}(\text{B}_{605}\text{S}_{605})_1$ was chosen. After the preparation of this barcode, the sample was divided into three equal portions. The first portion was used to measure the fluorescence intensity ratio of this barcode after the preparation and the second and third portions were stored at 4°C in PBS buffer containing 0.15% BSA for two months and ten months, respectively. After two months,

fluorescence intensity ratios were measured using single bead fluorescence spectroscopy and the data was plotted as a histogram for 100 beads. After 10 months, the third portion was taken out and fluorescence intensity ratios were measured using single bead fluorescence spectroscopy.

2.6. Application of Quantum Dot Barcodes to Multiplexed Immunoassays

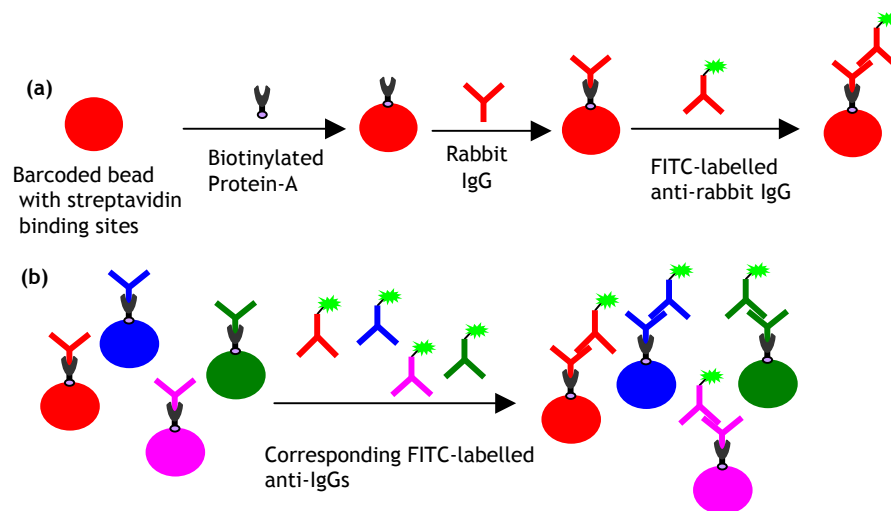
2.6.1. Materials

In addition to the materials used for the preparation of the barcodes described in **Section 2.2.1**, the detail of the materials used for performing multiplexed immunoassays is given below. Rabbit IgG, human IgG, mouse IgG and goat IgG were all polyclonal antibodies and were of reagent grade, purchased from Sigma-Aldrich, UK. Protein A-biotin, protein G-biotin and IgG free bovine serum albumin (BSA) were purchased from Sigma-Aldrich, UK. Fluorescein isothiocyanate (FITC) labelled anti-goat IgG whole molecule developed in rabbit, anti-mouse IgG (Fab specific), anti-human IgG whole molecule developed in goat were purchased from Sigma-Aldrich. FITC-labelled anti-rabbit IgG was purchased from Dako, UK.

Three different PBS buffers were used. PBS buffer without BSA, PBS with 0.15% BSA and PBS with 2% BSA. Aliquots of all IgGs, anti-IgG-FITC's, protein A-biotin and protein G-biotin were prepared in PBS using flash freezing with liquid nitrogen before being stored at -20°C. Before using, aliquots were equilibrated at room temperature.

2.6.2. Multiplexed Immunoassay using FITC-Labelled Anti-IgGs

As described in **Section 2.2.1**, different barcodes were prepared such that each barcode had a streptavidin as an outer layer, available for the binding of any biotinylated antibody. These biotin-binding sites can be used to immobilise different IgGs on the barcoded beads. In this type of multiplexed immunoassay, an FITC-labelled anti-IgG was used for detection. Four different barcodes were prepared to perform multiplexed immunoassay, namely, ●-B₆₀₅S₆₅₅, ●-B₆₀₅S₆₅₅(B₆₀₅S₆₀₅)₁, ●-B₆₀₅S₆₀₅ and ●-B₆₀₅S₅₆₅. **Scheme 2-5** shows the immunoassay scheme for a single IgG and for a solution containing four different IgGs. Following steps were followed to perform the multiplexed immunoassay.



Scheme 2-5: (a) Immunoassay scheme for a single rabbit IgG-anti-rabbit IgG pair; (b) Multiplexed immunoassay scheme showing rabbit IgG (red), human IgG (blue), mouse IgG (pink) and goat IgG (green) immobilised on barcoded beads. A cocktail of four anti-IgGs (rabbit, human, mouse, and goat) labelled with FITC (light green) is added to the mixture. Note that false colours are used to represent different barcoded beads and figures are not to scale.

2.6.2.1. Immobilisation of Protein A-Biotin or Protein G-Biotin

Protein A-biotin was immobilised on barcode ●-B₆₀₅S₆₅₅, ●-B₆₀₅S₆₅₅(B₆₀₅S₆₀₅)₁ and ●-B₆₀₅S₆₀₅. Briefly, 50µl (~2.3 × 10⁵ beads) from a 300µl barcode stock was added to an eppendorff tube. The barcoded beads were collected using MagnaRack and PBS buffer was discarded. To this, a 150µl aliquot of protein A-biotin (1mg/ml) was added and incubated for 45 min. The beads were agitated every 5-10 min using a pipette in order to ensure the mixing of barcoded beads in protein A-biotin solution. After this the barcodes were collected using MagnaRack and excess of protein A-biotin was removed. After washing, with the PBS, these barcoded beads were redispersed in 100µl PBS. A similar procedure was used for the immobilisation of protein G-biotin on the barcode ●-B₆₀₅S₅₆₅.

2.6.2.2. Immobilisation of Different Immunoglobulins (IgGs)

The barcoded beads ●-B₆₀₅S₆₅₅ , ●-B₆₀₅S₆₅₅(B₆₀₅S₆₀₅)₁ and ●-B₆₀₅S₆₀₅ with protein A-biotin were used for the immobilisation of rabbit IgG, human IgG and mouse IgG, respectively. The barcoded beads with protein A-biotin were collected by using MagnaRack and PBS buffer was discarded. To the barcoded beads ●-B₆₀₅S₆₅₅ , ●-B₆₀₅S₆₅₅(B₆₀₅S₆₀₅)₁ and ●-B₆₀₅S₆₀₅, onto which protein A-biotin had been immobilised, 300µl of rabbit IgG (1mg/ml), human IgG (1mg/ml) and mouse IgG (1mg/ml) were added respectively and incubated for 45 min. These barcoded beads were mixed every 5-10 min using a pipette. These barcodes were then washed exhaustively to remove excess of IgGs using PBS which contain 2% BSA. The same procedure was followed to immobilise goat IgG (1mg/ml) on the barcode ●-B₆₀₅S₅₆₅ using protein G-biotin. At this point a specific IgG had been bound to each of the different barcodes.

2.6.2.3. Detection of Different IgGs

The barcoded beads containing different IgGs were mixed in an equal proportion and collected using MagnaRack. This mixture was then redispersed in 300µl of PBS buffer containing 2% BSA. Equal concentration (1.5 mg/ml) of stock solutions of all four FITC-labelled anti-IgGs (anti-rabbit IgG-FITC, anti-human IgG-FITC, anti-mouse IgG-FITC and anti-goat IgG-FITC) were made. In the first assay, a cocktail (40µl) of four FITC-labelled anti-IgGs (10µl from each) was added to this mixture and incubated for 45 min in the dark by using a vortex mixer at a low speed. After this the beads were washed exhaustively with PBS containing 2% BSA to remove excess of FITC-labelled anti-IgGs. In a second assay, the procedure of the immunoassay was the same but anti-mouse IgG-FITC was not added to the cocktail whilst other three FITC-labelled anti-IgGs (anti-goat IgG , anti-human IgG and anti-rabbit IgG) were added. In a third assay, anti-human IgG-FITC was not added to the mixture and other three FITC-labelled anti-IgGs (anti-goat IgG , anti-mouse IgG and anti-rabbit IgG) were added. These beads were then analysed using single bead fluorescence spectroscopy.

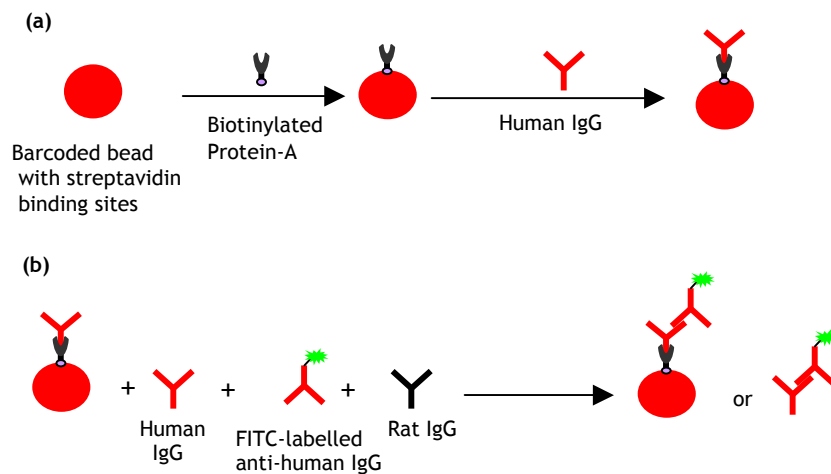
2.7. Binding Inhibition Immunoassay

In this immunoassay, FITC-labelled anti-human IgG was used as the detection antibodies to detect human IgG in solution. To perform this assay barcode ●-B₆₀₅S₆₅₅ was prepared using the same method as outlined in Section 2.2.1. After the preparation of this barcode, the barcoded beads were re-dispersed in 300µl of PBS buffer containing

0.15% BSA. The strategy for performing the assay is shown in **Scheme 2-6**. Following steps were followed to perform the immunoassay for human IgG quantification.

2.7.1. Immobilisation of Protein A-biotin

Briefly, 150µl ($\cong 7.0 \times 10^5$ beads) from a 300µl barcode stock was added to an eppendorff tube. The barcoded beads were collected using MagnaRack and PBS buffer was discarded. To this, a 450µl aliquot of protein A-biotin (1mg/ml) was added and incubated for 45 min, **Scheme 2-6a**. The beads were agitated every 5-10 min using a pipette in order to ensure the mixing of barcoded beads in protein A-biotin solution. After this the barcodes were collected using MagnaRack and excess of protein A-biotin was removed. After washing with the PBS containing 0.15% BSA, these barcoded beads were redispersed in 150µl PBS containing 0.15% BSA.



Scheme 2-6: Binding inhibition immunoassay of human IgG: (a) immobilisation of human IgG on the barcode \bullet -B₆₀₅S₆₅₅ using protein A-biotin; (b) Binding inhibition immunoassay scheme for human IgG. Different amounts of human IgG were added in the presence of fixed amounts of barcoded beads containing immobilised human IgG, FITC-labelled anti-human IgG and rat IgG.

2.7.2. Immobilisation of Human IgG onto Barcode ●-B₆₀₅S₆₅₅

The barcoded beads ●-B₆₀₅S₆₅₅ with protein A-biotin were used for the immobilisation of human IgG. These beads with protein A-biotin were collected by using MagnaRack and PBS buffer was discarded. To the barcoded beads ●-B₆₀₅S₆₅₅ containing protein A-biotin, 300µl of human IgG (3 mg/ml) was added and incubated for 45 min. These barcoded beads were mixed every 5-10 min using a pipette. As before, these barcodes were then washed exhaustively to remove excess of IgG using PBS which contain 2% BSA and redispersed in 300µl of the same buffer. At this point human IgG had been bound to the barcode ●-B₆₀₅S₆₅₅.

2.7.3. Optimisation of FITC Labelled Anti-Human IgG

The barcoded beads (●-B₆₀₅S₆₅₅) containing human IgG were incubated with different amounts of FITC-labelled anti-human IgG. Briefly, from 300µl of the barcoded beads containing human IgG, 40µl ($\approx 9.3 \times 10^4$ beads) were added in seven different eppendorf tubes. In each of the eppendorf tubes, different amounts of FITC labelled anti-human IgG were added and volume was made upto 200µl using PBS pH 7.4 containing 2% BSA in each eppendorf. This reaction mixture was incubated for 45 min. After this the beads were washed using the same buffer and analysed using single bead fluorescence spectroscopy.

2.7.4. Calibration Curve for the Determination of Human IgG in Solution

After optimisation of FITC-labelled anti-human IgG concentration, binding inhibition immunoassay was performed for the quantification of human IgG. The barcoded beads ($\approx 9.3 \times 10^4$ in each reaction mixture) were incubated with different concentrations of human IgG (0.5, 1, 5, 10, 20, 30 µg/ml) and fixed concentration of anti-human IgG-FITC (20µg/ml) and rat IgG (0.5 µg/ml) in the presence of PBS pH 7.4 containing 2% BSA and agitated for 45 min using a vortex mixer at a low speed. The beads were then washed exhaustively to remove excess of reagents using PBS pH 7.4 containing 2% BSA and re-dispersed in the same buffer. The beads were then analysed using single bead fluorescence spectroscopy.

2.8. References

1. Zhou DJ, Bruckbauer A, Abell C, Klenerman D, Kang DJ. Fabrication of three-dimensional surface structures with highly fluorescent quantum dots by surface-templated layer-by-layer assembly. *Advanced Materials* 2005;17(10):1243-+.
2. Goss CA, Charych DH, Majda M. Application of (3-Mercaptopropyl)Trimethoxysilane as a Molecular Adhesive in the Fabrication of Vapor-Deposited Gold Electrodes on Glass Substrates. *Analytical Chemistry* 1991;63(1):85-88.
3. Pacifico J, Jasieniak J, Gomez DE, Mulvaney P. Tunable D-3 Arrays of quantum dots: Synthesis and luminescence properties. *Small* 2006;2(2):199-203.
4. Qdot® Streptavidin Conjugates user manual. Invitrogen 2007.
5. Qdot® Biotin Conjugates user Manual. Invitrogen 2006.
6. Jiang L, Glidle A, Griffith A, McNeil CJ, Cooper JM. Characterising the formation of a bioelectrochemical interface at a self-assembled monolayer using X-ray photoelectron spectroscopy. *Bioelectrochemistry and Bioenergetics* 1997;42(1):15-23.
7. Glidle A, Yasukawa T, Hadyoon CS, Anicet N, Matsue T, Nomura M, et al. Analysis of protein adsorption and binding at biosensor polymer interfaces using X-ray photon spectroscopy and scanning electrochemical microscopy. *Analytical Chemistry* 2003;75(11):2559-2570.
8. http://www.chem.qmul.ac.uk/surfaces/scc/scat5_3.htm.
9. Romano EJ, Schulz KH. A XPS investigation of SO₂ adsorption on ceria-zirconia mixed-metal oxides. *Applied Surface Science* 2005;246(1-3):262-270.
10. Jun S, Jang EJ, Chung YS. Alkyl thiols as a sulfur precursor for the preparation of monodisperse metal sulfide nanostructures. *Nanotechnology* 2006;17(19):4806-4810.
11. Wu Y, Campos SK, Lopez GP, Ozbun MA, Sklar LA, Buranda T. The development of quantum dot calibration beads and quantitative multicolor bioassays in flow cytometry and microscopy. *Analytical Biochemistry* 2007;364(2):180-192.

Chapter 3

Layer-by-Layer Assembly of Quantum Dots

As described earlier in **Chapter 1**, the aim of work in this thesis is the immobilisation of quantum dots using layer-by-layer methodology to make a sequence of shells of quantum dots around the magnetic beads to produce a quantum dot encoded system. This chapter is concerned with the underpinning studies concerning the immobilisation of quantum dots onto solid substrates to characterise two different immobilisation strategies. The surfaces are characterised using X-ray photoelectron spectroscopy and fluorescence spectroscopy. Two approaches were used to make the multilayer assemblies. In the first approach, a dithiol linker was used to make multilayers of CdSe/ZnS quantum dots onto a glass substrate and magnetic beads. In the second approach, biotin and streptavidin conjugated CdSe/ZnS quantum dots were used to make multilayers of quantum dots onto a glass substrate. The experiments relating to the immobilisation of biotin and streptavidin conjugated quantum dots onto the magnetic beads is discussed in **Chapter 4**.

3.1. Layer-by-Layer Assembly of Quantum Dots onto Glass Substrates using a Dithiol Linker

Detailed descriptions of the basic Materials and Methods are provided in **Section**

2.1.2. For using a dithiol linker (1,9-nonanedithiol) to perform layer-by-layer assembly of quantum dots, the following procedure was adopted. First the glass substrates were cleaned by sonication in 5% vol/vol solution of Decon 90. A layer of (3-mercaptopropyl)trimethoxysilane (MPTS) was first immobilised on the glass substrate.⁽¹⁾ This layer provided thiol (-SH) functional groups for the binding of quantum dots. Next the glass slides were incubated into solution of quantum dots to make first layer of quantum dots onto the glass substrate. For making multilayers of quantum dots onto the substrate, the glass substrate was incubated in an ethanolic solution of 1,9-nonanedithiol. 1,9-nonanedithiol contains two terminal thiol groups, one at each end. One thiol (-SH) binds to the quantum dots onto the glass substrate leaving the second thiol functional group (-SH) for subsequent deposition of second layer of quantum dots as illustrated in **Scheme 2-1**. The above steps were repeated to make ten layers of quantum dots onto the glass substrate.

3.1.1. X-Ray Photoelectron Spectroscopy (XPS)

X-ray photoelectron spectroscopy was used to characterise the immobilisation of quantum dots onto the glass substrate. The principle of XPS or ESCA is based on the following conservation of energy equation, **Eq. 3-1**.

$$h\nu = E_b + E_{kin} \quad \text{Eq. 3-1}$$

“Where $h\nu$ is quantum energy, E_b the binding energy of the electron in the matter and E_{kin} the kinetic energy of the ejected electrons.”⁽²⁾ X-ray photoelectron spectroscopy involved “the measurement of kinetic energy of the inner or valence electron ejected by an incident photon with a known energy $h\nu$.”⁽²⁾ By knowing the values of $h\nu$ (determined by the X-ray source) and E_{kin} (measured experimentally), E_b which is a characteristic of chemical bonds in a compound, can be calculated. Binding energy values are specific for different elements and E_b can be used to identify different elements.

Figure 3-1 shows the XPS survey spectra of four different samples. **Figure 3-1a** shows the XPS survey spectrum of MPTS on the glass substrate. The presence of Si(2p), Si(2s), C(1s), O(1s) and S(2p) peaks in the spectrum confirmed the immobilisation of MPTS on the glass substrate. After the immobilisation of quantum dots onto the MPTS modified substrate, in addition to the previous peaks, a new set of peaks relating to Cd(3d), Se(3p),

Zn(2p_{3/2}), Zn(2p) appeared in the spectrum (Figure 3-1b) which confirmed the immobilisation of CdSe/ZnS quantum dots onto the MPTS modified glass substrate.

In the next step, the dithiol linker was immobilised on the monolayer of quantum dots (Figure 3-1c) and the second layer of quantum dots was immobilised on the dithiol modified quantum dot monolayer (Figure 3-1d). The ratio of Zn to C for the monolayer of

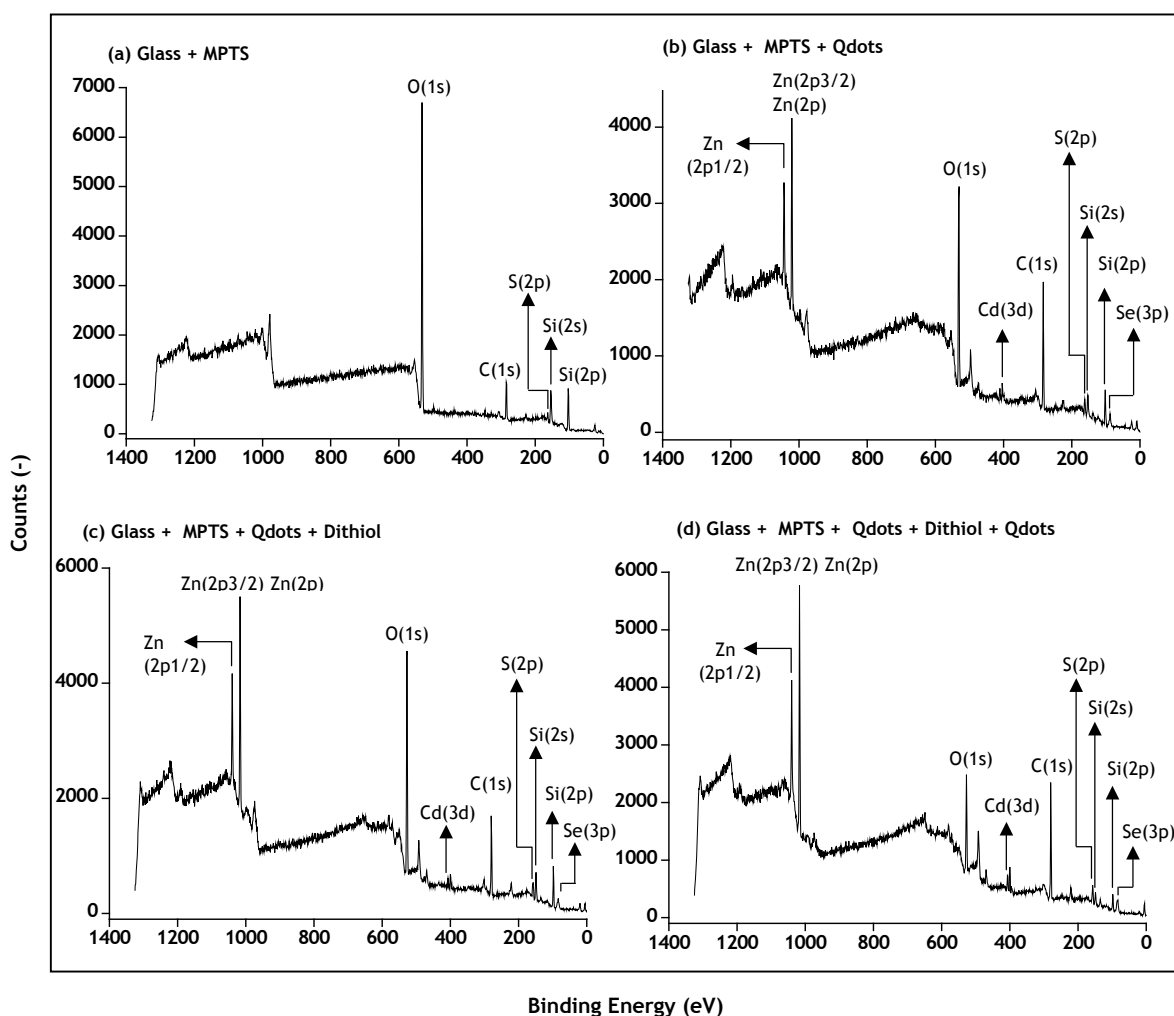


Figure 3-1: Comparison of XPS survey spectra of four different samples: (a) A layer of MPTS on glass; (b) Immobilisation of first layer of quantum dots onto MPTS modified glass substrate; (c) Immobilisation of dithiol linker on the monolayer of quantum dots immobilised by using MPTS; (d) Immobilisation of second layer of quantum dots onto dithiol modified substrate.

quantum dots is 2.0 and for the two layers of quantum dots it is 2.5, which indicates that the number of quantum dots increased after the second layer deposition. Ideally this value should be double than the first layer. The lower value may be due to the fact that in case of two layers of quantum dots, the photoelectrons generated in the inner layer of quantum dots lose their kinetic energy before reaching to the detector (the photoelectron escape depth is 5-10nm).⁽³⁾

For the attachment of quantum dots with the thiol (-SH) group from MPTS, high resolution XPS scans of S(2p) for the above four samples were taken (Figure 3-2). It can be

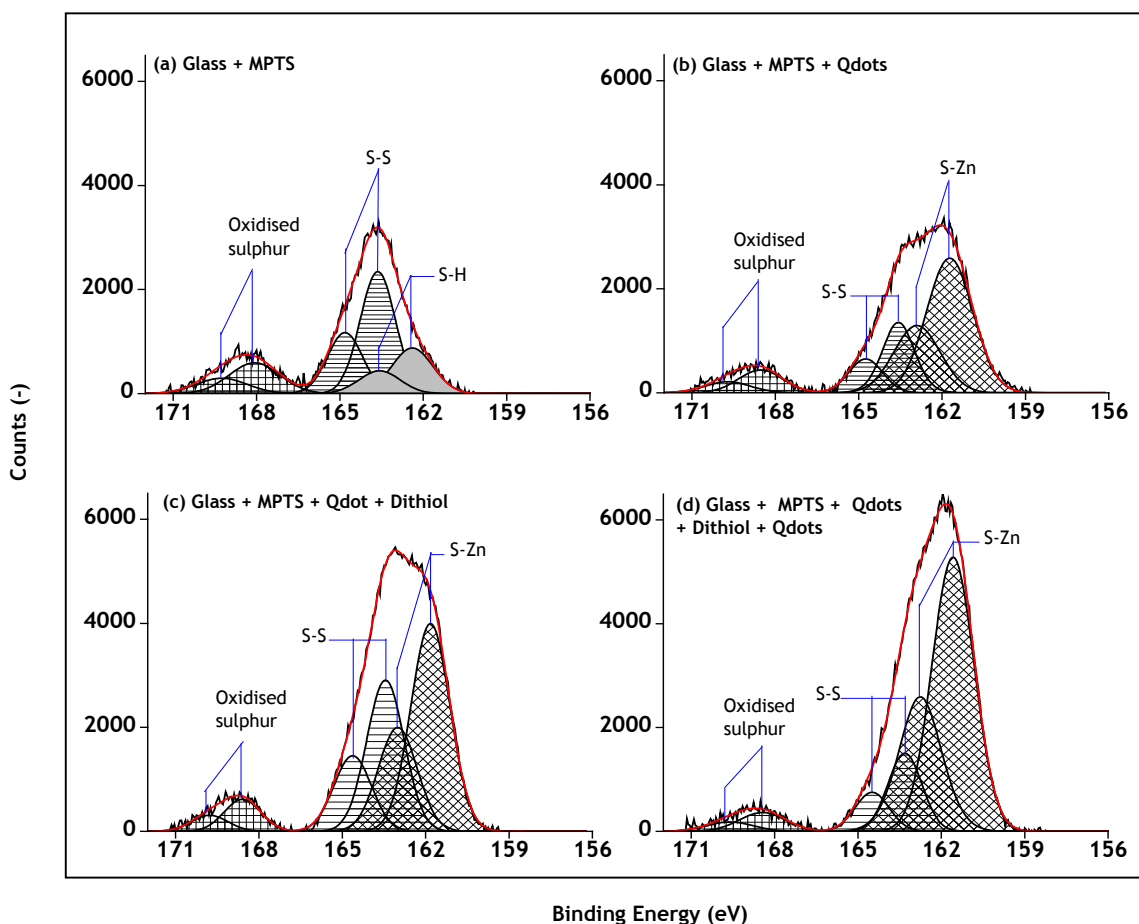


Figure 3-2: Comparison of S(2p) high resolution XPS spectra of: (a) A layer of MPTS on glass; (b) Immobilisation of first layer of quantum dots onto MPTS modified glass substrate; (c) Immobilisation of dithiol linker on the monolayer of quantum dots immobilised by using MPTS; (d) Immobilisation of second layer of quantum dots onto dithiol modified substrate.

seen that two S(2p) peaks appeared (**Figure 3-2a**). The main peak at 163.6 eV showed the presence of sulphur species from MPTS and the small peak at 168.5 eV showed the presence of oxidation of thiol (-SH) groups.⁽⁴⁾ The deconvolution of these peaks revealed the presence of two different species in the form of a pair of doublets at 162.3 eV and 163.6 eV. Each doublet was assigned after the deconvolution due to the known 2:1 ratio of S(2p_{1/2}) and S(2p_{3/2}) spin orbit states and by providing the value of their energy difference of 1.18 eV⁽⁵⁾ in the software. The doublet at 162.3 eV corresponds to the S-H and the doublet at 163.6 eV indicated the presence of (S-S) group.⁽⁶⁾

After the immobilisation of first layer of quantum dots (**Figure 3-2b**), the deconvolution of the S(2p) peaks indicated the presence of a doublet at 161.6 eV that can be assigned to the presence of S-Zn bonds⁽⁷⁾ in addition to the S-S doublet 163.6 eV and oxidised sulphur at 168.5 eV. Similar results have been reported in the case of silver deposition to the mercaptosilane layer.^(4, 8) After the deposition of dithiol linker on the monolayer of quantum dots, the same set of peaks was appeared again with a more contribution of S-S doublet as compared to S-Zn indicating the attachment of (-SH) to the quantum dots and the presence of free -SH groups (**Figure3-2c**).

When the second layer of quantum dots was immobilised, the deconvolution of the S(2p) peak revealed the same set of doublets with an increased contribution from the S-Zn doublet indicating the bonding of the second layer of quantum dots (S-Zn bonds). These studies support that the CdSe/ZnS quantum dots immobilised via layer-by-layer assembly.

Further, to confirm the immobilisation of quantum dots due to the presence of thiol groups on the glass substrate, a control experiment was carried out where the glass substrate, without prior modification using mercaptosilane, was incubated in a solution of quantum dots. **Figure 3-3** shows the high resolution XPS spectra of Zn(2p) in case of monolayer of quantum dots immobilised using MPTS and without using MPTS i.e. adsorption only. It can be seen that the signal from physisorbed quantum dots is five times smaller than when immobilisation is carried out using MPTS. Similar results were found when high resolution XPS spectra of Cd(3d) was compared for both samples (**Figure 3-4**).

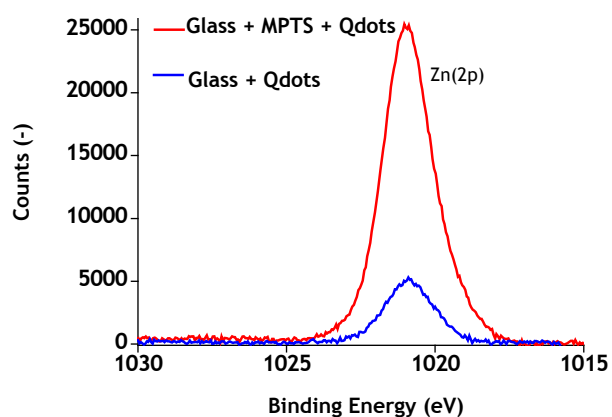


Figure 3-3: Comparison of Zn(2p) high resolution XPS spectra of quantum dots immobilised with or without using MPTS.

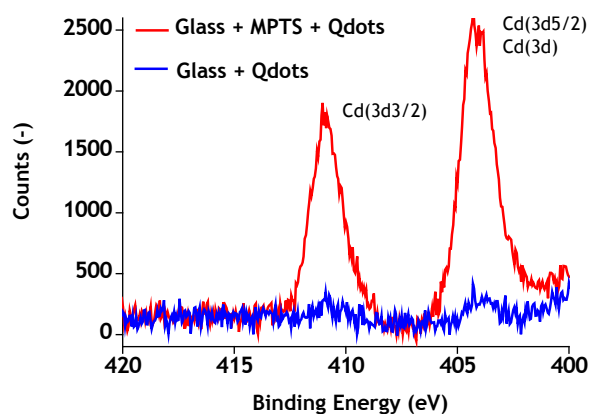


Figure 3-4: Comparison of Cd(3d) high resolution XPS spectra of quantum dots immobilised with or without using MPTS.

3.1.2. Fluorescence Spectroscopy

Thin films of different number of layers of quantum dots were prepared using the layer-by-layer assembly of quantum dots using a dithiol linker. Detailed Materials and Methods are described in Section 2.1.2. Figure 3-5 shows the fluorescence intensity plotted against number of layers of quantum dots. It can be seen that as the number of

layers increases the fluorescence intensity also increases. However, the increase in fluorescence is not linear after six layers. This may be due to the inner filter effect.⁽⁹⁾ This effect appears due to the absorption of the incident or excitation light before it reaches the point in the sample at which luminescence is observed and/or re-absorption of some of the emitted light, resulting in decrease in fluorescence intensity.⁽⁹⁾ Also, as the number of layers increased, the standard deviation of fluorescence measurements remained low, indicating that the quantum dot layer assemblies were uniform over the substrate.

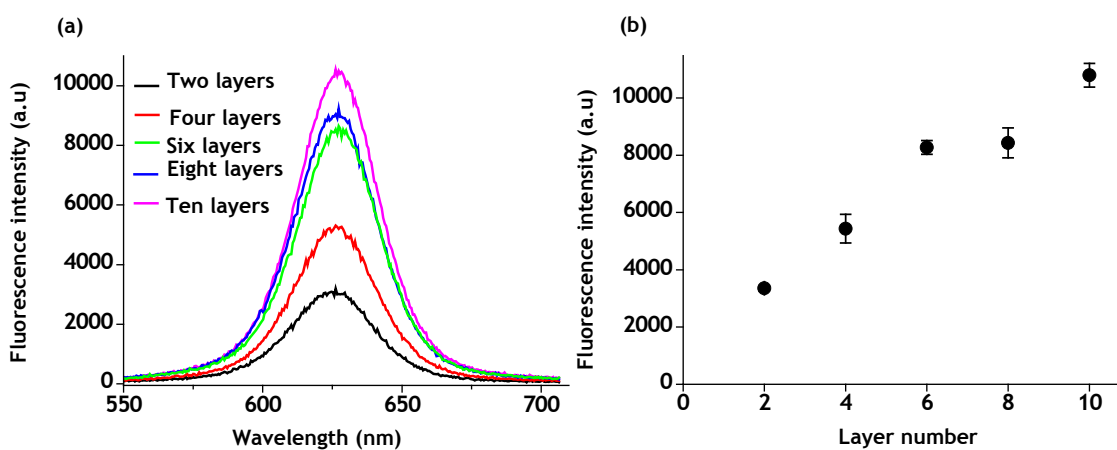


Figure 3-5: Layer-by-layer assemblies of CdSe/ZnS quantum dots (QD₆₂₆) onto glass substrate: (a) Fluorescence spectra of different layers of quantum dots onto the glass substrate; (b) Layer number vs Fluorescence intensity. The data points are the mean measurements and the error bars show the standard deviation for n=5 measurements in case of each layer assembly. Where “n” represents the number of measurements from a single sample in the case of each layer assembly. A UV-2A filter set was employed to excite the quantum dots in the UV-region using a mercury lamp and to collect the fluorescent signal. The UV-2A filter set consists of an excitation filter (330-380 nm), a dichroic mirror (cut-off wavelength 400 nm) and a 420 nm long-pass emission filter. The accumulation time was 0.1s in case of each measurement.

As a preliminary investigation prior to the development of barcode assemblies, described below, multicolour quantum dot multilayers were prepared using the same experimental procedure by immobilising quantum dot 626nm (QD₆₂₆) and quantum dot 555nm (QD₅₅₅) in an alternate fashion (**Figure 3-6**). Detailed descriptions of the Materials and Methods are provided in **Section 2.1.2**. Note that QD₅₅₅ was always the upper quantum dot layer in these assemblies and two layers refer to a first QD₆₂₆ layer and second QD₅₅₅ layer. Fluorescence emission spectra of these multilayers showed that signal from both types of quantum dots were increased as the number of layers increases. However, the increase in fluorescence is not linear in case of QD₅₅₅. This may be due to the inner filter effect as explained earlier.

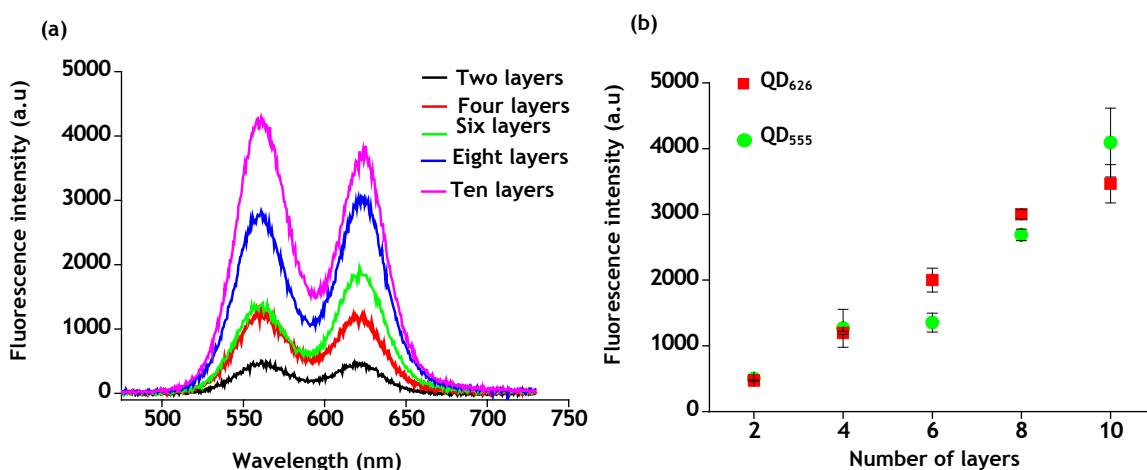


Figure 3-6: Layer-by-layer assemblies of QD₆₂₆ and QD₅₅₅ onto glass substrates: (a) Fluorescence spectra of different layers of quantum dots onto the glass substrate. Note that QD₅₅₅ is the outer layer in all the layer assemblies; (b) Layer number vs Fluorescence intensity. The data points are the mean measurements and the error bars show the standard deviation for n=5 measurements in case of each layer assembly. Where “n” represents the number of measurements from a single sample in the case of each layer assembly. A UV-2A filter set was employed to excite the quantum dots in the UV-region using a mercury lamp and to collect the fluorescent signal. The UV-2A filter set consists of an excitation filter (330-380 nm), a dichroic mirror (cut-off wavelength 400 nm) and a 420 nm long-pass emission filter. The accumulation time was 0.1s in case of each measurement.

3.2. Production of Quantum Dot Barcodes using a Dithiol Linker Via Layer-by-Layer Assembly onto Magnetic Beads

The above studies showed that mixed quantum dot layers can be assembled onto the glass slides. For the preparation of the barcodes onto magnetic beads, thiol (-SH) modified magnetic beads (1.0 μm)(●-) were used. Detailed descriptions of the Materials and Methods are provided in Section 2.1.3. The beads (●-) were incubated in a solution of quantum dot 626nm (QD₆₂₆) to make the first layer of quantum dots onto the magnetic bead surface (●-QD₆₂₆). To make a second layer of quantum dots these beads were then incubated in a solution of dithiol linker to introduce thiol groups on the bead surface so that the second layer of quantum dots could be attached to the bead surface. After the immobilisation of dithiol linker the beads were then incubated in quantum dot 555nm (QD₅₅₅) solution. After exhaustive washing, the beads (●-QD₆₂₆QD₅₅₅) were then incubated in 10 mM solution of cysteamine to introduce amine (-NH₂) groups on the bead surface in order to render them dispersible in water. This procedure was also used to render the completed barcode magnetic beads water dispersible. Two types of barcodes were prepared (●-QD₆₂₆) and (●-QD₆₂₆QD₅₅₅). The barcode (●-QD₆₂₆) has only one layer of quantum dots and the barcode (●-QD₆₂₆QD₅₅₅) has two layers of quantum dots. In case of barcode (●-QD₆₂₆QD₅₅₅), the first layer is QD₆₂₆ and the second or outer layer is QD₅₅₅. After the preparation, these barcodes were characterised using single bead fluorescence spectroscopy.

Figure 3-7 shows the fluorescence emission spectra of barcode (●-QD₆₂₆) and (●-QD₆₂₆QD₅₅₅). It can be seen that the barcode with a single colour (●-QD₆₂₆) can be recognised, however, a barcode with two layers of quantum dots did not give the fluorescence signal as expected. The signal related to QD₆₂₆, which is the underlying layer in this barcode did not appear in the spectrum. We hypothesised that this may be due to either the presence of the outer layer, which either quenches the inner layer signal and only the outer layer signal appeared or it may be due to the inner filter effect.⁽⁹⁾

To investigate this observation further, the barcoded beads (●-QD₆₂₆QD₅₅₅) were excited with two different excitation wavelengths. In addition to the excitation with a UV-2A filter set (UV excitation filter 330-380nm with a long pass emission filter 420nm), these beads were also excited with a G-2A filter set (green excitation filter 510-560 nm with a long pass emission filter 590nm). It can be seen (Figure 3-8) that the signal related to

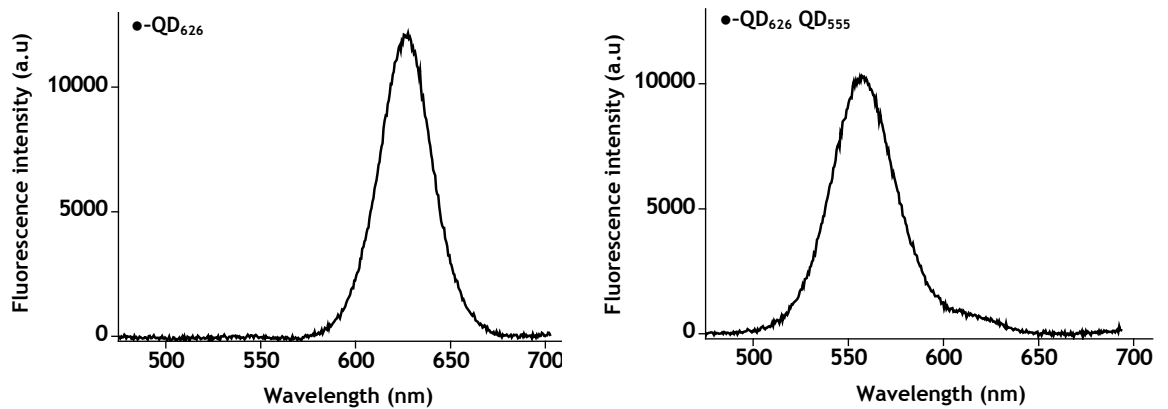
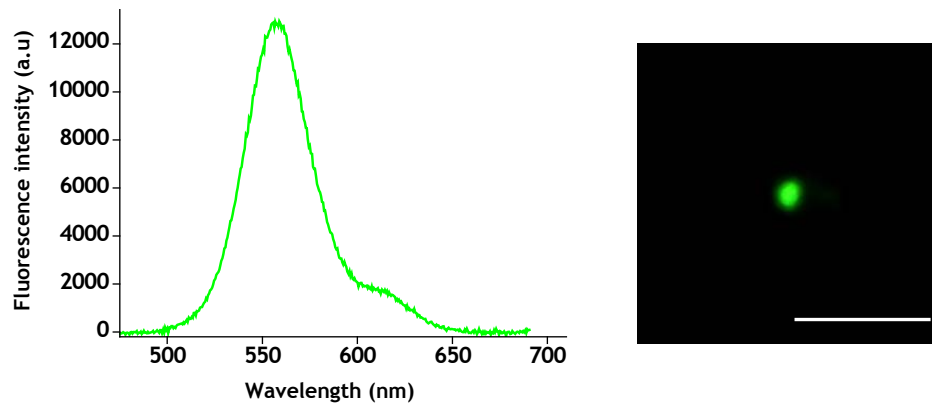


Figure 3-7: Single bead fluorescence spectra of barcode •-QD₆₂₆ (left) and barcode •-QD₆₂₆ QD₅₅₅ (right). A weak QD₆₂₆ signal appeared in the barcode •-QD₆₂₆QD₅₅₅. A UV-2A filter set was employed to excite the quantum dot encoded beads in the UV-region using a mercury lamp and to collect the fluorescent signal. The UV-2A filter set consists of an excitation filter (330-380 nm), a dichroic mirror (cut-off wavelength 400 nm) and a 420 nm long-pass emission filter. The accumulation time was 1s in case of each measurement.

QD₆₂₆ appeared when excited with a green excitation filter (510-560 nm). **Figure 3-8** shows the fluorescence micrographs of the barcode (•-QD₆₂₆QD₅₅₅) when excited using UV-2A and G-2A filter sets. This confirms that the QD₅₅₅ outer layer becomes transparent when excited at 510-560nm and which results in the fluorescent signal of QD₆₂₆. These results also support our hypothesis that the disappearance of inner layer QD₆₂₆ signal was due to the inner filter effect.

This indicated that in order to make the barcode using multilayers of quantum dots, a spacer should be used to separate the quantum dot layers allowing emitted light from the inner layer to emerge. Wang et al.,⁽¹⁰⁾ used a silica layer to create a spacing greater than 10nm between neighbouring quantum dot layers on magnetic nanoparticles to produce different colour barcodes. The silica layer prevents different layer quantum dots from interacting with each other so that each quantum dot layer can be efficiently excited.

(a) Excitation with 330-380nm



(b) Excitation with 510-56nm

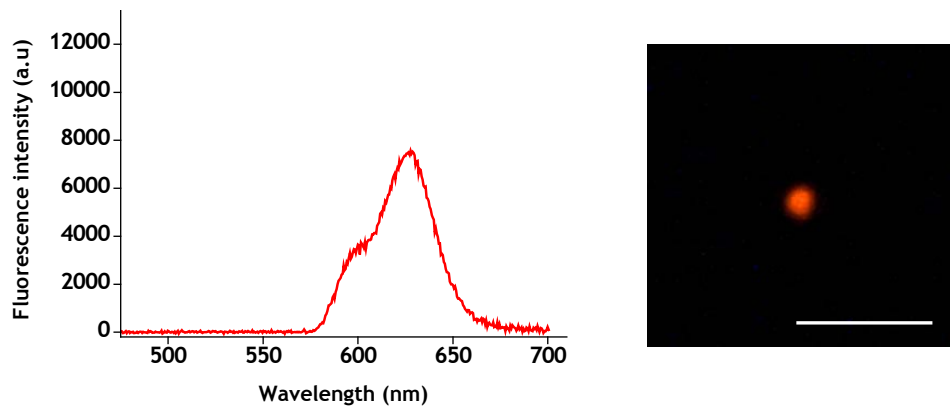


Figure 3-8: (a) Single bead fluorescence spectra (left) and fluorescence micrograph (right) of barcode \bullet -QD₆₂₆QD₅₅₅. A UV-2A filter set was used for excitation of quantum dots encoded bead in the UV-region using a mercury lamp and to collect the fluorescent signal or fluorescence micrograph. The UV-2A filter set consists of an excitation filter (330-380 nm), a dichroic mirror (cut-off wavelength 400 nm) and a 420 nm long-pass emission filter. The accumulation time was 1s. (b) Single bead fluorescence spectra (left) and fluorescence micrograph (right) of the same bead barcode \bullet -QD₆₂₆QD₅₅₅. A G-2A filter set was employed for excitation of quantum dots in the green-region using a mercury lamp and to collect the fluorescent signal or fluorescence micrograph. The G-2A filter set consists of an excitation filter (510-560 nm), a dichroic mirror (cut-off wavelength 565 nm) and a 590 nm long-pass emission filter. The accumulation time was 1s. The scale bar is 5 μ m.

3.3. Layer-by-Layer Assembly of Quantum Dot-Biotin and Quantum Dot-Streptavidin Conjugates onto Glass Substrates

In order to overcome the problem stated above, quantum dot-streptavidin and quantum dot-biotin conjugates were investigated as a means to produce the barcodes with suitably separated quantum dot layers. These biomolecules conjugated to the quantum dots can provide sufficient spacing to produce quantum dot barcodes. First of all these bioconjugates were immobilised on the glass substrate using layer-by-layer assembly of biotin-streptavidin interaction and characterised using X-ray photoelectron spectroscopy and fluorescence spectroscopy. The detailed procedure for the immobilisation has been described in the Materials and Methods Section 2.2.2.

3.3.1. X-Ray Photoelectron Spectroscopy (XPS)

X-ray photoelectron spectroscopy (XPS) was used to characterise the immobilisation of streptavidin and biotin quantum dot conjugates onto the glass surface. Glass substrates were cleaned and 3-aminopropyltriethoxysilane was immobilised on the glass surface. **Figure 3-9A(a)** shows N(1s) high resolution XPS spectrum of aminosilane on the glass substrate. The N(1s) spectrum confirmed the presence of two different nitrogen species occurring at (399.5 eV and 401.3 eV) two different binding energies separated by 1.8 - 2 eV.⁽¹¹⁾ This confirms the immobilisation of aminosilane on the glass substrate. The component at lower binding energy can be assigned to free aliphatic amino groups and component at higher binding energy can be assigned to the protonated aliphatic amino groups.⁽¹¹⁾

For the immobilisation of streptavidin conjugated quantum dots, glass slides were incubated in a solution of 1 mg/ml biotinamido hexanoic acid 3-sulfo-N-hydroxysuccinimide ester (NHS-Biotin) in the PBS at pH 8.0 for one hour at room temperature. **Figure 3-9A** shows the N(1s) and C(1s) spectra before (a) and after (b) immobilisation of biotin onto the aminosilane modified glass slides. Before immobilisation, the deconvolution of C(1s) spectrum shows the presence of two types of carbon species (C-C and C-N). After the immobilisation of biotin, one additional peak appeared at 288 eV which corresponded to the C=O group from biotin and confirmed the attachment of biotin on the glass substrate.^(12, 13)

To immobilise streptavidin conjugated quantum dots, samples were then incubated in a streptavidin conjugated quantum dot (S_{525}) solution in PBS pH 7.4 containing 0.15 % BSA for 1h to block non-specific adsorption of quantum dot conjugates. These substrates were then washed with quantum dot free PBS pH 7.4 containing 0.15% BSA. After the immobilisation of streptavidin conjugated quantum dots, the substrate was incubated in a biotin conjugated quantum dot (B_{655}) solution for 1h. The sample was then washed exhaustively to remove any unbound biotin-quantum dots. A control sample was prepared by the incubation of aminosilane modified glass substrate in PBS pH 7.4 containing 0.15% BSA for half an hour and then it was incubated in streptavidin conjugated quantum dot solution for 1h. After washing, the samples were dried under nitrogen gas.

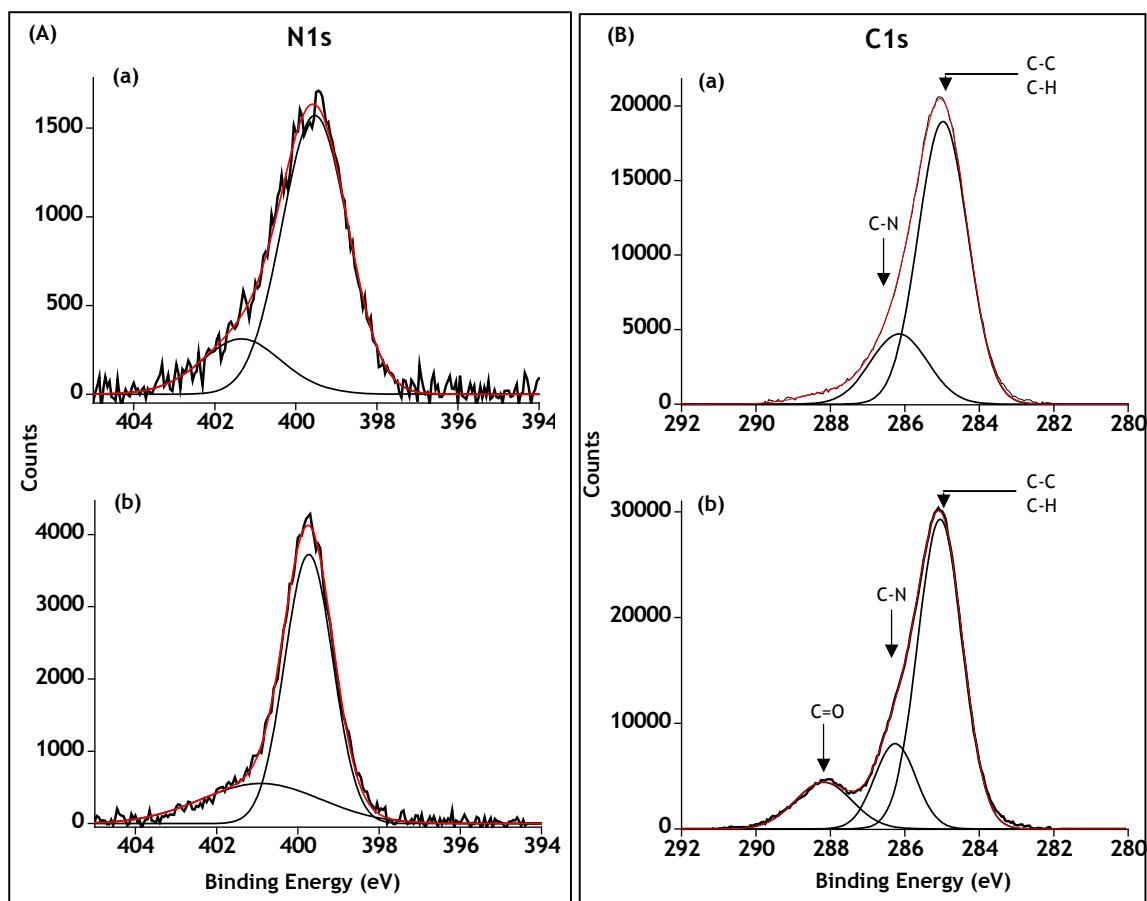


Figure 3-9: (A) N(1s) high resolution XPS spectra of aminosilane film on the glass substrate (a) before and (b) after the immobilisation of NHS-biotin; (B) C(1s) high resolution XPS spectra (a) before and (b) after immobilisation of NHS-biotin.

Figure 3-10 shows the survey spectra of four different samples prepared for the immobilisation of quantum dots using streptavidin and biotin conjugates. The survey scan for the glass substrate containing aminosilane and NHS-biotin shows the presence of Si(2p), Si(1s), S(2p), C(1s), N(1s) and O(1s) elements. After the immobilisation of streptavidin

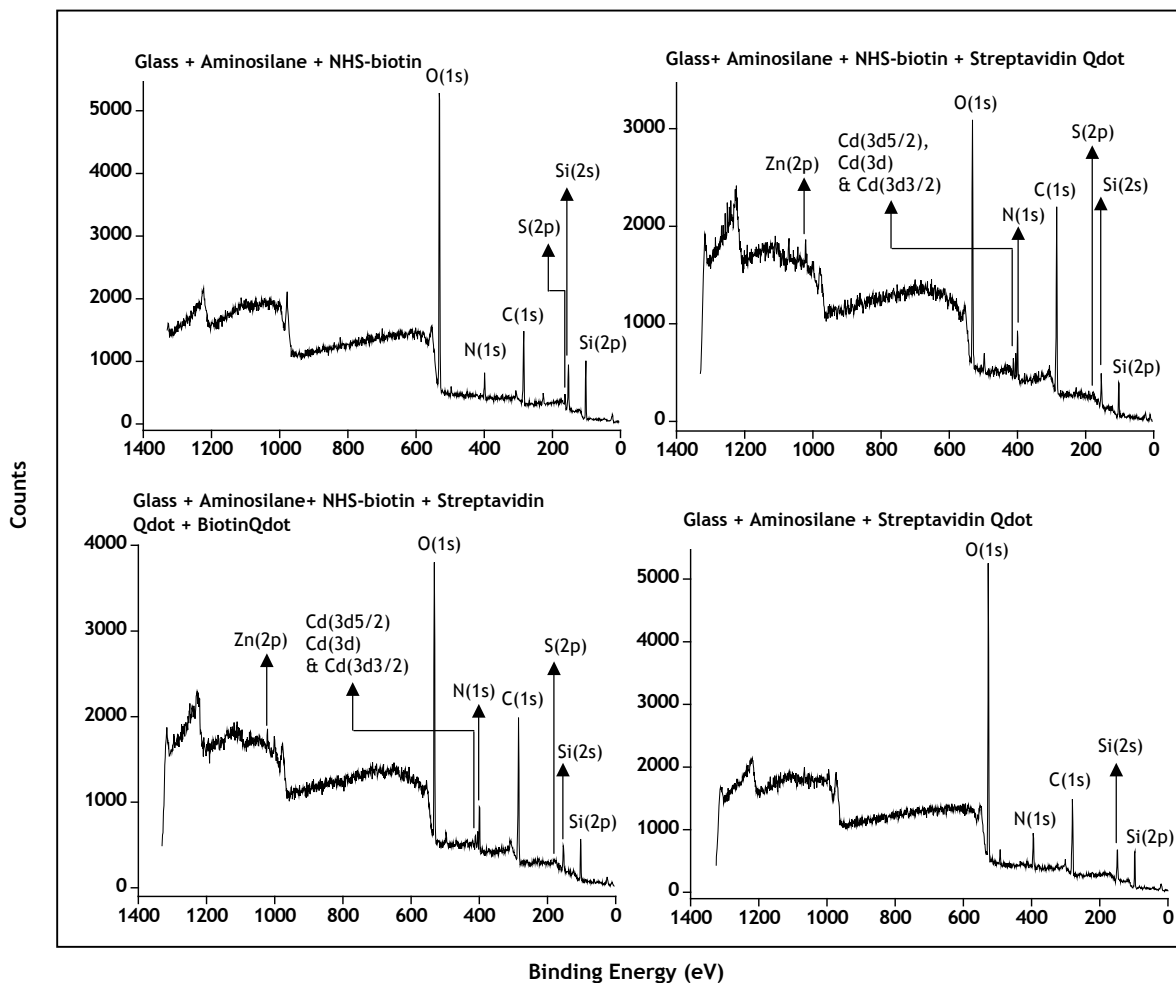


Figure 3-10: Comparison of XPS survey spectra of four different samples: (a) Immobilisation of biotin onto aminosilane modified glass substrate; (b) Immobilisation of first layer of streptavidin quantum dot conjugate (S_{525}) using biotin-streptavidin interaction; (c) Immobilisation of second layer of quantum dots using biotin conjugated quantum dots (B_{655}); (d) A control sample where the glass slides containing aminosilane were first incubated in BSA for half an hour and then incubated in streptavidin conjugated quantum dots.

conjugated and biotin conjugated quantum dots, two additional peaks related to Cd(3d5/2), Cd(3d) and Cd(3d3/2) appeared around 405.5 eV and 412.5 eV which confirmed the immobilisation of quantum dots. Also a weak signal related to Zn(2p) was found around 1022 eV.

The presence of these elements indicates that the streptavidin and biotin conjugated quantum dots were immobilised on the glass substrate using the layer-by-layer assembly. The ratio of N(1s) to Cd(3d5/2) for two layers (streptavidin quantum dots and biotin quantum dots) was found to be 2.55 which is higher than the value for the first layer (streptavidin quantum dots) 1.75. The ratio values are higher in case of two layers of quantum dot conjugates as compared to the monolayer of quantum dot conjugates. This is due to the fact that the number of quantum dots immobilised in the case of two layers is greater than the monolayer of quantum dots. This also confirms the immobilisation of biotin conjugated quantum dots (second layer) onto the streptavidin conjugated quantum dots (monolayer) in a layer-by-layer assembly.

In order to confirm that the immobilisation of quantum dot conjugates is via biotin-streptavidin interaction, high resolution XPS spectra of Cd(3d) and Zn(2p) were measured for the first layer and a control sample (**Figure 3-11**). A control sample was prepared by first incubating aminosilane functionalised glass substrate in PBS pH 7.4 containing 0.15% BSA for half an hour and then incubated in 10nM solution of QD₅₂₅-streptavidin (S₅₂₅) for 1h. **Figure 3-11** shows that streptavidin quantum dot conjugates were not immobilised on the control sample confirming that the immobilisation of quantum dot conjugates was via biotin-streptavidin interaction rather than the adsorption of quantum dot conjugates. Multilayers of quantum dot conjugates can be formed on the glass substrate using this layer-by-layer assembly.

3.3.2. Fluorescence Spectroscopy

Optical properties of thin films of quantum dot streptavidin and quantum dot biotin conjugates were also studied using fluorescence spectroscopy. In the first experiment, ten layers of quantum dot-streptavidin 655 nm (S₆₅₅) and quantum dot-biotin 655 nm (B₆₅₅) were prepared using layer-by-layer biological self-assembly of these conjugates on the glass substrate. **Figure 3-12** shows the fluorescence spectra of these thin films up to ten layers. It can be seen that the fluorescence intensity increased with

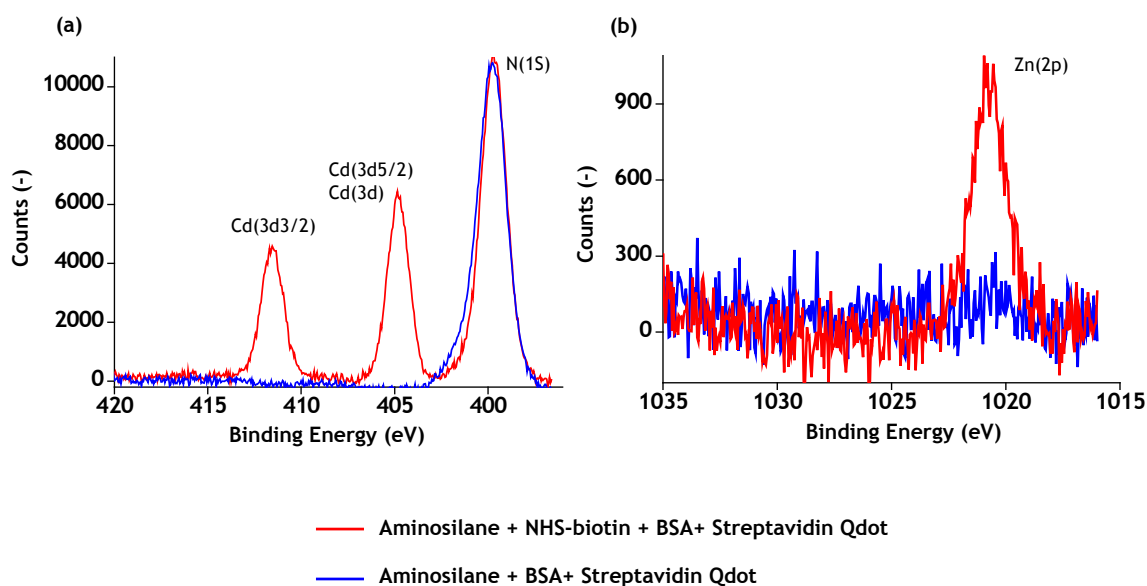


Figure 3-11: (a) Comparison of Cd(3d) high resolution XPS spectra of quantum dots immobilised with or without using biotin-streptavidin interaction; (b) Comparison of Zn(2p) high resolution XPS spectra of quantum dots immobilised with or without using biotin-streptavidin interaction.

the increase in number of layers of quantum dot conjugates. Also, and in contrast to studies involving quantum dots alone, **Figure 3-5** indicates that as the number of layers increases the standard deviation also increased.

Similarly, multicolour multilayers of quantum dot-streptavidin 525 nm (S_{525}) and quantum dot-biotin 655 nm (B_{655}) conjugates were prepared. **Figure 3-13** shows that the fluorescence intensity of both the quantum dots increases with the increase in number of layers. However, the fluorescence intensity of B_{655} is higher than the S_{525} quantum dots. Again in these multilayer quantum dot assemblies, the standard deviation is higher than the multicolour multilayers of quantum dots produced using a dithiol linker (**Figure 3-6**).

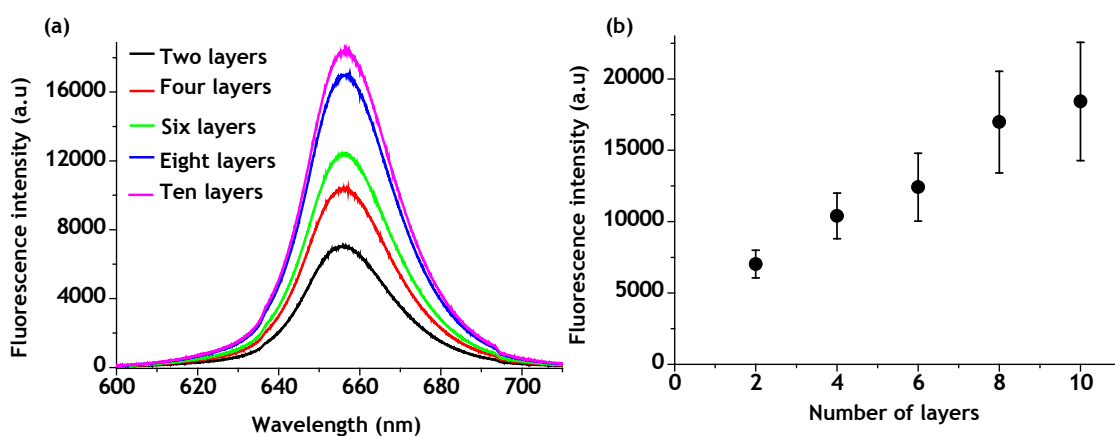


Figure 3-12: Layer-by-layer assemblies of quantum dot-streptavidin 655 nm (S_{655}) and quantum-dot biotin 655 nm (B_{655}) conjugates onto glass substrate: (a) Fluorescence spectra of different layers of quantum dots onto the glass substrate; (b) Layer number vs Fluorescence intensity. The data points are the mean measurements and the error bars show the standard deviation for $n=5$ measurements in case of each layer assembly. Where “ n ” represents the number of measurements from a single sample in the case of each layer assembly. A UV-2A filter set was employed to excite the quantum dots in the UV-region using a mercury lamp and to collect the fluorescent signal. The UV-2A filter set consists of an excitation filter (330-380 nm), a dichroic mirror (cut-off wavelength 400 nm) and a 420 nm long-pass emission filter. The accumulation time was 0.1s in case of each measurement.

This increase in standard deviation of fluorescence measurements may be due to the fact that streptavidin or biotin conjugates have 5-10 or 5-7 streptavidin or biotin molecules on each conjugate, respectively and this number varies from conjugate to conjugate. Therefore the streptavidin and biotin conjugate thin films are not as compact as the thin films of quantum dots formed using a dithiol linker, resulting in a higher standard deviation of measurements on different preparations.

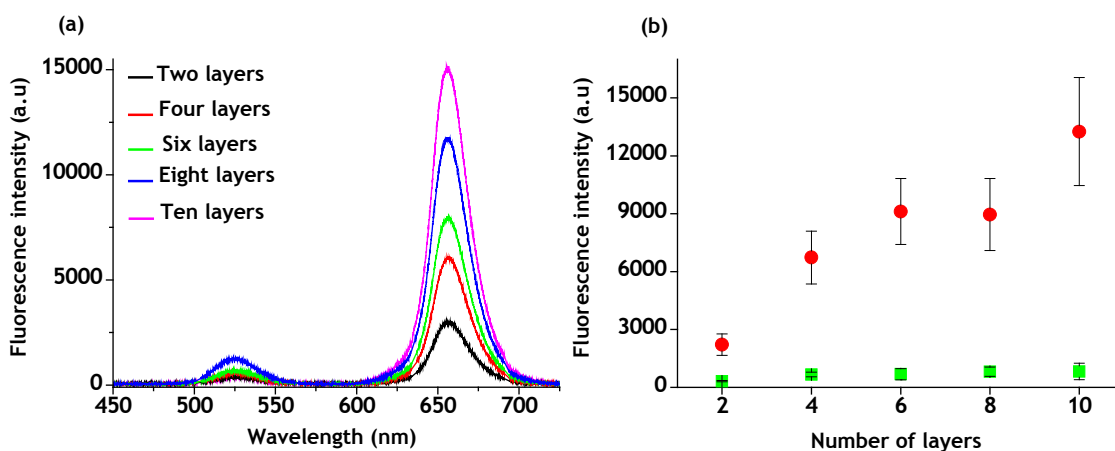


Figure 3-13: Layer-by-layer assemblies of quantum dot-streptavidin 525 nm (S_{525}) and quantum-dot biotin 655 nm (B_{655}) conjugates onto glass substrate; (a) Fluorescence spectra of different layers of quantum dots onto the glass substrate; (b) Layer number vs Fluorescence intensity. The data points are the mean measurements and the error bars show the standard deviation for $n=5$ measurements in case of each layer assembly. Where “ n ” represents the number of measurements from a single sample in the case of each layer assembly. A UV-2A filter set was used to excite the quantum dots in the UV-region using a mercury lamp and to collect the fluorescent signal. The UV-2A filter set consists of an excitation filter (330-380 nm), a dichroic mirror (cut-off wavelength 400 nm) and a 420 nm long-pass emission filter. The accumulation time was 0.1s in case of each measurement.

Despite the fact that the standard deviation for these quantum dot assemblies is higher, the XPS and fluorescence measurements of these multilayer assemblies indicate that the streptavidin and biotin conjugates of quantum dots can be used to produce multilayers of quantum dots onto magnetic beads. The production of quantum dot barcodes using quantum dot streptavidin and quantum dot biotin conjugates onto the magnetic beads is presented in **Chapter 4**.

3.4. References

1. Goss CA, Charych DH, Majda M. Application of (3-Mercaptopropyl)Trimethoxysilane as a Molecular Adhesive in the Fabrication of Vapor-Deposited Gold Electrodes on Glass Substrates. *Analytical Chemistry* 1991;63(1):85-88.
2. Nefedov VI. X-ray photoelectron spectroscopy of solid surfaces. Tokyo, Japan: Utrecht, The Netherlands; 1988.
3. Jun KAWA HA, Yoshinori KITAJIMA, Kuniko MAEDA, Shinjiro HAYAKAWA and Yohichi GoHSHI. The penetration depth of X-rays used in X-ray photoelectron in Ag determined by total reflection X-ray photoelectron spectroscopy. *Analytical Sciences* 1997;13:797-801.
4. Laibinis PE, Whitesides GM, Allara DL, Tao YT, Parikh AN, Nuzzo RG. Comparison of the Structures and Wetting Properties of Self-Assembled Monolayers of Normal-Alkanethiols on the Coinage Metal-Surfaces, Cu, Ag, Au. *Journal of the American Chemical Society* 1991;113(19):7152-7167.
5. Romano EJ, Schulz KH. A XPS investigation of SO₂ adsorption on ceria-zirconia mixed-metal oxides. *Applied Surface Science* 2005;246(1-3):262-270.
6. Siegbahn K, Nordling C, Fahlman A, Nordberg R, Hamrin K, Hedman J, et al. Atomic, Molecular and solid state structure studied by means of electron spectroscopy. 3rd ed: Uppsala; 1965.
7. Lang P, Nogues C. Self-assembled alkanethiol monolayers on a Zn substrate: Interface studied by XPS. *Surface Science* 2008;602(13):2137-2147.
8. Liu ZC, He QG, Xiao PF, Liang B, Tan JX, He NY, et al. Self-assembly monolayer of mercaptopropyltrimethoxysilane for electroless deposition of Ag. *Materials Chemistry and Physics* 2003;82(2):301-305.
9. Kubista M, Sjoback R, Eriksson S, Albinsson B. Experimental Correction for the Inner-Filter Effect in Fluorescence-Spectra. *Analyst* 1994;119(3):417-419.
10. Wang QB, Liu Y, Lin CX, Yan H. Layer-by-layer growth of superparamagnetic, fluorescent barcode nanospheres. *Nanotechnology* 2007;18(40):-.
11. Bierbaum K, Kinzler M, Woll C, Grunze M, Hahner G, Heid S, et al. A near-Edge X-Ray-Absorption Fine Structure Spectroscopy and X-Ray Photoelectron-Spectroscopy Study of the Film Properties of Self-Assembled Monolayers of Organosilanes on Oxidized Si(100). *Langmuir* 1995;11(2):512-518.
12. Zeng DW, Yung KC. XPS investigation on Upilex-S polyimide ablated by pulse TEA CO₂ laser. *Applied Surface Science* 2001;180(3-4):280-285.

13. Yam CM, Pradier CM, Salmain M, Marcus P, Jaouen G. Binding of biotin to gold surfaces functionalized by self-assembled monolayers of cystamine and cysteamine: Combined FT-IRRAS and XPS characterization. *Journal of Colloid and Interface Science* 2001;235(1):183-189.

Chapter 4

Production, Characterisation and Stability of Quantum Dot Barcodes

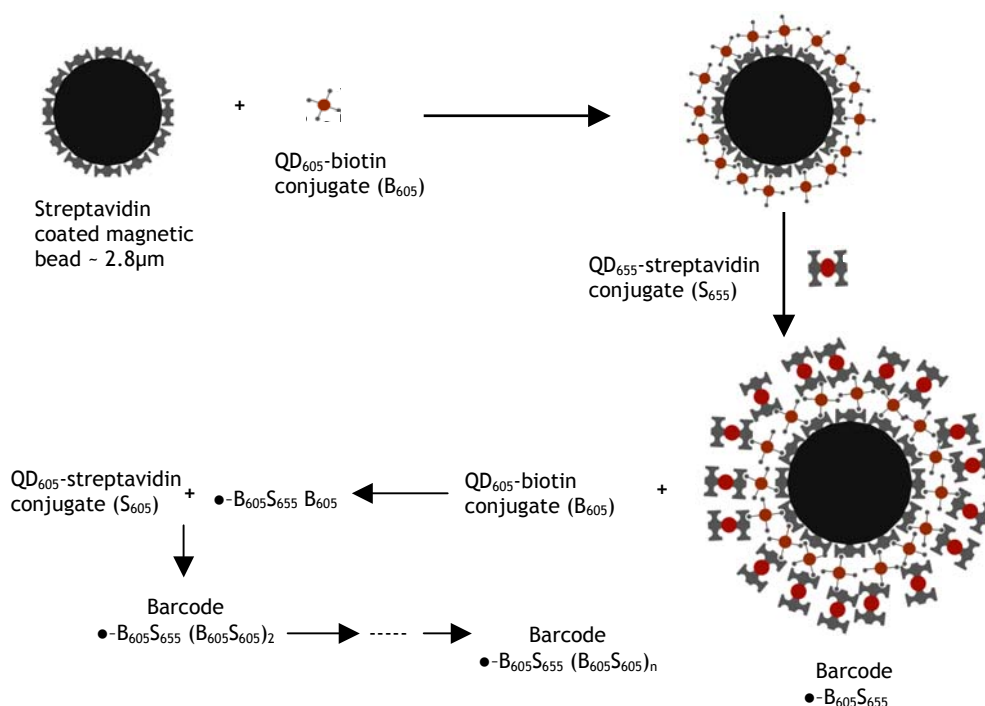
This Chapter discusses the assembly process, characterisation and stability of quantum dot barcodes produced by layer-by-layer assembly of streptavidin and biotin functionalised quantum dots, based upon biological self-assembly. The strong interaction between streptavidin and biotin is exploited to create constructs on the bead surface which can subsequently be read optically. The streptavidin-biotin interaction is sufficiently strong ($K_d \sim 4 \times 10^{-14}$ M) that the assembled codes are stable over extended periods.⁽¹⁻⁵⁾

4.1. Production of Quantum Dot Barcodes

Quantum dot barcodes were prepared by sequential assembly of layers of biotin and streptavidin conjugated CdSe/ZnS quantum dots onto streptavidin coated magnetic beads as described in detail in **Section 2.2.3**. The streptavidin coated magnetic beads ($\sim 2.8 \mu\text{m}$) were first incubated with a suspension of biotin conjugated quantum dots (QD₆₀₅-biotin) in 10 mM PBS buffer, pH 7.4, containing bovine serum albumin, BSA, (0.15% w/v), the latter acting to block any free sites for adventitious absorption. After incubation, the beads were washed exhaustively with the same buffer before a second incubation in a suspension of streptavidin conjugated quantum

dots (QD₆₅₅-streptavidin). Again, after exhaustive washing, the beads were re-suspended in the same PBS. The use of magnetic beads enabled the rapid manipulation of the beads providing a convenient method to wash and separate them after the assembly of the sequential layers.⁽⁶⁻⁸⁾ Using fluorescence microscopy, it was observed that the barcodes remained well dispersed in this supporting buffer, and there was no evidence of bead clustering, prior to the application of a magnetic field. After application of the magnetic field, when the beads were released, again there was no evidence of clustering.

The barcode construct, described above, was given the nomenclature ●-B₆₀₅S₆₅₅ as it comprised a first layer of QD₆₀₅-biotin (B₆₀₅), with a second layer of QD₆₅₅-streptavidin (S₆₅₅) assembled onto magnetic bead (●-). This assembly provided free outer streptavidin binding sites that have potential for subsequent assembly of biotinylated reagents, including quantum dot-biotin conjugates (e.g. QD₆₀₅-biotin), or affinity ligands. By using this assembly process in conjunction with the large numbers of commercially available quantum dots, having well defined surface chemistries there is the potential to create a large number of constructs as shown in Scheme 2-4.



Scheme 2-4: Barcode production using biological self-assembly of quantum dot-biotin and quantum dot-streptavidin conjugates. Copyright Wiley-VCH verlag GmbH & Co. KGaA. Reproduced with permission

4.2. Characterisation of Quantum Dot Barcodes

To confirm the formation of barcodes and to investigate the coding potential of the layer-by-layer assembly approach, single bead fluorescence spectroscopy was used to characterise the different bead assemblies, **Figure 2-2**. In order to discriminate between different barcodes, ratiometric measurements were used rather than measuring the absolute intensities of the quantum dots. The ratiometric measurement method has previously been proved to be well suited for barcode studies.⁽⁹⁻¹³⁾ The error in decoding of the barcodes is greater in case of using measurement of absolute intensities as a criteria for identifying different barcodes, than the ratiometric measurements⁽⁹⁾ due to the experimental and environmental factors. For example, in the current studies, it is difficult to control number of biotin binding sites on the magnetic beads and these varied from bead to bead. Similarly, there may be a variation in the size of the bead leading to different absolute number of binding sites. The ratiometric measurements reduces the error by normalising these factors, and by mitigating against other experimental or environmental variations. The method for performing single bead fluorescence spectroscopy is described in detail in **Section 2.4**.

As a proof of principle, to assemble multiple constructs, two different colour quantum dots conjugated to either biotin or streptavidin; QD₆₀₅-biotin, QD₆₀₅-streptavidin and QD₆₅₅-streptavidin were used. **Figure 4-1a** shows the spectral response of three different barcode constructs ●-B₆₀₅S₆₅₅, ●-B₆₀₅S₆₅₅(B₆₀₅S₆₀₅)₁ and ●-B₆₀₅S₆₅₅(B₆₀₅S₆₀₅)₂. **Figure 4-1b** shows the statistical distribution of 605 nm/655 nm ratiometric measurements of these three simplest barcode preparations, where the ratios of the relative fluorescence intensities are plotted as a histogram, each for 200 beads.

Figure 4-1b shows that the median values for three different barcodes are 0.94, 1.4 and 1.9 which are different from the expected ratio values of 1, 3 and 5 considering the number of layers of QD₆₀₅ and QD₆₅₅ quantum dots in three different barcodes. Moreover, as the number of biologically assembled layers increases, the relative standard deviation of the ratiometric measurement also increases. This may be due to the variation in the number of quantum dots on a given layer and also as a consequence of bead-bead variations in the number of quantum dots bound (It can be estimated that there are ~5-10 streptavidin or 5-7 biotin molecules per quantum dot).

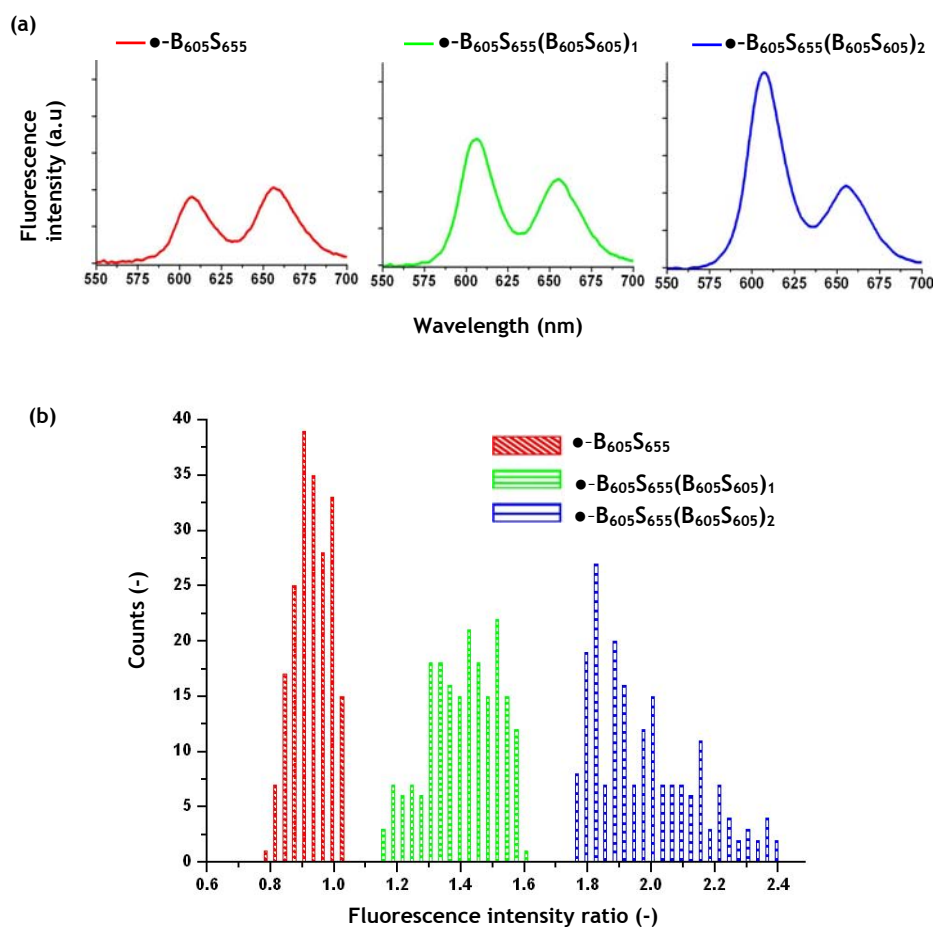


Figure 4-1: Characterisation of barcodes prepared by layer-by-layer assembly of QD₆₀₅-biotin, QD₆₀₅-streptavidin and QD₆₅₅-streptavidin: (a) A typical single bead fluorescence spectrum measured for $\bullet\text{-B}_{605}\text{S}_{655}$, $\bullet\text{-B}_{605}\text{S}_{655}(\text{B}_{605}\text{S}_{605})_1$ and $\bullet\text{-B}_{605}\text{S}_{655}(\text{B}_{605}\text{S}_{605})_2$ barcodes (in red, green and blue, respectively). A UV-2A filter set was employed to excite the quantum dot encoded beads in the UV-region using a mercury lamp and to collect the fluorescent signal. The UV-2A filter set consists of an excitation filter (330-380 nm), a dichroic mirror (cut-off wavelength 400 nm) and a 420 nm long-pass emission filter. The accumulation time was 1s for each single bead spectra; (b) Statistical distribution of barcodes calculated from fluorescence intensity ratio of QD₆₀₅ to QD₆₅₅ for three different barcodes using single bead fluorescence spectroscopy. The graph represents data collected from 200 beads for each preparation. For barcode $\bullet\text{-B}_{605}\text{S}_{655}$, the median value for this preparation is 0.94 with a relative standard deviation of 5.92%. For barcodes $\bullet\text{-B}_{605}\text{S}_{655}(\text{B}_{605}\text{S}_{605})_1$ and $\bullet\text{-B}_{605}\text{S}_{655}(\text{B}_{605}\text{S}_{605})_2$, the median values were 1.4 and 1.9 with relative standard deviations of 7.7% and 8.4% respectively. Copyright Wiley-VCH Verlag GmbH & Co. KGaA. Reproduced with permission.

Despite this variation in number of binding sites, the ratiometric intensity distribution reported here is comparable to, and in most cases much better than that previously reported for quantum dot-encoded beads.^{(13),(14-16)} For example, three intensity level quantum dot barcodes prepared using polyelectrolyte multilayers exhibit standard deviations of between 20-22%.⁽¹³⁾ However, the results show that when the difference between the highest and lowest fluorescence intensity ratios of adjacent barcodes is at least 0.15, different sequences can be identified, **Figure 4-1b**.

As one of the control experiments, in order to demonstrate that quantum dot assembly occurred via streptavidin-biotin conjugation, streptavidin coated magnetic beads were sequentially incubated with first QD₆₀₅-streptavidin and subsequently QD₆₅₅-streptavidin to prepare ●-S₆₀₅S₆₅₅. As expected this construct gave no fluorescent signal at 605 nm and 655 nm, as there were no available binding sites on the bead to bind either S₆₀₅ or S₆₅₅ as shown in **Figure 4-2**. These results provide clear evidence of the lack of non-specific adsorption of streptavidin moieties to themselves.

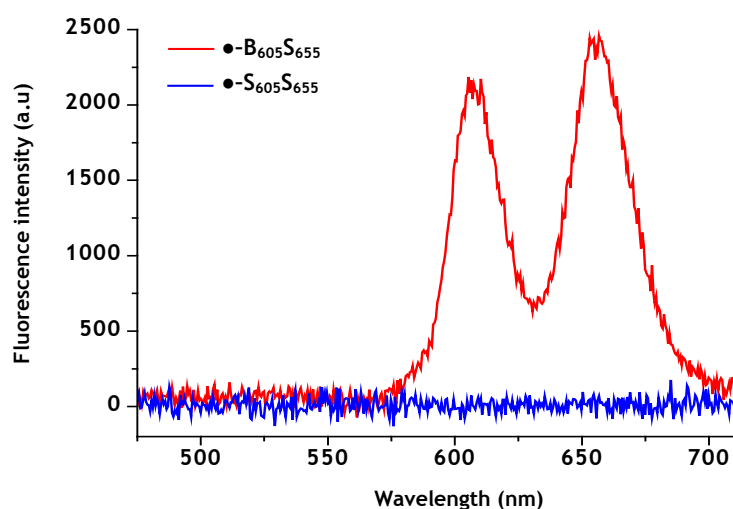


Figure 4-2: Single bead fluorescence emission spectra of barcode ●-B₆₀₅S₆₅₅ and ●-S₆₀₅S₆₅₅ shown in red and blue, respectively. A UV-2A filter set was employed to excite the quantum dot encoded beads in the UV-region using a mercury lamp and to collect the fluorescent signal. The UV-2A filter set consists of an excitation filter (330-380 nm), a dichroic mirror (cut-off wavelength 400 nm) and a 420 nm long-pass emission filter. The accumulation time was 1s for each single bead spectra.

In order to study the batch-to-batch variation in the preparation of barcodes, two different batches of barcode $\bullet\text{-B}_{605}\text{S}_{655}(\text{B}_{605}\text{S}_{605})_1$ were prepared and 605 nm/655 nm ratios for both were measured and plotted as a histogram as shown in **Figure 4-3**. The detailed description of Materials and Methods is described in **Section 2.2**. For two different batches, the relative standard deviations were found to be 6.7% and 8.3%. It is clear that the batch-to-batch variation is not large.

To quantify the number of quantum dots per bead, assays were performed by measuring the relative fluorescence intensities of assemblies on magnetic beads as detailed in the experimental **Section 2.4.1**.^(13, 17) For the first layer, $\bullet\text{-B}_{605}$, the

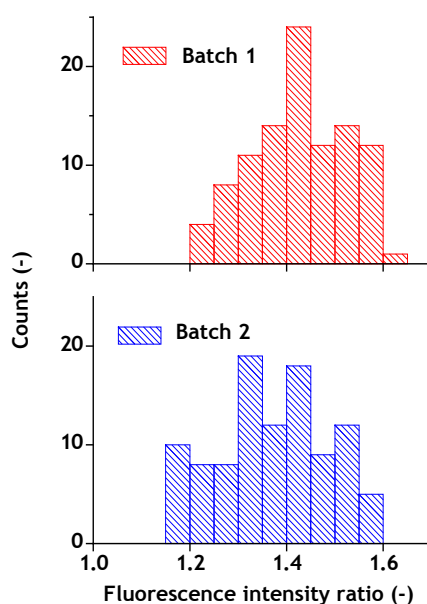


Figure 4-3: Batch to batch difference in the preparation of barcodes. Statistical distribution of barcodes $\bullet\text{-B}_{605}\text{S}_{655}(\text{B}_{605}\text{S}_{605})_1$ calculated from fluorescence intensity ratio of QD_{605} to QD_{655} using single bead fluorescence spectroscopy. The graph represents data collected from 100 beads for each preparation. For batch 1 and batch 2, the median values were 1.42 and 1.37 with standard deviations of 6.7% and 8.3% respectively. A UV-2A filter set was employed to excite the quantum dot encoded beads in the UV-region using a mercury lamp and to collect the fluorescent signal. The UV-2A filter set consists of an excitation filter (330-380 nm), a dichroic mirror (cut-off wavelength 400 nm) and a 420 nm long-pass emission filter. The accumulation time was 1s for each single bead spectra.

number of quantum dots was estimated to be $\sim 1.8 \times 10^5$ which is in close agreement with the $\sim 10^5$ estimated geometrically using a bead size of $2.8 \mu\text{m}$ and a quantum dot conjugate size of 15-20 nm. For the subsequent layers, the number of quantum dots per layer per bead was measured as between $\sim 10^4$ and $\sim 10^5$.

It was also found that the nature of the quantum dot conjugate was important for the immobilisation of quantum dot conjugates on streptavidin beads. Streptavidin quantum dot conjugate having a PEG-linker was found to bind to the magnetic beads having biotin binding sites resulted in the immobilisation of quantum dot biotin conjugate. On the other hand, streptavidin quantum dot conjugate with no PEG-linker (ITKTM quantum dot-streptavidin conjugate, Invitrogen) did not bind to the barcode having biotin binding sites. Detailed descriptions of the Materials and Methods are provided in **Section 2.2.3.1**. In the preparation of these quantum dot conjugates, streptavidin was covalently attached to the quantum dots without the use of a PEG-linker. Two different wavelength quantum dot conjugates (without PEG-linker) were used namely these are QD₆₅₅ ITKTM-streptavidin conjugate (S^*_{655}) and QD₆₀₅ITKTM-streptavidin conjugate (S^*_{605}), **Figure 4-4**.

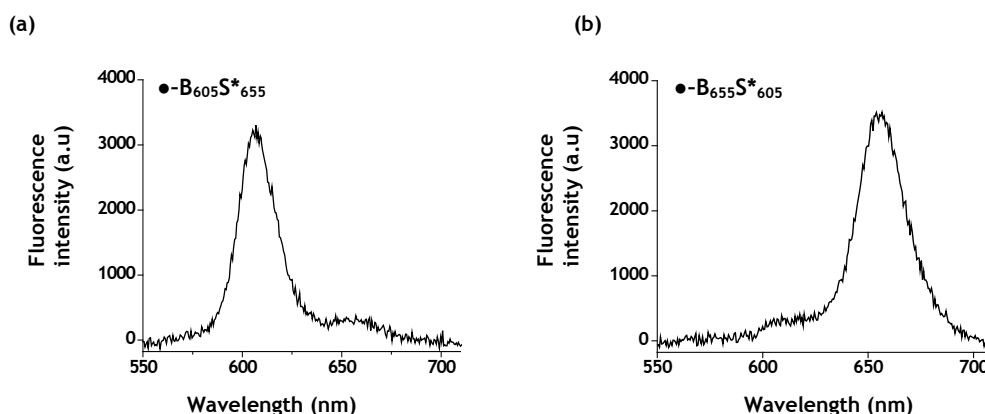


Figure 4-4: (a) Fluorescence spectra after immobilisation of QD₆₅₅ ITKTM-streptavidin conjugate (S^*_{655}) on magnetic bead having QD₆₀₅-biotin conjugate (\bullet -B₆₀₅); (b) Fluorescence spectra after immobilisation of QD₆₀₅ITKTM-streptavidin conjugate (S^*_{605}) on magnetic bead having QD₆₅₅-biotin conjugate (\bullet -B₆₅₅). A UV-2A filter set was employed to excite the quantum dot encoded beads in the UV-region using a mercury lamp and to collect the fluorescent signal. The UV-2A filter set consists of an excitation filter (330-380 nm), a dichroic mirror (cut-off wavelength 400 nm) and a 420 nm long-pass emission filter. The accumulation time was 1s for each single bead spectra.

It can be seen that a weak signal was found when ITKTM-streptavidin quantum dot conjugates were used. This shows that the binding of streptavidin quantum dot conjugate to biotin quantum dot conjugate was strongly dependent on the steric hindrance. It is hypothesised that the presence of PEG-linker provides flexibility to the streptavidin quantum dot conjugate and assist in binding to the bead surface.

Quantum dot barcodes produced by layer-by-layer assembly of biotin and streptavidin quantum dot conjugates have streptavidin binding sites for further binding of different biotinylated molecules. In order to confirm the presence of streptavidin binding sites on barcoded beads and to demonstrate the application of the barcodes as sensors to detect an arbitrary biotinylated molecule, biotin-fluorescein was immobilised on ●-B₆₀₅S₆₅₅, and subsequently washed with PBS containing 0.15% BSA to make ●-B₆₀₅S₆₅₅-fluorescein. This barcode was mixed with unlabelled ●-B₆₀₅S₆₅₅, and analysed using single bead fluorescence spectroscopy. **Figure 4-5a** shows that both labelled (●-B₆₀₅S₆₅₅-fluorescein) and un-labelled (●-B₆₀₅S₆₅₅) barcodes can be identified. The characteristic spectra of the ●-B₆₀₅S₆₅₅ bead remains unchanged after the binding of biotin-fluorescein (**Figure 4-5b**), showing that the barcode information was intact and independent of the nature of the molecule being detected.

Further, to detect ●-B₆₀₅S₆₅₅-fluorescein in the presence of a second, multilayer, barcode, ●-B₆₀₅S₆₅₅-fluorescein was mixed with ●-B₆₀₅S₆₅₅(B₆₀₅S₆₀₅)₁ in PBS and analysed using single bead fluorescence spectroscopy. As expected, fluorescein was detected on barcode ●-B₆₀₅S₆₅₅ (**Figure 4-6a** and **Figure 4-6b**) only. Note that in **Figure 4-6a** one bead has weak emission because of low level of 605 nm and 655 nm bleeding through the green band pass filter. In the absence of green band pass filter, the barcode ●-B₆₀₅S₆₅₅ appears with a weak emission because it has two layers of quantum dots i.e., QD₆₀₅ and QD₆₅₅, whilst the barcode ●-B₆₀₅S₆₅₅(B₆₀₅S₆₀₅)₁, which appears brighter, has four layers of quantum dots i.e., three QD₆₀₅ and one QD₆₅₅. Importantly, **Figure 4-5b** and **Figure 4-6b** also show the presence of fluorescein on barcode ●-B₆₀₅S₆₅₅ through a significant shoulder peak in the spectrum at ~530 nm. **Figure 4-6b** also shows that different barcodes can still be identified using the ratio of 605 nm/655 nm fluorescence emission intensity in the presence of an additional conjugated molecule. It is clear that both of these barcodes can be identified, proving the concept for a range of biological assays to be developed in future.

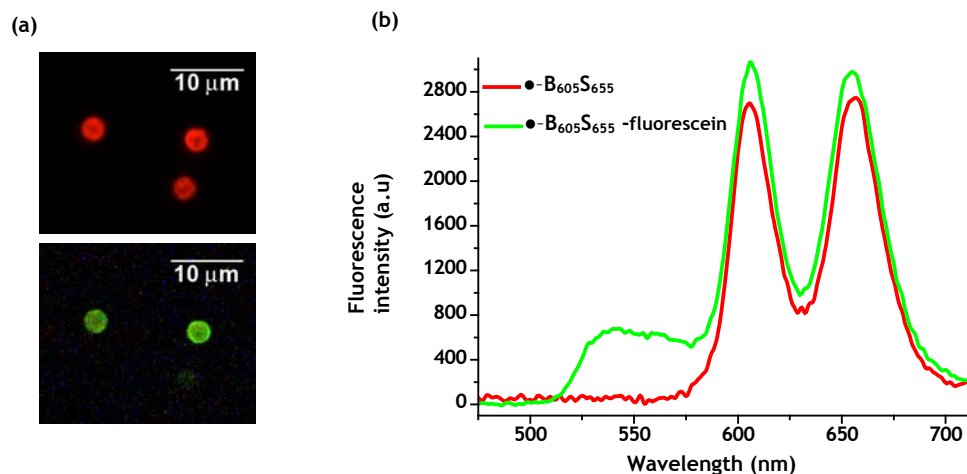


Figure 4-5: (a) Fluorescence micrographs of barcode \bullet - $B_{605}S_{655}$ and \bullet - $B_{605}S_{655}$ -fluorescein beads in the absence (top) and presence (bottom) of green band pass filter (500 nm-550 nm). The micrographs show the presence of both fluorescein labelled and un-labelled barcodes. Micrographs also show that beads are not cross linked and show no tendency to cluster; (b) Single bead fluorescence emission spectra of barcode \bullet - $B_{605}S_{655}$ and \bullet - $B_{605}S_{655}$ -fluorescein. Note that after assembly of biotin-fluorescein to \bullet - $B_{605}S_{655}$, there is a shoulder at \sim 530 nm whilst there is no change in fluorescence of quantum dots. For fluorescence spectra, A B-2A filter set was employed to excite the quantum dots and fluorescein encoded beads in the blue-region using a mercury lamp and to collect the fluorescent signal. The B-2A filter set consists of an excitation filter (450-490 nm), a dichroic mirror (cut-off wavelength 500 nm) and a 515 nm long-pass emission filter. The accumulation time was 1s for each single bead spectra. Copyright Wiley-VCH verlag GmbH & Co. KGaA. Reproduced with permission.

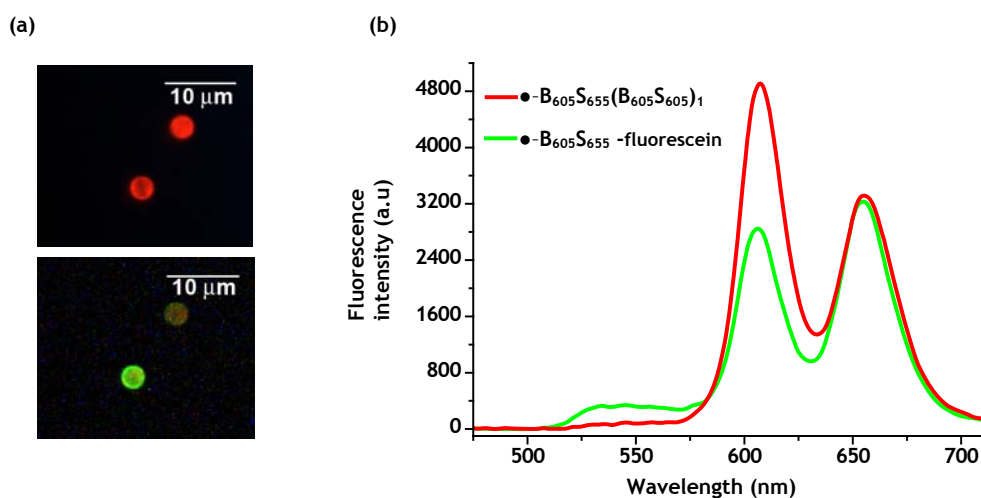


Figure 4-6: (a) Fluorescence microscopy image of barcodes \bullet - $B_{605}S_{655}(B_{605}S_{605})_1$ and \bullet - $B_{605}S_{655}$ -fluorescein beads in the absence (top) and presence (bottom) of a green band pass filter. Note a vestigial colour is seen for the non fluoresceinated bead in the lower micrograph due to bleed-through of the intense 605 nm and 655 nm emission from the \bullet - $B_{605}S_{655}(B_{605}S_{605})_1$ assemblies; (b) Single bead fluorescence emission spectra of barcode \bullet - $B_{605}S_{655}(B_{605}S_{605})_1$ and \bullet - $B_{605}S_{655}$ -fluorescein. Note that after assembly of biotin-fluorescein to \bullet - $B_{605}S_{655}$, there is a shoulder at \sim 530 nm whilst there is no change in fluorescence of quantum dots. A B-2A filter set was employed to excite the quantum dots and fluorescein encoded beads in the blue-region using a mercury lamp and to collect the fluorescent signal. The B-2A filter set consists of an excitation filter (450-490 nm), a dichroic mirror (cut-off wavelength 500 nm) and a 515 nm long-pass emission filter. The accumulation time was 1s for each single bead spectra. Copyright Wiley-VCH verlag GmbH & Co. KGaA. Reproduced with permission.

4.3. Stability Studies of Quantum Dot Barcodes

The stability of the barcodes is an important parameter to identify the possible applications of a barcode system. This section presents the data about the stability studies of quantum dot barcodes produced by using biotin-streptavidin interaction of quantum dot conjugates on streptavidin magnetic beads. The parameters that have been studied are stability of the barcodes at high temperature, incubation in different concentrations of biotin, and the long-term stability of barcodes when stored in PBS pH 7.4 containing 0.15% BSA.

4.3.1. Thermal Stability

Stability of the barcodes at higher temperatures is important where higher temperatures are required in certain applications like PCR. In order to study the stability of the barcodes, $\bullet\text{-B}_{605}\text{S}_{655}(\text{B}_{605}\text{S}_{605})_1$ was treated at an elevated temperature (95°C) for 15 min in the PBS buffer pH 7.4 containing 0.15% BSA. Detailed descriptions of the Materials and Methods are provided in Section 2.5.1. Single bead fluorescence spectra were measured and fluorescence intensity ratio (QD_{605} to QD_{655}) before and after the treatment at higher temperature was calculated and plotted as a histogram as shown in Figure 4-7.

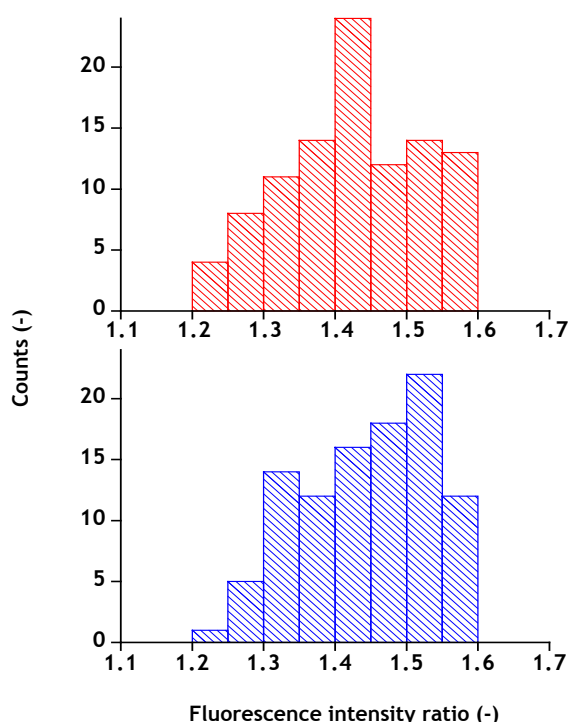


Figure 4-7: Heat treatment of barcode $\bullet\text{-B}_{605}\text{S}_{655}(\text{B}_{605}\text{S}_{605})_1$. Barcoded beads were heated and maintained at 95°C for 15 min in PBS containing 0.15% BSA. Single bead fluorescence spectra were taken before and after the treatment. The statistical distribution of the barcodes was calculated by collating fluorescence intensity ratios of QD_{605} to QD_{655} for 100 beads, in each case. A UV-2A filter set was employed to excite the quantum dot encoded beads in the UV-region using a mercury lamp and to collect the fluorescent signal. The UV-2A filter set consists of an excitation filter (330-380 nm), a dichroic mirror (cut-off wavelength 400 nm) and a 420 nm long-pass emission filter. The accumulation time was 1s for each single bead spectra.

It is clear that the barcode information is intact and no change in the distribution of fluorescence emission ratios was observed. Although the fluorescence intensity ratio distribution is different after treatment at higher temperature but it lies in the same range as before the treatment at higher temperature. This experiment confirms the stability of the barcodes prepared by using biotin-streptavidin interaction.

4.3.2. Stability in Biotin Solution

To further assess the stability of the barcodes, $\bullet\text{-B}_{655}\text{S}_{605}(\text{B}_{605}\text{S}_{605})_1$ was incubated in solutions of different concentrations of biotin. This barcode has one inner layer of QD_{655} and three outer layers of QD_{605} . The decrease in the fluorescence ratio measurements gave information about the disassembly of the barcode produced by layer-by-layer assembly of QD-biotin and QD-streptavidin conjugates. The barcoded beads were incubated in solutions of biotin at concentrations between 1 and 100 mM at room temperature (**Figure 4-8**). Detailed descriptions of the Materials and Methods are provided in **Section 2.5.2**. It can be seen that 1mM biotin has nearly no effect on the barcode assembly. Interestingly the barcode did not disassemble completely when exposed to 100mM biotin, even after 1400 min at room temperature. However, the first two layers of QD_{605} -streptavidin and QD_{605} -biotin were disassembled after 1400 min incubation in 10mM, 50mM and 100mM biotin solutions.

It can be hypothesised that, as the number of layers of biotin and streptavidin quantum dot conjugates increases, the compactness of the layers decreases. The first two outer layers were disassembled quickly as compared to the inner two layers. Due to the compactness of the film for the first two inner layers, biotin molecules could not displace the QD-conjugates and more energy is required for biotin molecules to displace QD-conjugates from the streptavidin bead.

Therefore, in order to see whether this hypothesis was true, $\bullet\text{-B}_{655}\text{S}_{605}(\text{B}_{605}\text{S}_{605})_1$ barcode was incubated in 100mM biotin solution at 37°C for different time intervals (**Figure 4-9**). It is clear from the Figure 4-9 that the disassembly process is slow and requires 1400 min for the barcode to disassemble completely after incubation at 37°C. Fluorescence intensity ratio values showed that after 200 min, the two outer layers of the barcodes were disassembled as the ratio values are in the range of barcode $\bullet\text{-B}_{655}\text{S}_{605}$ which

is two layers less than the barcode $\bullet\text{-B}_{655}\text{S}_{605}(\text{B}_{605}\text{S}_{605})_1$. After 600 min nearly 20% of the beads showed that the barcode completely disassembled while other beads still have

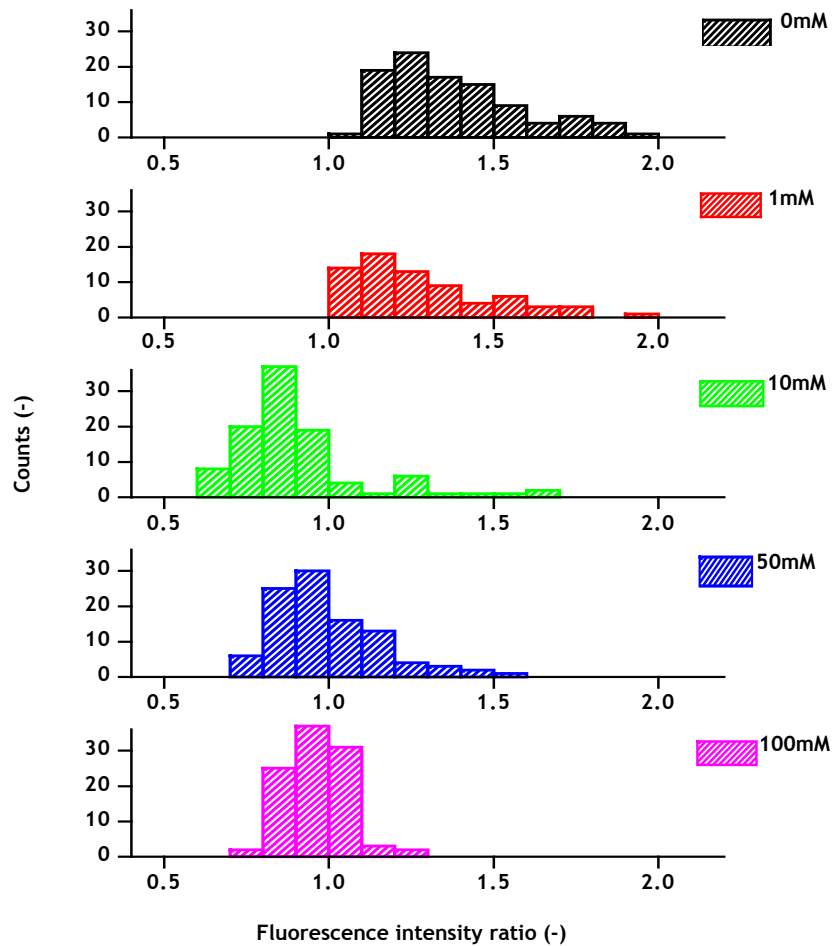


Figure 4-8: Statistical distribution of $(\text{QD}_{605} \text{ to } \text{QD}_{655})$ fluorescence intensity ratio of barcode $\bullet\text{-B}_{655}\text{S}_{605}(\text{B}_{605}\text{S}_{605})_1$ incubated for 1400 min at different concentrations of biotin (0-100mM). Data collected from 100 single bead spectra for each concentration. A UV-2A filter set was employed to excite the quantum dots in the UV-region using a mercury lamp and to collect the fluorescent signal. The UV-2A filter set consists of an excitation filter (330-380 nm), a dichroic mirror (cut-off wavelength 400 nm) and a 420 nm long-pass emission filter. The accumulation time was 1s for each single bead spectra.

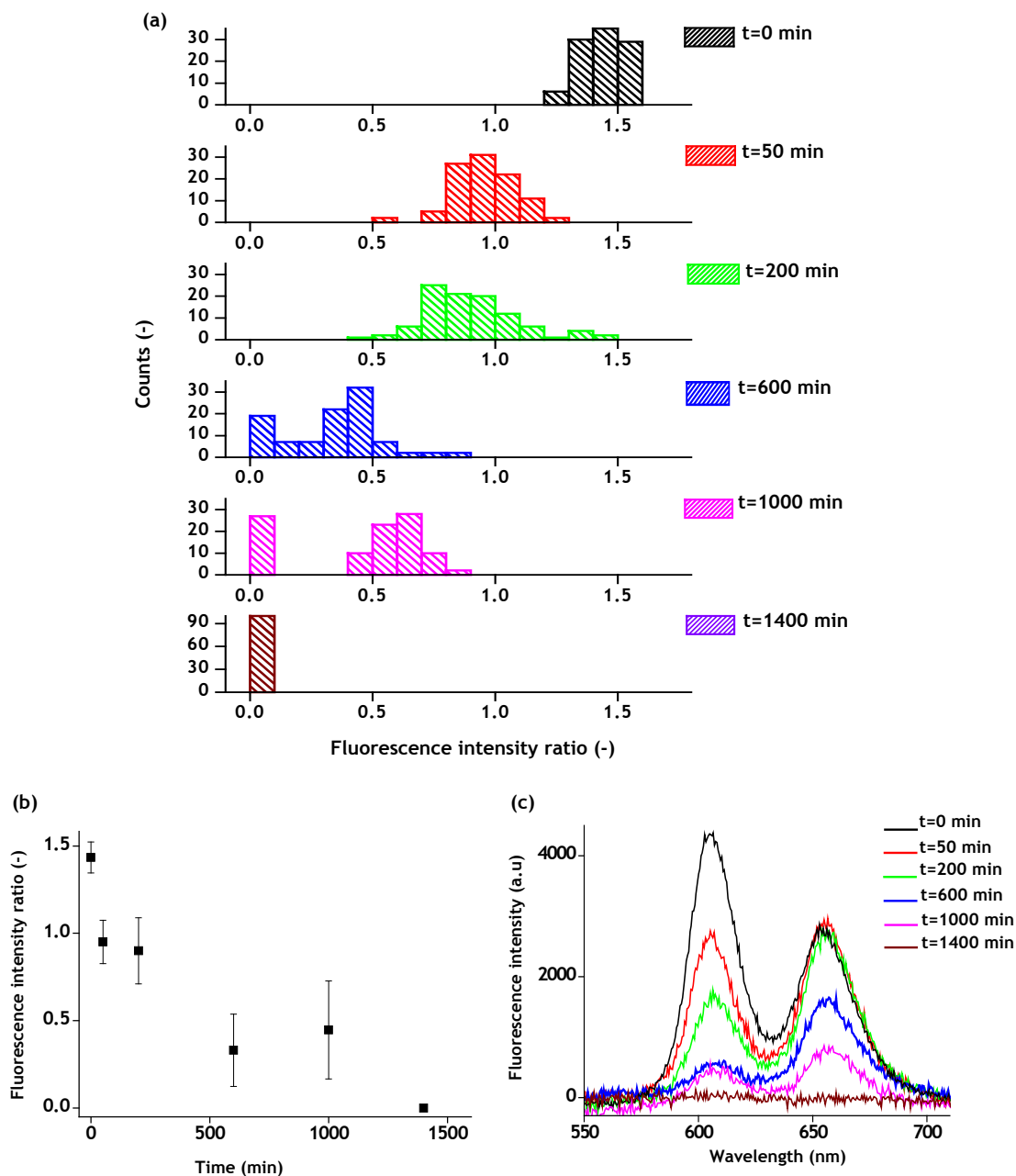


Figure 4-9: (a) Statistical distribution of QD_{605} to QD_{655} fluorescence intensity ratio of barcode \bullet - $B_{655}S_{605}(B_{605}S_{605})_1$ incubated in 100mM biotin solution at 37°C for different time intervals. Data collected from 100 single bead spectra for each time interval; (b) The decrease in fluorescence intensity ratio is plotted against time by using data from a. The error bars show standard deviation from data collected for 100 beads at each time interval; and (c) Corresponding fluorescence emission spectra of the barcode \bullet - $B_{655}S_{605}(B_{605}S_{605})_1$ at different time intervals after incubation in 100mM biotin solution at 37°C. A UV-2A filter set was employed to excite the quantum dot encoded beads in the UV-region using a mercury lamp and to collect the fluorescent signal. The UV-2A filter set consists of an excitation filter (330-380 nm), a dichroic mirror (cut-off wavelength 400 nm) and a 420 nm long-pass emission filter. The accumulation time was 1s for each single bead spectra.

remaining two layers of quantum dot conjugates. Notably at 1000 min, the ratio values again increased due to the disassembly of both B₆₅₅ and S₆₀₅ layers at nearly equal rates and in addition, the overall fluorescence intensity decreased. Also the number of beads with no quantum dots has also increased. This disassembly process also supports the hypothesis that the barcodes were produced by the layer-by-layer assembly of quantum dot conjugates.

4.3.3. Long-Term Stability

An important indicator of the stability of barcodes is the long-term stability. The stability of the barcode was studied by measuring the fluorescence intensity ratio of barcode •-B₆₀₅S₆₅₅(B₆₀₅S₆₀₅)₁ after 2 months and 10 months. Detailed descriptions of the Materials and Methods are provided in **Section 2.5.3**. The fluorescence intensity ratio of QD₆₀₅ to QD₆₅₅ of barcode •-B₆₀₅S₆₅₅(B₆₀₅S₆₀₅)₁ when it was prepared and after 2 months was plotted as a histogram for comparison (**Figure 4-10**).

It can be seen that the barcode fluorescence intensity ratio was changed slightly after storage in PBS containing 0.15% BSA for 2 months at 4°C. However, this change did not affect the identification of the barcode. On the other hand, in case of 10 months storage, the barcode disassembled completely giving no fluorescence. This may be due to the instability of the quantum dot-conjugates after long-term storage and quantum dot conjugates were no longer attached to the bead surface.

To assess this assumption and to find out whether streptavidin beads retain streptavidin-binding sites, these beads were incubated again with QD₆₀₅-biotin and QD₆₅₅-streptavidin to prepare •-B₆₀₅S₆₅₅. It can be seen that the barcode can be prepared by re-using the streptavidin beads as shown in **Figure 4-10b** which support the fact that the quantum dot conjugates were unstable and disassembled from the bead surface leaving the streptavidin beads with no fluorescence. Although the fluorescence signal can be obtained for barcode •-B₆₀₅S₆₅₅ not all the beads gave the same fluorescence signal. This is because the streptavidin beads were already coated with the biotin, therefore there were fewer of biotin binding sites remain on these beads and this number of binding sites varied greatly from bead to bead as compared to the fresh streptavidin beads used to prepare the barcode.

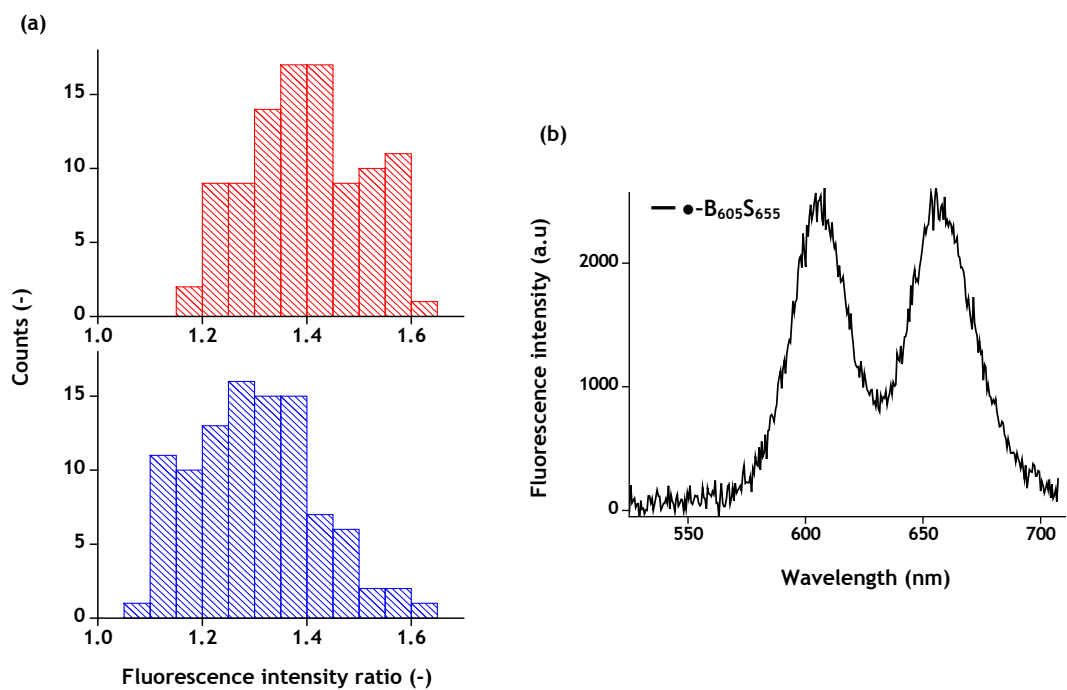


Figure 4-10: (a) Long term stability of barcode $\bullet\text{-B}_{605}\text{S}_{655}(\text{B}_{605}\text{S}_{605})_1$. Single bead fluorescence spectra were measured before (red) and after the storage of the barcode at 4°C for two months (blue). A UV-2A filter set was employed to excite the quantum dots in the UV-region using a mercury lamp and to collect the fluorescent signal. The UV-2A filter set consists of an excitation filter (330-380 nm), a dichroic mirror (cut-off wavelength 400 nm) and a 420 nm long-pass emission filter. The accumulation time was 1s for each single bead spectra. The statistical distribution of the barcodes was calculated by collating fluorescence intensity ratios of QD₆₀₅ to QD₆₅₅ for 100 beads, in each case. Barcodes stored for 10 months gave no fluorescence; **(b)** Fluorescence emission spectra of barcode $\bullet\text{-B}_{605}\text{S}_{655}$ prepared by re-using streptavidin beads from the barcodes $\bullet\text{-B}_{605}\text{S}_{655}(\text{B}_{605}\text{S}_{605})_1$ which were stored for 10 months.

4.4. References

1. Holmberg A, Blomstergren A, Nord O, Lukacs M, Lundeberg J, Uhlen M. The biotin-streptavidin interaction can be reversibly broken using water at elevated temperatures. *Electrophoresis* 2005;26(3):501-510.
2. Su XL, Li YB. Quantum dot biolabeling coupled with immunomagnetic separation for detection of Escherichia coli O157 : H7. *Analytical Chemistry* 2004;76(16):4806-4810.
3. Geho D, Lahar N, Gurnani P, Huebschman M, Herrmann P, Espina V, et al. Pegylated, streptavidin-conjugated quantum dots are effective detection elements for reverse-phase protein microarrays. *Bioconjugate Chemistry* 2005;16(3):559-566.
4. Shingyoji M, Gerion D, Pinkel D, Gray JW, Chen FQ. Quantum dots-based reverse phase protein microarray. *Talanta* 2005;67(3):472-478.
5. Bakalova R, Zhelev Z, Ohba H, Baba Y. Quantum dot-based western blot technology for ultrasensitive detection of tracer proteins. *Journal of the American Chemical Society* 2005;127(26):9328-9329.
6. Maeda Y, Yoshino T, Takahashi M, Ginya H, Asahina J, Tajima H, et al. Noncovalent immobilization of streptavidin on in vitro- and in vivo-biotinylated bacterial magnetic particles. *Applied and Environmental Microbiology* 2008;74(16):5139-5145.
7. Liu HL, Sonn CH, Wu JH, Lee KM, Kim YK. Synthesis of streptavidin-FITC-conjugated core-shell Fe₃O₄-Au nanocrystals and their application for the purification of CD4(+) lymphocytes. *Biomaterials* 2008;29(29):4003-4011.
8. Wu H, Liu GD, Wang J, Lin YH. Quantum-dots based electrochemical immunoassay of interleukin-1 alpha. *Electrochemistry Communications* 2007;9(7):1573-1577.
9. Lee JA, Mardiyani S, Hung A, Rhee A, Klostranec J, Mu Y, et al. Toward the accurate read-out of quantum dot barcodes: Design of deconvolution algorithms and assessment of fluorescence signals in buffer. *Advanced Materials* 2007;19(20):3113-+.
10. Vaidya SV, Gilchrist ML, Maldarelli C, Couzis A. Spectral bar coding of polystyrene microbeads using multicolored quantum dots. *Analytical Chemistry* 2007;79(22):8520-8530.

11. Yang J, Dave SR, Gao XH. Quantum dot nanobarcodes: Epitaxial assembly of nanoparticle-polymer complexes in homogeneous solution. *Journal of the American Chemical Society* 2008;130(15):5286-5292.
12. Wang L, Tan WH. Multicolor FRET silica nanoparticles by single wavelength excitation. *Nano Letters* 2006;6(1):84-88.
13. Allen CN, Lequeux N, Chassenieux C, Tessier G, Dubertret B. Optical analysis of beads encoded with quantum dots coated with a cationic polymer. *Advanced Materials* 2007;19(24):4420-+.
14. Han MY, Gao XH, Su JZ, Nie S. Quantum-dot-tagged microbeads for multiplexed optical coding of biomolecules. *Nature Biotechnology* 2001;19(7):631-635.
15. Gao XH, Nie SM. Doping mesoporous materials with multicolor quantum dots. *Journal of Physical Chemistry B* 2003;107(42):11575-11578.
16. Gao XH, Nie SM. Quantum dot-encoded mesoporous beads with high brightness and uniformity: Rapid readout using flow cytometry. *Analytical Chemistry* 2004;76(8):2406-2410.
17. Wu Y, Lopez GP, Sklar LA, Buranda T. Spectroscopic characterization of streptavidin functionalized quantum dots. *Analytical Biochemistry* 2007;364(2):193-203.

Chapter 5

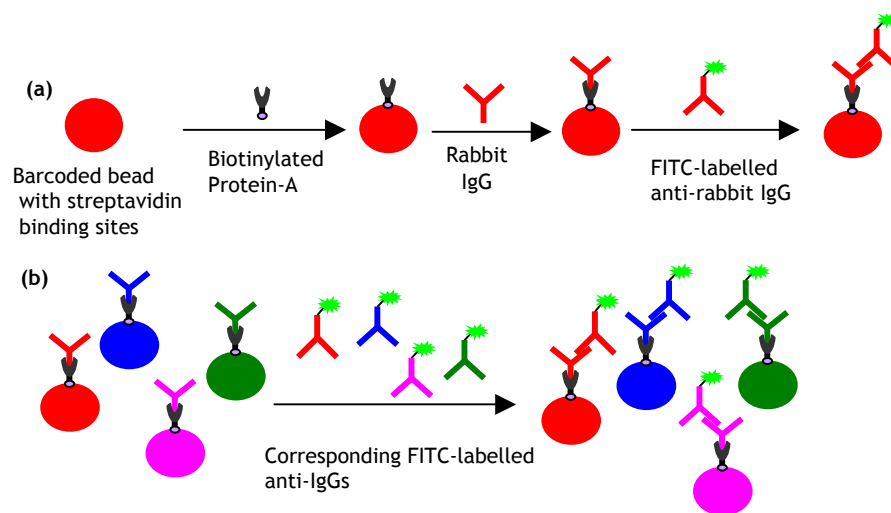
Applications of Quantum Dot Barcodes in Immunoassays

In recent years, the development of barcoded beads for multiplexed analysis has received great attention in analytical biotechnology. The encoded bead (barcode) technology has promising applications for multiplexing bioassays and can overcome many of the disadvantages in microarray technology. Over recent years different strategies have been reported for the preparation of barcodes, which are discussed in detail in **Chapter 1**. Unlike the microarray technology, barcoded beads benefited from different mass transfer characteristics giving enhanced solution kinetics when compared with planar diffusion as the case of microarray. This Chapter discusses the application of quantum dot barcodes produced by layer-by-layer assembly of quantum dot-biotin and quantum dot-streptavidin conjugates on a magnetic bead surface for multiplexing immunoassays.

5.1. Application of Quantum Dot Barcodes in Multiplexing Bioanalysis

Quantum dot barcodes prepared by layer-by-layer assembly of quantum dot conjugates on magnetic beads (**Section 2.2.3**) were characterised using single bead fluorescence spectroscopy (**Section 4.3**) and tested for the multiplexed immunoassays. Detailed descriptions of the Materials and Methods for performing multiplexed immunoassays are provided in **Section 2.6**. The magnetic bead based barcodes can be

identified upon the basis of different spectral responses from different quantum dots assembled on the bead surface, using the biological self-assembly of quantum dot biotin and quantum dot streptavidin conjugates. The barcode preparation is such that each barcode has streptavidin binding sites available for binding of any subsequent biotinylated molecule. For performing multiplexed immunoassays, four different IgGs namely, rabbit IgG, human IgG, mouse IgG and goat IgG with their corresponding anti-IgGs labelled with FITC were chosen. **Scheme 2-5**, shows the immunoassay scheme for single IgG and in case of the four different IgGs.



Scheme 2-5: (a) Immunoassay scheme for a single rabbit IgG-anti-rabbit IgG pair; (b) Multiplexed immunoassay scheme showing rabbit IgG (red), human IgG (blue), mouse IgG (pink) and goat IgG (green) immobilized on barcoded beads. A cocktail of four anti-IgGs (rabbit, human, mouse, and goat) labelled with FITC (light green) is added to the mixture. Note that false colours are used to represent different barcoded beads and figures are not to scale.

Four different quantum dot barcodes were prepared on the magnetic bead surface (\bullet -), namely, \bullet -B₆₀₅S₆₅₅, \bullet -B₆₀₅S₆₅₅(B₆₀₅S₆₀₅)₁, \bullet -B₆₀₅S₆₀₅ and \bullet -B₆₀₅S₅₆₅. After the preparation of four different barcodes, the fluorescent signal was measured by using single bead fluorescence spectroscopy as shown in **Figure 5-1**.

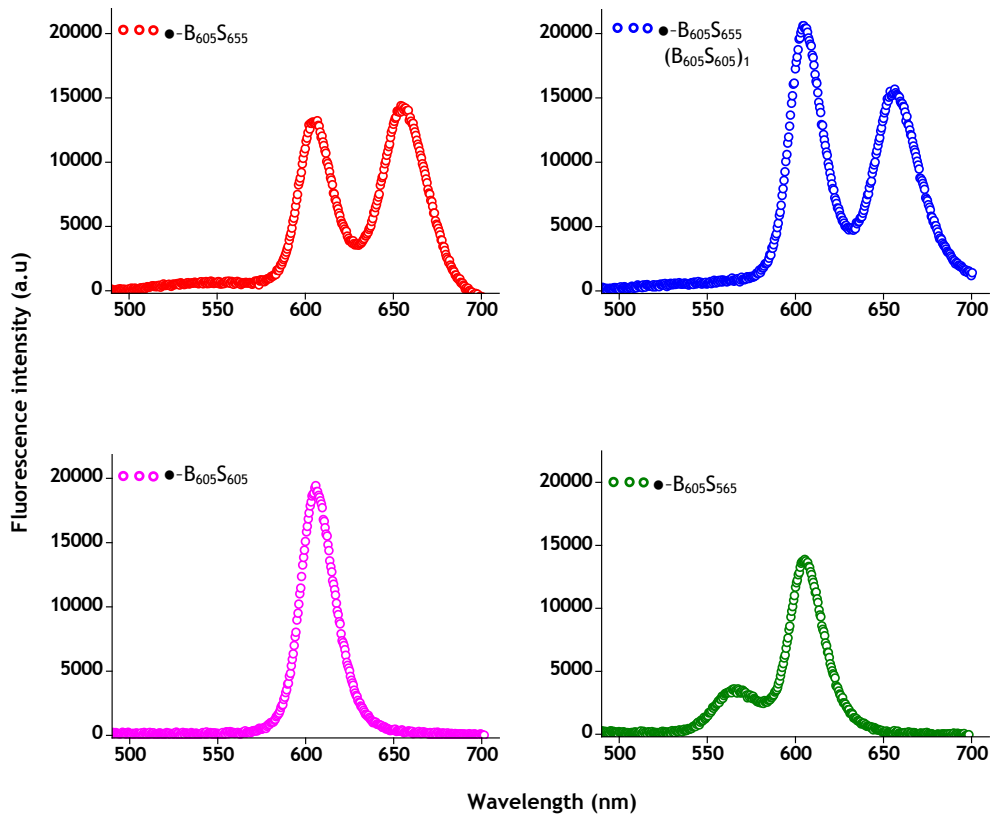


Figure 5-1: Single bead fluorescence spectra of four different barcodes prepared using layer-by-layer assembly of quantum dot biotin (QD605-biotin) and quantum dot streptavidin (QD-655, QD605 and QD565) conjugates on a streptavidin coated magnetic bead (●-). A B-2A filter set was employed to excite the quantum dots in the blue-region using a mercury lamp and to collect the fluorescent signal. The B-2A filter set consists of an excitation filter (450-490 nm), a dichroic mirror (cut-off wavelength 500 nm) and a 515 nm long-pass emission filter. The accumulation time was 1s for each single bead spectra.

As can be seen from **Figure 5-1**, these barcodes can be clearly distinguished from each other. As stated, each barcode has streptavidin as an outer protein layer, which can be used for the immobilisation of any biotinylated molecule. Therefore for performing multiplexed immunoassay, protein A-biotin or protein G-biotin was used to capture different IgGs. Protein A and Protein G are bacterial antibody binding proteins which bind to the Fc region of the IgGs.¹ The binding capacity of these proteins vary with the species and subclass of IgG.²

Biotin labelled protein A was immobilised on ●-B₆₀₅S₆₅₅, ●-B₆₀₅S₆₅₅(B₆₀₅S₆₀₅)₁ and ●-B₆₀₅S₆₀₅ to capture rabbit IgG, human IgG and mouse IgG, respectively (**Scheme 2-5**). Protein G-biotin was immobilised on ●-B₆₀₅S₅₆₅ to capture goat IgG from the solution due to its strong binding with goat IgG as compared to protein A.³ Each barcode was washed exhaustively with PBS pH 7.4 containing 2% BSA to remove excess IgGs using a magnet to separate the beads from the washing solution. After immobilisation, each barcode has a specific IgG available for capture of the complementary specific anti-IgG. To measure these IgGs immobilised on the barcode surface, FITC labelled anti-IgGs of all four species were used. For performing multiplexed immunoassay, appropriate amount of each barcode labelled with specific IgG were mixed together. To this mixture, a cocktail of anti-IgGs labelled with FITC (anti-rabbit IgG-FITC, anti-human IgG-FITC, anti-mouse IgG-FITC and anti-goat IgG-FITC) was added and the measured single bead fluorescence spectra of the barcoded beads were as shown in **Figure 5-2**.

The fluorescein signal appeared as a shoulder at ~530 nm in each barcode spectra confirming the attachment of all four FITC-labelled anti-IgGs to their corresponding IgGs, **Figure 5-2** and **Figure 5-3**.

In order to demonstrate the specificity of these IgG-anti-IgG pairs and also to confirm whether the signal appeared on each barcode was specific, anti-rabbit, anti-human and anti-goat FITC-labelled IgGs were added to a mixture of four barcodes, as constructed above (anti-mouse IgG-FITC was not added to the mixture). A strong FITC signal (shoulder at 530 nm) only appeared on three barcodes for which corresponding anti-IgGs-FITC were added, **Figure 5-4A**.

The weak FITC signal appeared in the case of barcode ●-B₆₀₅S₆₀₅ (pink) which has mouse IgG immobilised on its surface. Similarly, in further analogous experiments, anti-human IgG-FITC was not added to the four bead constructs and a similar outcome was achieved with a weak FITC signal generated (namely ●-B₆₀₅S₆₅₅ (B₆₀₅S₆₀₅)₁, blue, **Figure 5-4B**).

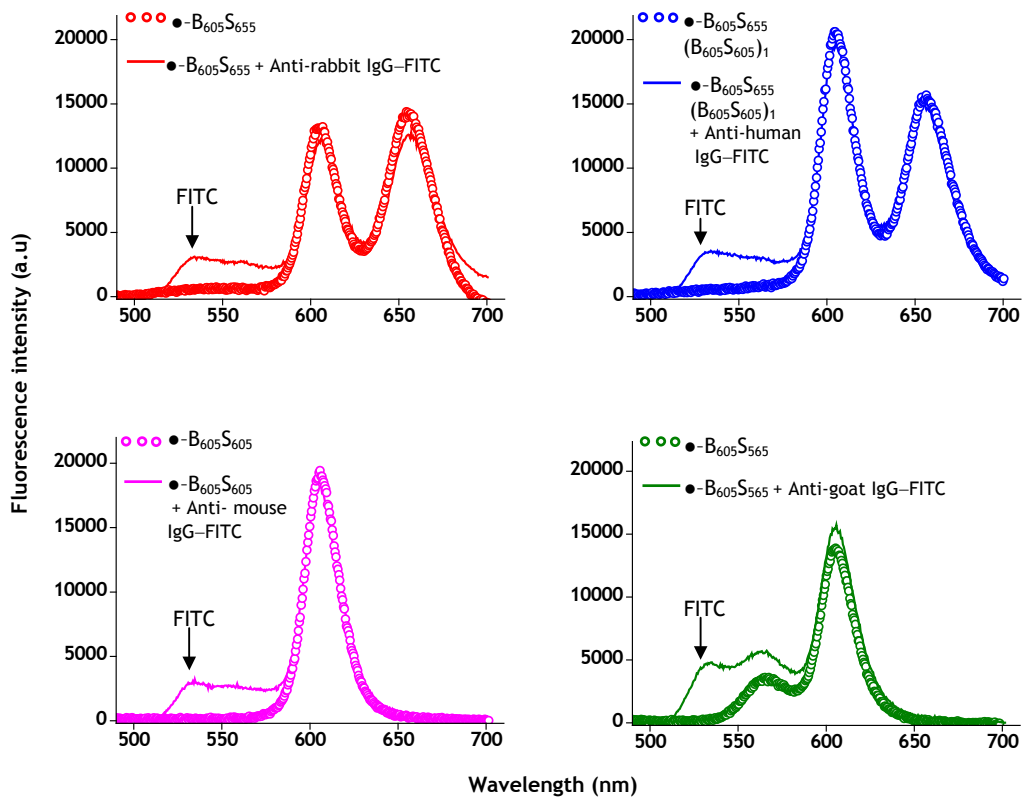


Figure 5-2: Single bead fluorescence spectra of four different barcodes measured before and after performing multiplexed immunoassay. A B-2A filter set was employed to excite the quantum dots and fluorescein in the blue-region using a mercury lamp and to collect the fluorescent signal. The B-2A filter set consists of an excitation filter (450-490 nm), a dichroic mirror (cut-off wavelength 500 nm) and a 515 nm long-pass emission filter. The accumulation time was 1s for each single bead spectra. Rabbit IgG was immobilised on barcode \bullet -B₆₀₅S₆₅₅ (red), human IgG was immobilised on barcode \bullet -B₆₀₅S₆₅₅ (B₆₀₅S₆₀₅)₁ (blue), mouse IgG was immobilised on barcode \bullet -B₆₀₅S₆₀₅ (pink) and goat IgG was immobilised on barcode \bullet -B₆₀₅S₅₆₅ (green). All the spectra are on the same scale.

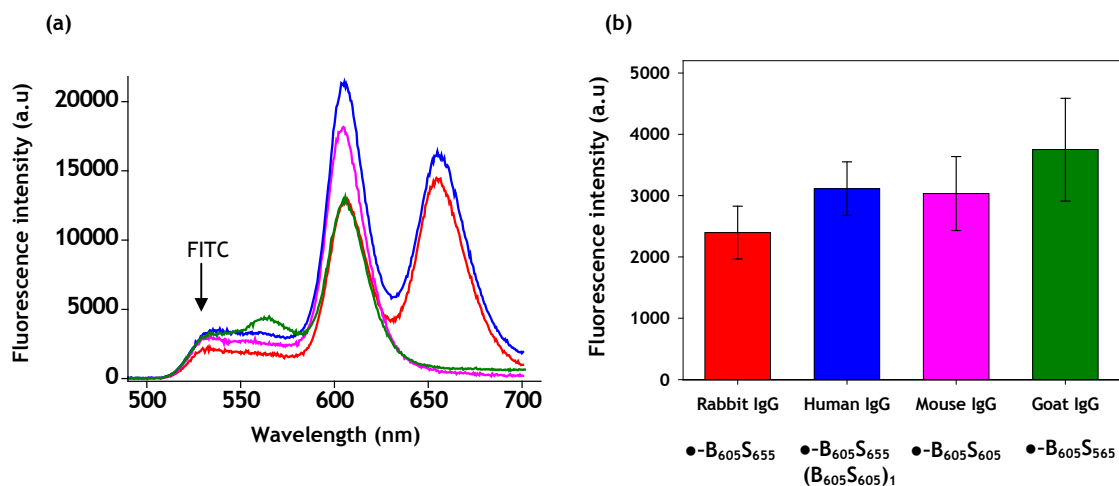


Figure 5-3: Multiplexed immunoassay using four different IgGs immobilised on four different barcodes. Rabbit IgG was immobilised on barcode ●-B₆₀₅S₆₅₅ (red), human IgG was immobilised on barcode ●-B₆₀₅S₆₅₅ (B₆₀₅S₆₀₅)₁ (blue), mouse IgG was immobilised on barcode ●-B₆₀₅S₆₀₅ (pink) and goat IgG was immobilised on barcode ●-B₆₀₅S₅₆₅ (green): (a) Single bead fluorescence spectra of four different IgG functionalised barcodes after the addition of a cocktail of four different FITC-labelled anti-IgGs. A B-2A filter set was employed to excite the quantum dots and fluorescein in the blue-region using a mercury lamp and to collect the fluorescent signal. The accumulation time was 1s for each single bead spectra; (b) The data represent mean fluorescence intensity (n=25 single bead spectra) measured from barcoded beads in each case at 530 nm. Where “n” represents number of single beads analysed using single bead spectroscopy.

To determine the origin of this signal and whether it was due to the cross reactivity of immunoglobulins or non-specific binding (NSB) of anti-IgGs-FITC on the barcode surface, control experiments were performed where FITC labelled anti-IgGs were added to the barcode ●-B₆₀₅S₅₆₅ without immobilising IgGs on the barcode surface.

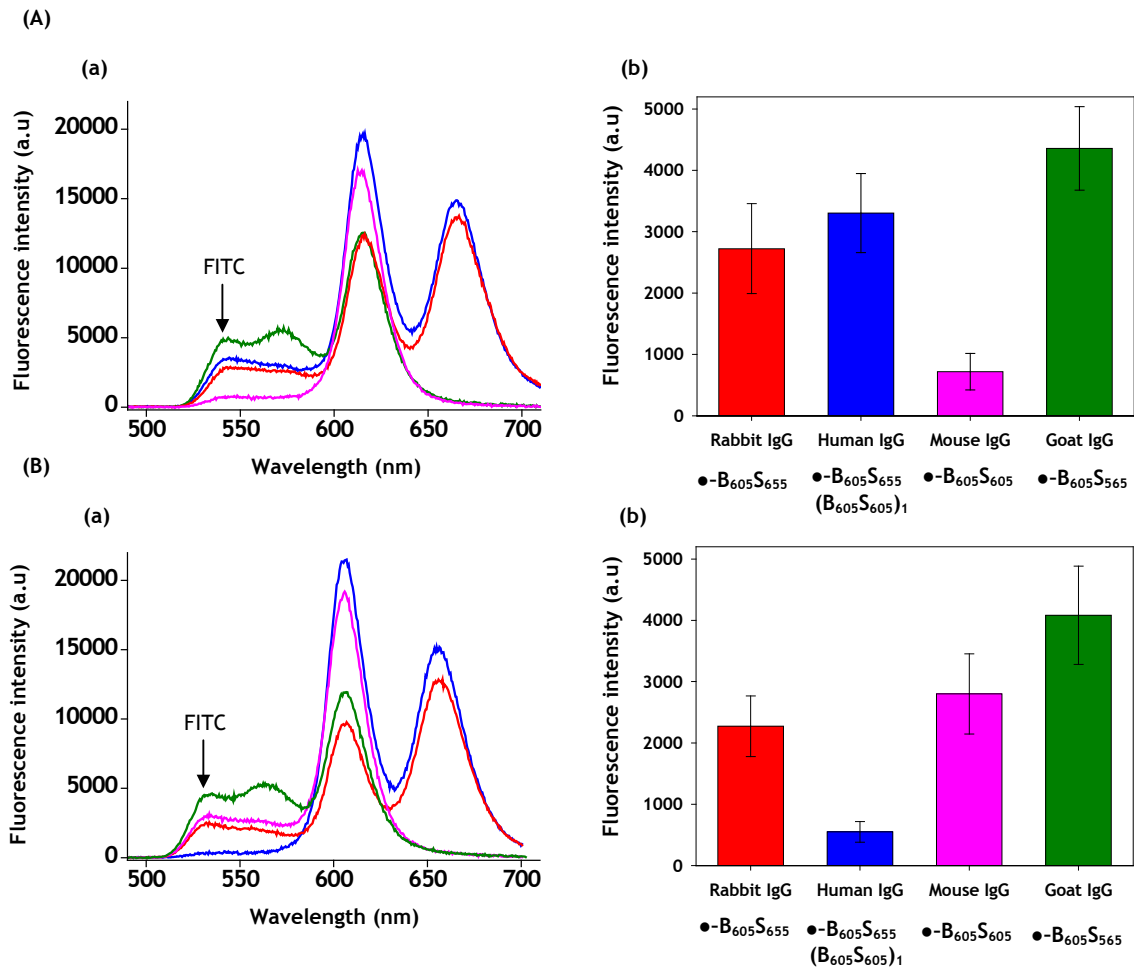


Figure 5-4: Multiplexed immunoassay using four different IgGs immobilised on four different barcodes. Rabbit IgG was immobilised on barcode ●-B₆₀₅S₆₅₅ (red), human IgG was immobilised on barcode ●-B₆₀₅S₆₅₅ (B₆₀₅S₆₀₅)₁ (blue), mouse IgG was immobilised on barcode ●-B₆₀₅S₆₀₅ (pink) and goat IgG was immobilised on barcode ●-B₆₀₅S₅₆₅ (green): **(A)** Anti-mouse IgG-FITC was not added to the mixture of barcodes. Other three FITC-labelled anti-IgGs were added; **(a)** Single bead fluorescence spectra of four different IgG functionalised barcodes after the addition of a cocktail of three different FITC-labelled anti-IgGs; **(b)** The data represent mean fluorescence intensity (n=25 single bead spectra) measured from barcoded beads in each case at 530 nm; Where “n” represents number of single beads analysed using single bead spectroscopy. **(B)** Anti-human IgG-FITC was not added to the mixture of barcodes and three other FITC-labelled anti-IgGs were added to the barcode mixture; **(a)** Single bead fluorescence spectra of four different IgG functionalised barcodes after the addition of a cocktail of three different FITC-labelled anti-IgGs; **(b)** The data represent mean fluorescence intensity (n=25 single bead spectra) measured from barcoded beads in each case at 530 nm. Where “n” represents number of single beads analysed using single bead spectroscopy. A B-2A filter set was employed to excite the quantum dots in the blue-region using a mercury lamp and to collect the fluorescent signal. The accumulation time was 1s for each single bead spectra.

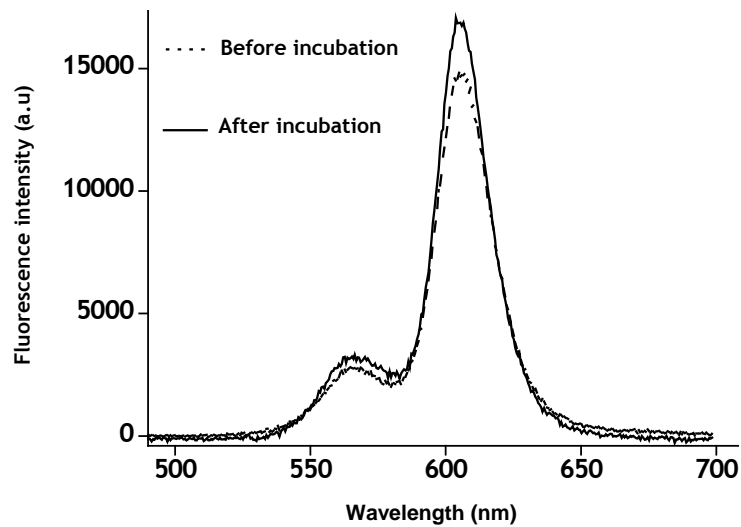


Figure 5-5: Control experiment showing the single bead spectra of the barcode \bullet -B₆₀₅S₅₆₅ before and after incubation in a cocktail of four different FITC-labelled anti-IgGs. The shoulder peak around 530 nm did not appear after incubation of the barcode in the FITC-labelled anti-IgGs. Note this is a representative spectra. In this control experiment 25 single bead spectra were taken. A B-2A filter set was employed to excite the quantum dots in the blue-region using a mercury lamp and to collect the fluorescent signal. The B-2A filter set consists of an excitation filter (450-490 nm), a dichroic mirror (cut-off wavelength 500 nm) and a 515 nm long-pass emission filter. The accumulation time was 1s for each single bead spectra.

No FITC signal was recorded in the barcode spectra (**Figure 5-5**), confirming that the background signal was not due to NSB but instead was probably as a consequence of the cross-reactivity of the polyclonal immunoglobulins.⁴ These findings are consistent with the known observation that streptavidin can generate a protein resistant coating (evidenced by its established application in functionalising microtitre plate wells for conventional immunoassays).

Instead of measuring the spectral response, the immunoassay on the beads could be readily visualised using an optical microscope with a green band pass filter (500 nm-550

nm) to discriminate between bound and unbound antibodies. Two barcodes were used for these experiments, \bullet -B₆₀₅S₆₅₅ and \bullet -B₆₀₅S₆₅₅(B₆₀₅S₆₀₅)₁ labelled with rabbit IgG and human IgG, respectively. To this mixture anti-rabbit IgG-FITC was added and incubated for 45 min. Note that anti-human IgG-FITC was not added to the mixture. After exhaustive washing these beads were imaged in the presence and absence of green band pass filter. When a green band pass filter was used, only the barcode \bullet -B₆₀₅S₆₅₅ immobilised with rabbit IgG gave a strong FITC signal (confirming the binding of anti-rabbit IgG to rabbit IgG immobilised on barcoded \bullet -B₆₀₅S₆₅₅ bead), **Figure 5-6**. The weak FITC fluorescent signal seen on the barcode \bullet -B₆₀₅S₆₅₅(B₆₀₅S₆₀₅)₁, **Figure 5-6**, can again be attributed to the cross reactivity of anti-rabbit IgG with human IgG as noted in **Figure 5-4**.

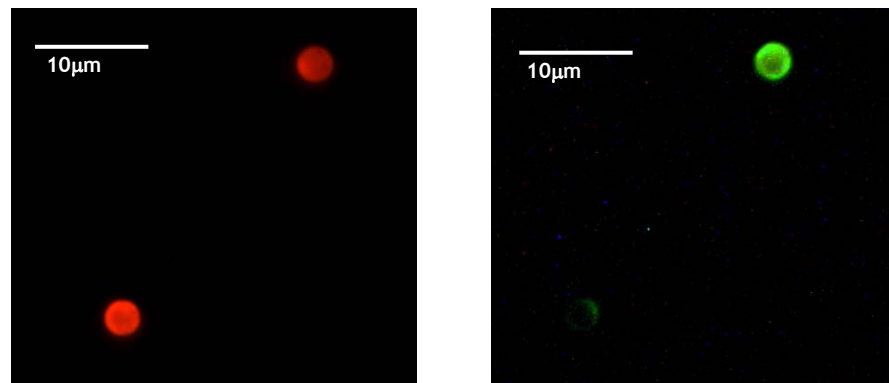
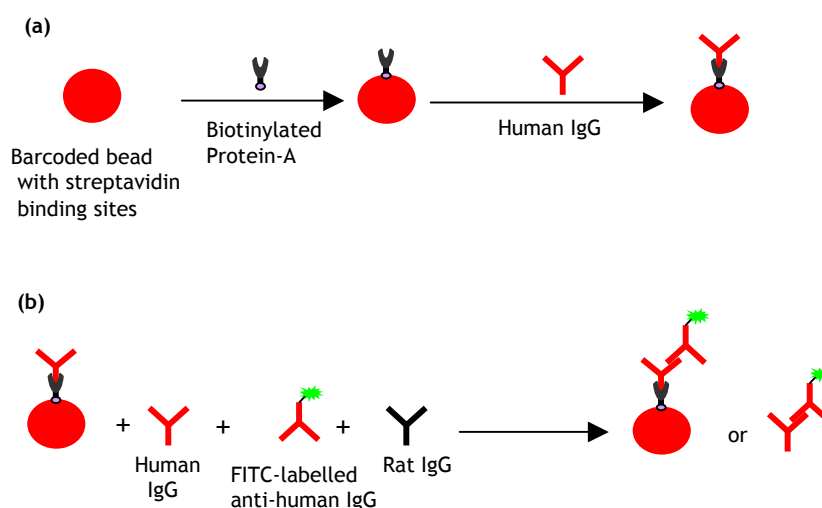


Figure 5-6: Shows fluorescence micrographs of barcodes \bullet -B₆₀₅S₆₅₅ and \bullet -B₆₀₅S₆₅₅(B₆₀₅S₆₀₅)₁ containing rabbit IgG and human IgG, respectively after the addition of FITC-labelled anti-rabbit IgG in the absence (left) and presence (right) of a green band pass filter (500 nm-550 nm). The image at left was taken by exciting quantum dots using UV-2A filter. The UV-2A filter set consists of an excitation filter (330-380 nm), a dichroic mirror (cut-off wavelength 400 nm) and a 420 nm long-pass emission filter. The image at right was taken by excitation of quantum dots in the blue region using B-2A filter set containing band pass emission filter (500 nm-550 nm) instead of 515 nm long-pass emission filter.

5.2. Binding Inhibition Immunoassay using Quantum Dot Barcodes

The above experiments in **Section 5.1** showed that quantum dot encoded beads prepared using quantum dot-biotin and quantum dot-streptavidin conjugates are suitable for performing multiplexed immunoassays. The above experiments however showed a qualitative measure of the multiplexed immunoassay. This section describes the quantitative immunoassay for human IgG to show that these barcodes can also be used to perform a quantitative immunoassay (**Scheme 2-6**). Detailed descriptions of the Materials and Methods for performing binding inhibition immunoassay are provided in **Section 2.7**.



Scheme 2-6: Binding inhibition immunoassay of human IgG: (a) immobilisation of human IgG on the barcode \bullet -B₆₀₅S₆₅₅ using protein A-biotin; (b) Binding inhibition immunoassay scheme for human IgG. Different amounts of human IgG were added in the presence of fixed amounts of barcoded beads containing immobilised human IgG, FITC-labelled anti-human IgG and rat IgG.

Human IgG was used as the analyte and FITC labelled anti-human IgG was used as the detection antibody. Also rat IgG was used as a control for non-specific binding. The first step involved the determination of the amount of anti-human IgG-FITC that can be added for the detection of human IgG. For this purpose, human IgG was immobilised on

the barcoded bead (\bullet -B₆₀₅S₆₅₅) using protein A-biotin as described in **Section 2.7**. After this the beads were incubated with different concentrations of anti-human IgG-FITC (0.25, 0.5, 1, 5, 10, 20, 30 μ g/ml) in the presence of PBS pH 7.4 containing 2% BSA and agitated for 45 min using a vortex mixer at a low speed. After exhaustive washing, the barcoded beads were analysed using single bead fluorescence spectroscopy and measurement of the FITC signal at 530 nm. Fluorescence signals were plotted for different concentrations of anti-human IgG-FITC, **Figure 5-7**. It can be seen that above 20 μ g/ml of anti-human IgG-FITC, the FITC signal saturated. The assumption is made that at this concentration, all binding sites on the bead are occupied. This concentration of anti-human IgG-FITC was subsequently used to perform the binding inhibition immunoassay for human IgG.

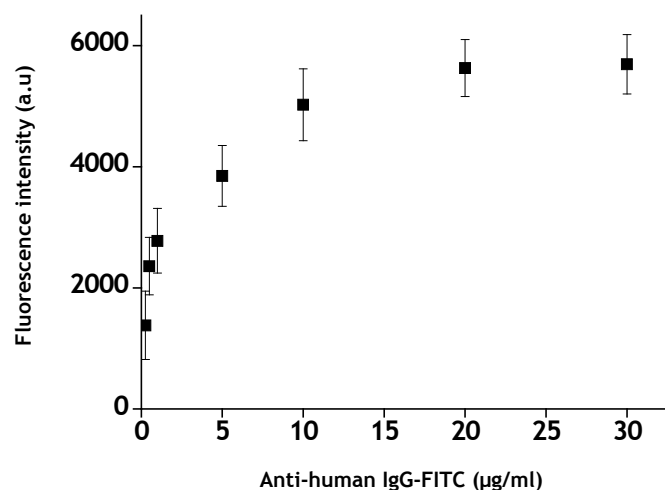


Figure 5-7: Optimisation of FITC labelled anti-human IgG concentration for performing binding inhibition immunoassay for human IgG using the barcode \bullet -B₆₀₅S₆₅₅. The data points are the mean measurements of the fluorescence intensity of FITC at 530 nm and the error bars show the standard deviation for n=25 measurements. Where “n=25” represents 25 single bead spectra from 25 beads in case of each reaction mixture. A B-2A filter set was employed to excite the quantum dots and fluorescein in the blue-region using a mercury lamp and to collect the fluorescent signal. The B-2A filter set consists of an excitation filter (450-490 nm), a dichroic mirror (cut-off wavelength 500 nm) and a 515 nm long-pass emission filter. The accumulation time was 1s for each single bead spectra.

After the optimisation of FITC labelled anti-human IgG, immunoassay was performed for the determination of human IgG in a mixture of human IgG and rat IgG. In order to perform this, human IgG was first immobilised on the barcoded bead (\bullet -B₆₀₅S₆₅₅) using protein A-biotin as described in Section 2.7. The beads ($\cong 9.3 \times 10^4$ in each reaction mixture) were then incubated with different concentrations of human IgG (0.5, 1, 5, 10, 20, 30 $\mu\text{g/ml}$) and fixed concentrations of anti-human IgG-FITC (20 $\mu\text{g/ml}$) and rat IgG (0.5 $\mu\text{g/ml}$) in the presence of PBS pH 7.4 containing 2% BSA and agitated for 45 min using a vortex mixer at a low speed. After exhaustive washing with the same buffer, these beads were analysed using single bead fluorescence spectroscopy to measure different concentrations of human IgG added to the reaction mixture, Figure 5-8. It can be seen

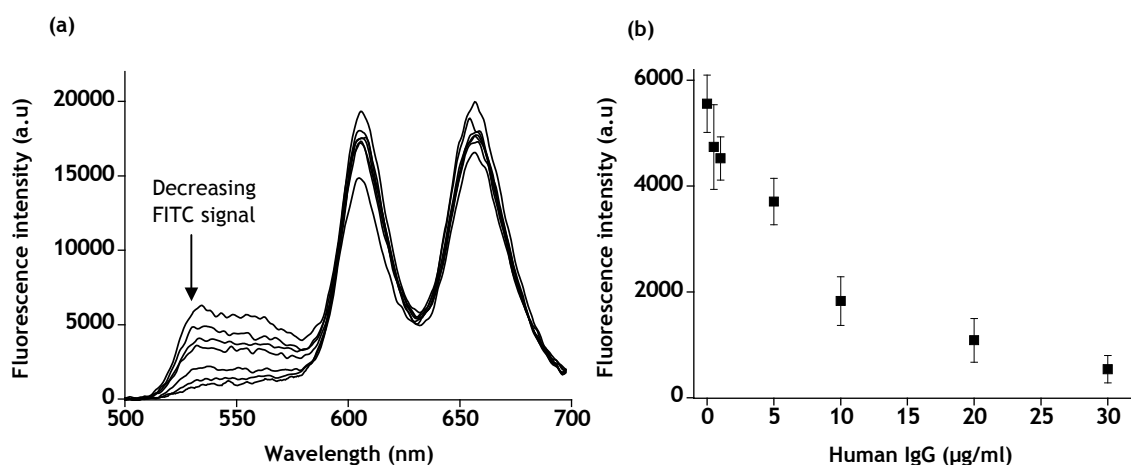


Figure 5-8: Shows the binding inhibition immunoassay using the barcode \bullet -B₆₀₅S₆₅₅ for the determination of different concentrations of human IgG: (a) Fluorescent signal of FITC labelled anti-human IgG decreases with the increase in human IgG concentration; (b) An exponential decay curve was obtained by fitting the plotted data using exponential decay model. The data points are the mean measurements of the fluorescence intensity of FITC at 530 nm and the error bars show the standard deviation for n=25 measurements in each case. Where “n=25” represents 25 single bead spectra from 25 beads in case of each reaction mixture. A B-2A filter set was employed to excite the quantum dots and fluorescein in the blue-region using a mercury lamp and to collect the fluorescent signal. The B-2A filter set consists of an excitation filter (450-490 nm), a dichroic mirror (cut-off wavelength 500 nm) and a 515 nm long-pass emission filter. The accumulation time was 1s for each single bead spectra.

that as the human IgG concentration increases, FITC signal decreases with the increase in concentration of human IgG in the reaction mixture. This is due to the fact that free human IgG binds with anti-human IgG-FITC resulting in the decrease of anti-human IgG-FITC signal on the barcoded bead. These results show that the barcodes prepared by using quantum dot-biotin and quantum dot-streptavidin conjugates can be used for the measurement of different immunoglobulins.

5.3. References

- 1 B. Guss, M. Eliasson, A. Olsson, M. Uhlen, A. K. Frej, H. Jornvall, J. I. Flock, and M. Lindberg, *Embo Journal*, 1986, **5**, 1567.
- 2 L. Bjorck and G. Kronvall, *Journal of Immunology*, 1984, **133**, 969.
- 3 M. Eliasson, R. Andersson, A. Olsson, H. Wigzell, and M. Uhlen, *Journal of Immunology*, 1989, **142**, 575.
- 4 G. F. Wang, H. Y. Park, and R. J. Lipert, *Analytical Chemistry*, 2009, **81**, 9643.

Chapter 6

Summary, Conclusions and Future Prospects

The experimental work in this thesis employed layer-by-layer assembly of different colour quantum dots to prepare encoded magnetic beads. The use of magnetic beads to prepare barcodes provides a simple technique to separate the beads from the incubation and washing solutions during the course of a biological assay. The magnetic collection method associated with the separation and washing of the encoded magnetic beads has great advantage over the centrifugation methods required for similar silica or latex bead based constructs. This magnetic method provides an easy way to separate bound and unbound antibodies in a biosensing assay.

Two approaches were used to prepare quantum dot encoded magnetic beads. The first approach was based on making layer-by-layer assembly of CdSe/ZnS quantum dots onto the magnetic beads using thiol chemistry. Before assembling the quantum dots onto the magnetic beads using this approach, the quantum dots were immobilised onto glass substrate using layer-by-layer assembly, in order to characterise the immobilisation method using X-ray photoelectron spectroscopy and fluorescence spectroscopy (Section 3.1).

The XPS studies showed that the quantum dots were bound to the glass substrate

using S–Zn bonding. These studies also showed that the attachment of dithiol linker was a suitable means to bond successive quantum dot layers (Section 3.1.1). Moreover, fluorescence spectroscopy studies confirmed that as the number of layers of quantum dots increased, the standard deviation of the fluorescence signal for different layers remained low, indicating that the quantum dot layer assemblies were uniform over the substrate (Section 3.1.2). To test this method further, multicolour quantum dot multilayers were prepared on glass substrate using the same method as described above. Fluorescence emission spectra of these multilayers showed that signal from both types of quantum dots were increased as the number of layers increases, confirming the suitability of this method to prepare quantum dot encoded beads (Section 3.1.2).

By using the dithiol linker method, two different barcodes namely (●-QD₆₂₆) and (●-QD₆₂₆QD₅₅₅) were prepared onto magnetic beads (●-) (Section 3.2). It was found that the barcode ●-QD₆₂₆ can be read optically when excited at 330-380nm (UV-2A) as confirmed from its characteristic emission spectrum with emission maximum at 626nm. However, in the presence of the second layer of quantum dots as in the case of ●-QD₆₂₆QD₅₅₅, the spectral response of the first inner layer of quantum dots QD₆₂₆, did not appear in the emission spectrum of barcode ●-QD₆₂₆QD₅₅₅.

It was found that QD₆₂₆ emission signal appeared when excited with a 510-560 nm (G-2A) excitation filter. This is because QD₅₅₅ outer layer is transparent to these wavelengths and so excitation of a fluorescent signal from QD₆₂₆ can occur from the inner layer. However, a desirable characteristic of a barcode is that it should give signal from both the quantum dots simultaneously. As a consequence, this barcoding scheme was not pursued.

It was thought that the spatial separation between different layers of quantum dots might be essential to produce barcodes using layer-by-layer assembly of quantum dots.⁽¹⁾ Magnetic fluorescent silica nanospheres were prepared using a thin silica shell (>10nm) as a spacer between different layers of quantum dots immobilised in a layer-by-layer assembly to produce different barcodes.⁽¹⁾ Therefore, quantum dot-biotin and quantum dot-streptavidin conjugates were used to prepare barcoded beads. In these conjugates, CdSe/ZnS quantum dots were conjugated to streptavidin and biotin. The size of the quantum dot streptavidin conjugate is ~15-20nm and that of biotin conjugate is ~10-12nm.^(2, 3) When these conjugates bound in a layer-by-layer assembly, the spacing between

different layers of quantum dots becomes greater than 10nm.

Quantum dot-biotin and quantum dot-streptavidin conjugates were subsequently used to prepare quantum dot barcodes using biological self-assembly in a layer-by-layer approach onto magnetic beads. First to test this method of immobilisation, the quantum dot-biotin and quantum dot-streptavidin conjugates were immobilised onto glass substrates and the immobilisation procedure was characterised using XPS and fluorescence spectroscopy (Section 3.3). First the glass slides were modified using aminosilane to immobilise biotin onto the glass substrate using NHS-biotin. These biotin functionalised glass substrates were then incubated in quantum dot-streptavidin conjugate solution to immobilise the first layer of quantum dots. These substrates were then incubated in quantum dot-biotin conjugate solution to make a second layer of quantum dots. In this manner ten layers of CdSe/ZnS quantum dots were formed.

XPS studies showed the immobilisation of aminosilane, biotin, quantum dot-streptavidin and quantum dot-biotin conjugates onto glass substrate. These studies confirmed that the immobilisation of multilayers of quantum dots is via biotin-streptavidin interaction (Section 3.3.1). Fluorescence spectroscopy also confirmed that the fluorescent signal was increased as the number of layers of quantum dot conjugates increased (Section 3.3.2). However, in contrast to studies involving quantum dots alone as described earlier using thiol chemistry, as the number of layers increases the standard deviation also increased. Multicolour quantum dot-conjugate multilayers were also prepared on glass substrate using the same method as described above. Fluorescence emission spectra of these multicolour multilayers showed that the signal from both types of quantum dots was increased as the number of layers increased with a subsequent increase in the standard deviation of fluorescent signal. The increase in standard deviation may be due to the fact that streptavidin or biotin conjugates have 5-10 or 5-7 streptavidin or biotin molecules on each conjugate, respectively and these varied from conjugate to conjugate. Therefore these films were not compact, resulting in a higher standard deviation of measurements on different preparations. However, the fluorescent signal from both the quantum dots in a multicolour multilayer assembly confirmed the suitability of this method to prepare quantum dot encoded beads.

Quantum dot barcodes were prepared using layer-by-layer assembly of quantum dot-biotin and quantum dot-streptavidin conjugates onto streptavidin magnetic beads.

Three different barcodes were prepared namely: ●-B₆₀₅S₆₅₅ ; ●-B₆₀₅S₆₅₅(B₆₀₅S₆₀₅)₁ ; and ●-B₆₀₅S₆₅₅(B₆₀₅S₆₀₅)₂. Single bead fluorescence spectra of these barcodes showed that the barcodes can be identified on the basis of their different spectral response (Section 4.1). The barcodes were characterised using ratiometric measurements of fluorescence intensity of different quantum dot conjugates assembled on the bead surface, using the biological self-assembly of quantum dot biotin and quantum dot streptavidin conjugates. It was found that the ratiometric measurements are comparable to, and in most cases much better than that previously reported for quantum dot-encoded beads.⁽⁴⁻⁸⁾ These barcodes were then characterised against batch to batch difference in the preparation of barcodes and it was found that the batch to batch variation is negligible (Section 4.2).

Biotin-streptavidin based barcodes were tested for stability at higher temperature and long term stability after storage (Section 4.3). It was found that barcode information remained intact after heat treatment at 95°C for 15 min. In the case of long-term stability, barcode information was found to be intact after two month storage at 4°C. However, after 10 months storage, the barcode had disassembled completely giving no fluorescence. This may be due to the inherent instability of the quantum dot-conjugates immobilised onto the bead after long-term storage and quantum dot conjugates were no longer attached to the bead surface.

As the barcodes were prepared using biological self-assembly of quantum dots conjugates, therefore it was important to study their stability in different concentrations of biotin solution (Section 4.3). The barcodes prepared above were incubated in different concentrations of biotin at room temperature and at 37°C for different time intervals. It was found that the barcodes were disassembled completely in the presence of 100mM biotin at 37°C in 24h. This disassembly process using different concentrations of biotin also confirmed that the barcode assembly was due to biotin-streptavidin interaction.

The quantum dot barcodes as described earlier were used to develop multiplexed immunoassays. For this purpose, a model immunoassay was designed where four different IgGs namely: Rabbit IgG; Human IgG; Mouse IgG and ; Goat IgG were immobilised on four different barcodes ●-B₆₀₅S₆₅₅, ●-B₆₀₅S₆₅₅ (B₆₀₅S₆₀₅)₁, ●-B₆₀₅S₆₀₅ and ●-B₆₀₅S₅₆₅, respectively. These IgGs were detected using their corresponding FITC labelled anti-IgGs (Section 5.1). It was found that different IgG-anti-IgG pairs can be identified on the basis

of different barcode signals. Control experiments showed that the FITC signal that appeared on each barcode was specific i.e. due to the specific IgG-anti-IgG pairs. However, a slight cross reactivity was observed among different polyclonal antibodies. As a control experiment, barcode ●-B₆₀₅S₅₆₅ without the immobilisation of any IgGs was incubated in a mixture of four different anti-IgGs-FITC mixture. No FITC signal was found on the barcode. This finding is consistent with the observation that streptavidin can generate a resistant coating as is exploited in established applications that use microtitre plate wells for conventional immunoassays.

The above experiments proved that the quantum dot barcodes prepared using quantum dot-biotin and quantum dot-streptavidin conjugates can be used to perform multiplexed immunoassays. Moreover, these barcodes were also used to perform a quantitative immunoassay (Section 5.2). Barcode ●-B₆₀₅S₆₅₅ was used to perform a quantitative binding inhibition immunoassay for human IgG. It was found that different concentrations of human IgG can be determined using these barcodes which open up a possibility of using these barcodes for performing a range of different multiplexed quantitative immunoassays.

In future work, the barcoded technology demonstrated above could be applied to perform a range of clinically relevant quantitative multiplexed immunoassays and nucleic acid hybridisation assays. Moreover, these barcodes can also be introduced into different cells for intracellular studies. The present work involved the readout of the barcodes using single bead fluorescence spectroscopy, which is laborious and time consuming. These barcodes could also be read using suitably adopted flow cytometry.⁽⁶⁾ The next step is the convergence of this barcode technology with the high throughput methods for barcode measurement and identification methods. Klostranec *et al.*, developed a microfluidic system in conjunction with quantum dot encoded beads for the determination of different biomarkers related to hepatitis B, hepatitis C and HIV.⁽⁹⁾ This system contains four main components: different quantum dot encoded beads to identify different target molecules; electrokinetically driven microfluidic system to enable sequential and high throughput readout of different barcodes; photon counting detection system which enables real time readout of the barcodes flowing through the microfluidic channels and; signal processing system for the deconvolution of the quantum dot encoded beads signal.⁽⁹⁾ This type of method can be used for the high throughput readout of the barcode technology developed in the present studies.

Another route for the development of high throughput measurement system for these barcodes could be the patterning of the encoded beads using electrostatic or magnetic properties of the beads. Streptavidin coated magnetic beads were patterned at the micron scale using positive charge aminosilane patterns as a template for selective immobilisation of streptavidin coated magnetic beads.⁽¹⁰⁾ Other patterning methods include patterning of magnetic beads using patterned polyelectrolyte multilayers, magnetic gradients and using PDMS stamps.⁽¹¹⁻¹³⁾

In conclusion, a new strategy to make barcodes by using biological self-assembly in a layer-by-layer approach is demonstrated. The analytical figures of merit for this technique were characterised showing the potential that the technology has for multiplexing immunoassays. Given the widespread use of streptavidin and biotin as ligand binding motifs in analytical biotechnology, the method will have broad applicability in a range of measurements including multiplexed immunoassays and nucleic acid hybridisation assays.

References

1. Wang QB, Liu Y, Lin CX, Yan H. Layer-by-layer growth of superparamagnetic, fluorescent barcode nanospheres. *Nanotechnology* 2007;18(40):pp7.
2. Qdot® Biotin Conjugates user Manual. Invitrogen 2006.
3. Qdot® Streptavidin Conjugates user manual. Invitrogen 2007.
4. Allen CN, Lequeux N, Chassenieux C, Tessier G, Dubertret B. Optical analysis of beads encoded with quantum dots coated with a cationic polymer. *Advanced Materials* 2007;19(24):4420-4425.
5. Gao XH, Nie SM. Doping mesoporous materials with multicolor quantum dots. *Journal of Physical Chemistry B* 2003;107(42):11575-11578.
6. Gao XH, Nie SM. Quantum dot-encoded mesoporous beads with high brightness and uniformity: Rapid readout using flow cytometry. *Analytical Chemistry* 2004;76(8):2406-2410.
7. Han MY, Gao XH, Su JZ, Nie S. Quantum-dot-tagged microbeads for multiplexed optical coding of biomolecules. *Nature Biotechnology* 2001;19(7):631-635.
8. Yang J, Dave SR, Gao XH. Quantum dot nanobarcodes: Epitaxial assembly of nanoparticle-polymer complexes in homogeneous solution. *Journal of the American Chemical Society* 2008;130(15):5286-5292.

9. Klostranec JM, Xiang Q, Farcas GA, Lee JA, Rhee A, Lafferty EI, et al. Convergence of quantum dot barcodes with microfluidics and signal processing for multiplexed high-throughput infectious disease diagnostics. *Nano Letters* 2007;7(9):2812-2818.
10. Sivagnanam V, Sayah A, Vandevyver C, Gijs MAM. Micropatterning of protein-functionalized magnetic beads on glass using electrostatic self-assembly. *Sensors and Actuators B-Chemical* 2008;132(2):361-367.
11. Lyles BF, Terrot MS, Hammond PT, Gast AP. Directed patterned adsorption of magnetic beads on polyelectrolyte multilayers on glass. *Langmuir* 2004;20(8):3028-3031.
12. Anandakumar S, Rani VS, Jeong JR, Kim C, Kim KW, Rao BP. Translocation of magnetic beads using patterned magnetic pathways for biosensing applications. *Journal of Applied Physics* 2009;105(07B312):1-3.
13. Issle J, Pla-Roca M, Martfnez E, Hartmann U. Patterning of magnetic nanobeads on surfaces by poly(dimethylsiloxane) stamps. *Langmuir* 2008;24(3):888-893.